UNIVERSITY OF CALIFORNIA SAN DIEGO

Tissue-specific roles of endoplasmic reticulum – plasma membrane contact site proteins in *Caenorhabditis elegans*

A dissertation submitted in partial satisfaction of

the requirements for the degree Doctor of Philosophy

in

Biology

by

Christopher Piggott

Committee in charge:

Professor Yishi Jin, Chair
Professor Shelley Halpain
Professor Peter Novick
Professor Michael Petrascheck
Professor James Wilhelm
Professor Binhai Zheng

2020

The Dissertation of Christopher Piggott is approved, and it is acceptable in quality and form for publication on microfilm and electronically:

_____

_____

_____

_____

_____

_____
Chair

University of California San Diego

2020

TABLE OF CONTENTS

LIST OF FIGURES

LIST OF TABLES

ACKNOWLEDGEMENTS

I would like acknowledge Professor Yishi Jin for her guidance and support as my advisor and always pushing me to do better. I am grateful to all past and present members of the Jin and Chisholm labs, particularly the postdocs and grad students who gave me advice and guided me when I first joined the lab, and all the members who contributed to the friendly, stimulating environment. I thank my thesis committee members for their advice and support.

I would like to thank my cohort and the many friends that have supported me throughout graduate school, with special thanks to Javier How for always being up for a drink and making Scrubs references; to Samuel Lin for always being there to chat and the many workday workouts; to Robert Pulido for taking the surf class with us; to Jeanae Kaneshiro for all the hangouts throughout grad school; to Kent Phuong and Jonah Chevrier for always being down to hang when I'm home for the holidays; and to Galina Gheihman for the spring break road trips exploring America's national parks.

I would especially like to thank my girlfriend Antonia Darragh for her unwavering support for me throughout grad school, and the many adventures we have shared all over the world. I also thank her family for being welcoming and taking care of me.

Finally, I would like to thank my family, who, despite being far away, always provided a warm home to return to for the holidays.

Chapter 2, in large part, is a reprint of the material as it appears in Kim KW, Tang NH, Piggott CA, Andrusiak MG, Park S, Zhu M, Kurup N, Cherra SJ, Wu Z, Chisholm AD, Jin Y. 2018. Expanded genetic screening in *Caenorhabditis elegans* identifies new regulators and an inhibitory role for NAD + in axon regeneration. *Elife* 7:e39756. The dissertation author was a co-author of this material.

Chapter 3, in full, has been submitted for publication as it may appear in Piggott CA, Wu Z, Nurrish S, Xu S, Kaplan JM, Chisholm AD, Jin Y. 2020. *Caenorhabditis elegans* junctophilin has tissue-specific functions and regulates neurotransmission with extended-synaptotagmin. The dissertation author was the primary investigator and author of this material.

VITA

2014 Bachelor of Science, University of Toronto

2020 Doctor of Philosophy, University of California San Diego

PUBLICATIONS

Bin NR, Jung CH, **Piggott C**, Sugita S. 2013. Crucial role of the hydrophobic pocket region of Munc18 protein in mast cell degranulation. *Proc Natl Acad Sci U S A* 110:4610-4615.

Zeqiraj E, Tian L, **Piggott CA**, Pillon MC, Duffy NM, Ceccarelli DF, Keszei AFA, Lorenzen K, Kurinov I, Orlicky S, Gish GD, Heck AJR, Guarné A, Greenberg RA, Sicheri F. 2015. Higher-Order Assembly of BRCC36-KIAA0157 Is Required for DUB Activity and Biological Function. *Mol Cell* 59:970-983.

Kim KW, Thakur N, **Piggott CA**, Omi S, Polanowska J, Jin Y, Pujol N. 2016. Coordinated inhibition of C/EBP by Tribbles in multiple tissues is essential for Caenorhabditis elegans development. *BMC Biol* 14.

Kim KW, Tang NH, **Piggott CA**, Andrusiak MG, Park S, Zhu M, Kurup N, Cherra SJ, Wu Z, Chisholm AD, Jin Y. 2018. Expanded genetic screening in caenorhabditis elegans identifies new regulators and an inhibitory role for NAD + in axon regeneration. *Elife* 7:e39756.

Piggott CA, Wu Z, Nurrish S, Xu S, Kaplan JM, Chisholm AD, Jin Y. 2020. *Caenorhabditis elegans* junctophilin has tissue-specific functions and regulates neurotransmission with extended-synaptotagmin. (submitted).

ABSTRACT OF THE DISSERTATION

Tissue-specific roles of endoplasmic reticulum – plasma membrane contact site proteins in *Caenorhabditis elegans*

by

Christopher Piggott

Doctor of Philosophy in Biology

University of California San Diego, 2020

Professor Yishi Jin, Chair

This dissertation explores the roles of endoplasmic reticulum (ER) – plasma membrane (PM) contact site proteins in *Caenorhabditis elegans* physiology. I first investigated the roles of ER-PM contact site proteins in axon regeneration after injury by examining mutants affecting conserved ER-PM contact site components. While most ER-PM components are individually dispensable, the sole *C. elegans* junctophilin *jph-1* is required for axon regeneration. Additionally, the partial deletion allele *jph-1(ok2823)* enhances regenerative axon fusion. I further studied junctophilin using *jph-1(0)* null alleles generated by CRISPR-Cas9. By *in vivo* confocal imaging of tagged proteins, I found that junctophilin is expressed in muscles and neurons. In muscles, JPH-1 co-localizes with calcium channels EGL-19 and UNC-68 at ER-PM contact sites. I used tissue-

specific rescue constructs to demonstrate that junctophilin is required in the pharyngeal and body wall muscles for feeding and locomotion, respectively. In neurons, JPH-1 co-localizes with the neuronal ER-PM contact site protein ESYT-2. Using pharmacological assays, I showed that both *jph-1* and *esyt-2* modulate neurotransmission at the neuromuscular junction. Interestingly, *jph-1* and *esyt-2* mutants displayed mutual suppression in their responses to the drug aldicarb, suggesting that they have antagonistic roles in neuromuscular synaptic transmission. Lastly, I investigated the interactions between *jph-1* and calcium channels by generating double mutants, which revealed that junctophilin functions in overlapping pathways with ER- and PM-localized calcium channels for animal health and development. My data demonstrates that ER-PM contact site proteins play critical roles in diverse tissue types and support tissue-specific functions.

Chapter 1:

Introduction to membrane contact sites and junctophilin

1.1 Overview of endoplasmic reticulum – plasma membrane contact sites

Membrane contact sites (MCSs) are regions of close contact, generally within 10 to 30 nm, between organelles or between an organelle and the plasma membrane (PM). Since the first observation of MCSs by electron microscopy in the 1950s (Porter and Palade, 1957), every membrane-bound organelle, from mitochondria to peroxisomes, has been found to be involved in at least one MCS (Prinz et al., 2020). Many of these involve the endoplasmic reticulum (ER), which is the largest membrane-bound organelle and forms a contiguous network of sheets and tubules spread through the entire cell (Phillips and Voeltz, 2016). The ER forms MCSs with many organelles, including mitochondria and endosomes, as well as with the PM.

ER-PM MCSs have important roles in cellular physiology, particularly in non-vesicular lipid transfer and calcium channeling. For example, lipid transfer proteins ORP5 and ORP8 transfer phosphatidylinositol-4-phosphate (PI4P) from the PM to the ER in exchange for countertransport of phosphatidylserine (PS), clearing PI4P from the PM and enriching PS in the PM (Chung et al., 2015). An example of calcium channeling is store-operated calcium entry (SOCE), which replenishes ER calcium when stores are low (Hogan and Rao, 2015). The ER calcium sensor STIM1 relocalizes to ER-PM contact sites, where it activates Orai1 calcium channels on the PM. Calcium enters the cell through the Orai1 calcium channels and is taken up by nearby sarcoplasmic reticulum/ER Ca^{2+}-ATPase (SERCA) transporters into the ER. By entering the cell at ER-PM contact sites, calcium bypasses the bulk of the cytoplasm and is transported into the ER without raising the cytoplasmic calcium concentration.

ER-PM MCSs are maintained by proteins or protein complexes that bind to both membranes simultaneously and tether them together. In yeast, six ER-anchored proteins were identified that act independently from each other to tether the ER to the PM (Manford et al., 2012).

Ist2 is a multi-pass ER membrane protein related to the TMEM16 family of calcium-activated chloride channels. The tricalbins Tcb1/2/3 are homologous to the mammalian extended-synaptotagmins, which are anchored in the ER by a hydrophobic hairpin and bind to the inner leaflet of the plasma membrane (Giordano et al., 2013). Scs2 and Sc22 are vesicle-associated membrane protein (VAMP)-associated proteins (VAPs), which have an ER transmembrane segment and a cytoplasmic domain that bind a variety of lipid transfer proteins (Gallo et al., 2016). In mammals, two additional ER-PM tethers have been identified: junctophilins and Sec22b-Stx1 non-fusogenic SNARE complexes (Gallo et al., 2016). Among these tethers, extended-synaptotagmins and junctophilins are of the clearest physiological importance.

1.2 Extended-synaptotagmins (E-Syts)

Extended-synaptotagmins (E-Syts) were originally identified in a search for proteins similar to synaptotagmins, which regulate the fusion of vesicles to the plasma membrane (Fernández-Chacón et al., 2001; Geppert et al., 1994). Synaptotagmins contain a transmembrane region and two C2 domains separated by a short linker (Min et al., 2007; Südhof and Rizo, 1996). C2 domains have lipid-binding capabilities that can be enhanced by the presence of calcium (Nalefski and Falke, 1996). Extended synaptotagmins are so named because they are longer than synaptotagmins; E-Syts contain three or five C2 domains, a synaptotagmin-like mitochondrial and lipid-binding protein (SMP) domain, and a hydrophobic region (Min et al., 2007).

E-Syts are conserved throughout animals, with most vertebrates having three E-Syts (Min et al., 2007). E-Syt1 has five C2 domains, while E-Syt2 and 3 each have three C2 domains. Invertebrates, including *C. elegans* and *D. melanogaster*, have one E-Syt, which contains three C2 domains and is therefore most similar to E-Syt2 and 3. The E-Syt family is conserved all the way to yeast, which have the related tricalbins Tcb1/2/3 (Schulz and Creutz, 2004).

Studies in mammalian cell lines showed that E-Syts localize to ER-PM contact sites (Giordano et al., 2013). An N-terminal hairpin transmembrane domain anchors E-Syts in the ER membrane. E-Syt2 and 3 bind the plasma membrane and are constitutively localized at ER-PM contact sites (Giordano et al., 2013). In contrast, E-Syt1 localizes to the ER at resting Ca2+ levels. Upon an influx of calcium from the extracellular medium, E-Syt1 translocates to the PM, leading to an expansion of ER-PM contact sites (Idevall-Hagren et al., 2015). E-Syt2 and 3 respond to calcium by tightening their binding to the PM, decreasing the distance between the ER and the PM. Therefore, E-Syts play a role in regulating ER-PM contact sites in response to calcium.

The C2 domains play a key role in regulating E-Syt membrane binding. The C2 domains are referred to as C2A, C2B, C2C, C2D, and C2E from N- to C-terminal ends of the protein. Homology analysis suggests that C2C and C2D in E-Syt1 are likely duplicates of C2A and C2B (Min et al., 2007). Constitutive localization of E-Syt2 and 3 is achieved by binding of the C2C domain to phosphatidylinositol 4,5-bisphosphate (PI(4,5)P2) on the inner leaflet of the PM (Giordano et al., 2013). Upon calcium influx, the Ca2+-dependent C2A domain also binds the PM, causing a "zipping up" of the protein to the membrane and decreasing the distance between the ER and PM. In E-Syt1, calcium influx causes the Ca2+-dependent C2C domain (which is homologous to the C2A domain of E-Syt2 and 3) to bind the PM, localizing E-Syt1 to ER-PM contact sites (Idevall-Hagren et al., 2015). It is thought that the other C2 domains in E-Syts are unable to bind calcium but work cooperatively to aid binding of the protein to the plasma membrane (Jean et al., 2010; Min et al., 2007).

While intracellular imaging and biochemical assays have established that E-Syts regulate ER-PM contact sites in response to calcium, it is still unclear what physiological role this plays. E-Syt triple knockout mice are viable and show normal development (Sclip et al., 2016; Tremblay and Moss, 2016). A clue to E-Syt function comes from the presence of SMP domains. These domains belong to the TULIP superfamily and are found in proteins implicated in lipid binding and transfer (Kopec et al., 2010). The X-ray structure of the E-Syt2 SMP domain revealed that it forms a hydrophobic channel that could transport lipids (Schauder et al., 2014). Recently, E-Syt1 was shown to be capable of transporting lipid between liposomes *in vitro* (Saheki et al., 2016; Yu et al., 2016). Unexpectedly, knocking out all three E-Syts in HeLa cells had no effect on constitutive lipid levels at the plasma membrane (Saheki et al., 2016). However, triple knockout did lead to accumulation of diacylglycerol (DAG) at the PM after phospholipase C (PLC) signaling.

E-Syt1 was shown to be capable of transferring DAG *in vitro* and E-Syt1 expression in the triple knockout restored wild-type DAG levels, suggesting that E-Syt1 may be important for clearing DAG from the plasma membrane. Taken together, this data indicates that E-Syts are a calcium-sensitive protein that likely plays a role in lipid regulation.

1.3 Junctophilin protein family

Junctional membrane complexes between the endoplasmic reticulum and plasma membrane

Among the contacts between the ER and PM, a subset are termed Junctional Membrane Complexes (JMCs). These contacts are stable, and distinct from transient ER-PM contacts such as STIM1-Orai1 interactions in SOCE (Hogan and Rao, 2015). JMCs are found in excitable cells, particularly muscles and neurons, and couple electrical excitation of the PM to ER calcium release. Muscles have specialized structures known as transverse tubules (t-tubules) that are tubular invaginations of the PM (Silverthorn, 2013). T-tubules extend the PM deep into the muscle cell where they make JMCs with the sarcoplasmic reticulum (SR, muscle equivalent of ER). In skeletal muscle, t-tubules are sandwiched between two SR compartments. By electron microscopy, these appear as three compartments in a row and hence are called “triads”. In cardiac muscle, t-tubules are adjacent to only one SR compartment at a time and hence these are called “diads”. Triads and diads are critical for excitation-contraction coupling.

Excitation-contraction coupling

Muscle contraction begins with electrical excitation of the PM (Silverthorn, 2013). In skeletal muscle, this causes the voltage sensing, dihydropyridine sensitive, L-type calcium channel Cav1.1 (known as the dihydropyridine receptor (DHPR) or Cav1.1) to undergo a conformational change. DHPRs, through physical linkage, trigger the opening of Ryanodine Receptor (RyR) calcium channels on the SR surface. RyRs release calcium from SR calcium stores and the calcium binds muscle filaments and allows muscle contraction. In cardiac muscle, DHPRs are not physically linked to RyRs, and activation of RyRs is dependent on entry of extracellular calcium through DHPRs. In skeletal muscle, DHPRs and RyRs localize to triads where the PM and SR

membranes form JMCs, allowing DHPRs and RyRs to physically interact. In cardiac muscle, DHPRs and RyRs localize to diads, where extracellular calcium entering through DHPRs efficiently triggers the opening of nearby RyRs.

The discovery of junctophilins at triad junctions

In the late 1990s, the molecular basis of triad formation was still unclear. Knocking out DHPRs and RyRs in mouse skeletal muscle reduced triad junction frequency, but the remaining triads were structural intact (Franzini-Armstrong et al., 1991; Ikemoto et al., 1997). The SR transmembrane proteins triadin and junctin localize to triads, but hydropathy and topology analysis placed the bulk of both proteins in the SR lumen, making it unlikely that the small cytoplasmic portions could directly interact with the PM (Jones et al., 1995; Knudson et al., 1993). This data suggested that other, yet undiscovered, molecules were the primary structural component of triad junctions.

To identify proteins that might be involved in triad formation, Takeshima and colleagues performed an antibody screen (Takeshima et al., 1998). SR vesicles enriched for junctional membranes were isolated from rabbit skeletal muscle and injected into mice to generate antibodies. These antibodies were then screened against rabbit skeletal muscle cryosections. Among these, an antibody was found that labeled transverse rows corresponding to the location of triad junctions. This antibody was found to bind to a novel protein, which was named junctophilin 1 (JPH1) (Takeshima et al., 2000). Through cross-hybridization with mouse cDNA libraries, two other junctophilins were identified which were named junctophilin 2 (JPH2) and junctophilin 3 (JPH3). A fourth junctophilin, junctophilin 4 (JPH4), was later identified by sequence homology (Nishi et al., 2003).

Subsequent work established that junctophilins are the primary component responsible for the generation of JMCs at triads and diads. Furthermore, junctophilins directly bind PM- and ER-localized calcium channels and ensure their localization to JMCs, enabling efficient trans-membrane signaling. Junctophilins have even been shown to play a role in directly gating RyRs. These functions make junctophilins important in health and disease.

Tissue specificity of junctophilin isotypes

The four junctophilins show different patterns of tissue expression. JPH1 and JPH2 are expressed in both skeletal and cardiac muscle (Ito et al., 2001; Minamisawa et al., 2004; Nishi et al., 2000; Takeshima et al., 2000). JPH1 and JPH2 appear to be expressed at similar levels in skeletal muscle (Ito et al., 2001), and most studies in skeletal muscle have examined both proteins. In contrast, JPH2 appears to be the main isotype in heart muscle, and studies in the heart have mostly focused on JPH2. JPH1 and JPH2 are also expressed in the smooth muscle surrounding arteries, although RT-qPCR suggests that JPH2 is more highly expressed than JPH1 (Pritchard et al., 2019; Saeki et al., 2019). JPH2 mRNA was also found in mouse stomach and lung (Takeshima et al., 2000), consistent with expression of JPH2 in the smooth muscle of these tissues. JPH3 and JPH4 are broadly expressed in neurons of the brain and nervous system (Nishi et al., 2003, 2000; Takeshima et al., 2000). In addition, JPH3 is expressed in pancreatic beta cells (Li et al., 2016) and JPH4 is expressed in T-cells (Woo et al., 2016), both of which are excitable cell types.

Junctophilin structure

Junctophilins have a domain structure that is conserved from *C. elegans* to humans (Garbino et al., 2009). All junctophilins have eight N-terminal MORN (Membrane Occupation

and Recognition Nexus) motifs, which are 14 amino acid motifs with the consensus sequence YxGxWxxGKRHGYG (Takeshima et al., 2000). The first six and last two MORN motifs are separated by a joining region of approximately 150 aa. Following the MORN motifs is a computationally predicted α-helical domain, which averages 70 amino acids in length (Garbino et al., 2009). This is followed by the divergent region, which takes up approximately half the length of the protein. The divergent region has very low conservation between isotypes (for example, between human JPH1 and human JPH2) but has high conservation when comparing the same isotype in different species (for example, between human JPH1 and mouse JPH1) (Garbino et al., 2009). This suggests that the divergent region might be important for the isotype-specific functions of junctophilin, such as tissue-specific binding sites. At the C-terminus of junctophilin is a hydrophobic transmembrane domain.

1.4 Functional studies of junctophilins in muscle

Junctophilins localize to ER-PM membrane contact sites

JPH1 was initially identified at the skeletal muscle triad junction, where the PM and SR membranes form JMCs 10-12 nanometres apart. Electron microscopy with immunogold labeling showed that JPH1 localizes between PM and SR membranes in rabbit skeletal muscle, confirming its localization to JMCs and consistent with a structural role in JMC formation (Takeshima et al., 2000). To dissect the role of individual domains in JPH1 localization, Takeshima and colleauges expressed GFP-tagged truncation constructs in amphibian embryos. Full-length JPH1 and a truncated JPH1 lacking the C-terminal transmembrane domain localize along the plasma membrane. In contrast, constructs lacking MORN 7 and 8, and to a lesser degree MORN 1-6, do not go to the plasma membrane. This evidence suggests that the MORN motifs target JPH1 to the plasma membrane, with the total number of MORN motifs and the presence of specific MORN motifs both being important.

Biochemical studies shed further light on the functions of the MORN motifs. Recombinant rabbit JPH1 lacking the transmembrane domain was purified from *E. coli* and reacted with a microarray of phospholipids (Kakizawa et al., 2008). Purified JPH1 was found to bind phosphorylated forms of phosphatidylinositol (PI), which are enriched on the plasma membrane and in the endocytic pathway, but not phosphatidylcholine (PC), phosphatidylethanolamine (PE), or unphosphorylated PI, which are distributed more broadly across intracellular membranes (Van Meer et al., 2008). Similarly, recombinant human JPH2 lacking the transmembrane domain binds to phosphorylated forms of PI (Bennett et al., 2013). Microarray binding and lipid bilayer assays showed that JPH2 also binds to PS, which is found on the inner leaflet of the plasma membrane. Depletion of PI(4,5)P2 in HeLa cells causes transgenic JPH1 to redistribute from the plasma

membrane to the cytoplasmic ER (Rossi et al., 2019). Taken together, this data suggests that MORN domains directly bind phospholipids to target junctophilin to the plasma membrane.

Although no study has directly shown that the transmembrane domain of junctophilin is inserted in the ER/SR membrane, this conclusion can be drawn from the localization of JPH1 at ER-PM JMCs and the observation that the transmembrane domain is dispensable for plasma membrane localization. Furthermore, as we will discuss next, overexpression of junctophilin generates ER-PM contacts, suggesting that it is able to bind to both plasma membrane and ER simultaneously.

Junctophilins tether ER and PM membranes

Due to its localization at membrane ER-PM membrane contact sites and a domain organization that allows it to simultaneously bind the ER and PM, it was hypothesized that junctophilin may be a membrane tether. The predicted α-helical region of junctophilin would provide a flexible linker 10.5 nm long, enough to span the 10-12 nm JMCs where junctophilins are found (Garbino et al., 2009). Furthermore, transmission electron microscopy showed that recombinant human JPH2 forms an elongated structure approximately 15 nm long and 2 nm wide (Bennett et al., 2013).

Expression of JPH1 in amphibian embryos generated ER-PM contacts as well as unnatural ER stacks visible by electron microscopy, demonstrating that junctophilins are capable of tethering membranes (Takeshima et al., 2000). JPH1 lacking the transmembrane domain did not generate ER-PM contacts, providing further evidence that the transmembrane domain is inserted in the ER membrane. To further study the role of junctophilins in ER-PM contact formation, Takeshima and colleagues generated JPH2 knockout mice and examined JMCs with electron microscopy. While

JPH2 knockout mice were embryonic lethal, cardiac myocytes obtained from JPH2 knockout embryos had fewer 12 nm JMCs (Takeshima et al., 2000), suggesting that JPH2 is required for ER-PM coupling. An inducible heart-specific shRNA knockdown of JPH2 bypassed the embryonic lethality of JPH2 knockout and allowed the study of JPH2 in adult animals (Van Oort et al., 2011). Ventricular myocytes isolated from adult JPH2 knockdown animals were examined by electron microscopy and found to have fewer ER-PM contact sites and more variability in the ER-PM interval at these sites (Van Oort et al., 2011). In the reverse experiment, heart-specific overexpression of JPH2 in mouse increased ER-PM contact site area and also generated convoluted membrane structures visible by electron microscopy (Guo et al., 2014), reminiscent of the ER stacks generated by JPH1 overexpression in amphibian embryos (Takeshima et al., 2000). JPH1 or JPH2 overexpression in HeLa cells increases the proportion of PM-localized ER (Rossi et al., 2019). Altogether, this evidence indicates that junctophilin is an ER-PM tether.

Junctophilins stabilize triad junctions and T-tubules

Junctophilins were originally identified in a screen designed to understand the structural basis of triad junctions. Triads are found in skeletal muscle, where both JPH1 and JPH2 are expressed. Although JPH1 knockout mice die within a day of birth, electron microscopy revealed that newly born JPH1 knockout mice have abnormal SR morphology and fewer triads (Ito et al., 2001). Adenovirus-mediated knockdown of both JPH1 and JPH2 in adult mice disrupted existing triad junctions (Hirata et al., 2006). These results indicated that junctophilins are required for both triad development and stabilization. Although effects on diad formation was not specifically reported in JPH2 knockout embryonic myocytes, the authors observed fewer 12 nm JMCs (Takeshima et al., 2000).

Junctophilins are also involved in the development and stabilization of T-tubules. Immunofluorescent labeling of isolated rat cardiomyocytes shows that the arrival of JPH2 at T-tubules coincides with the start of membrane invagination at P10 (Ziman et al., 2010). Two studies conducted in mice of different genetic backgrounds showed that constitutive heart-specific knockdown of JPH2 impedes T-tubule development (Chen et al., 2013; Reynolds et al., 2013). Knockdown of JPH2 in rat myocytes disrupts the organization of existing T-tubules (Wei et al., 2010), indicating that JPH2 is required for T-tubule maintenance. In a tamoxifen-inducible Gαq mouse heart failure model, where JPH2 undergoes proteolytic cleavage, T-tubules are disrupted (Wu et al., 2014). Junctophilin overexpression has the opposite effect on T-tubule organization. Heart-specific JPH2 overexpression in mouse accelerates T-tubules development (Reynolds et al., 2013). In trans-aortic banded (TAB) mice, which normally exhibit T-tubule disruption, JPH2 overexpression maintains T-tubule organization (Guo et al., 2014). It is unclear if junctophilin's role in T-tubule development and maintenance is mediated by its membrane tethering function or through interactions with other proteins.

Junctophilins bind PM- and SR-localized ion channels and caveolin

At membrane contact sites, in addition to tethering membranes, junctophilins bind to channels and membrane proteins. As much of the evidence was collected by co-immunoprecipitation, in most cases it is not clear if junctophilin directly binds to its targets or is part of larger complexes.

JPH1 was shown to bind RyR1 through co-immunoprecipitation in rabbit skeletal muscle in two separate studies (Golini et al., 2011; Phimister et al., 2007). Cross-linking followed by mass spectrometry showed JPH1 and RyR1 in the same complex with several other proteins (Woo et al.,

2008). Co-immunoprecipitation in mouse skeletal muscle microsomes showed that JPH1 and JPH2 both bind RyR (Nakada et al., 2018). In the mouse heart, where JPH2 is the primary isotype, coimmunoprecipitation showed that JPH2 binds RyR2 (Beavers et al., 2013; Van Oort et al., 2011). The residue E169 in the joining region of JPH2 is involved in this interaction (Beavers et al., 2013). Super-resolution microscopy shows that the majority of junctophilin and RyR molecules are found together. In isolated rat cardiomyocytes, 57% of RyR co-localizes with JPH2, which further increases to 81% when including a 30nm band around JPH2 clusters (Jayasinghe et al., 2012). This was corroborated by dSTORM in rat heart sections, where 60% of RyR co-localizes with JPH2, which further increases to 77% when including a 30nm band around JPH2 clusters . A similar proportion of JPH2 co-localizes with RyR. In rat skeletal muscle sections, dSTORM showed that JPH1 is present throughout the RyR2 distribution while JPH2 is confined to smaller nanodomains within the RyR2 distribution (Jayasinghe et al., 2014).

Junctophilins also bind L-type calcium channels. Golini and colleagues showed that both JPH1 and JPH2 bind DHPR by co-immunoprecipitation in rabbit skeletal muscle (Golini et al., 2011). Through transient transfection of HEK293 cells, they further showed that the interaction between human JPH1 and DHPR is direct, and occurs through JPH1 aa 232-369, the region including MORN 7 and 8. Transient transfection of HEK293 cells did not result in co-immunoprecipitation of human JPH2 and DHPR, suggesting that the interaction between these proteins is indirect. Co-immunoprecipitation using rabbit muscle lysate shows JPH2 aa 216-399 binds DHPR, which covers MORN 7 and 8. Co-immunoprecipitation in mouse skeletal muscle microsomes confirms that JPH1 and JPH2 both bind CaV1.1 (Nakada et al., 2018). The binding region was narrowed down to a 12aa fragment of CaV1.1 that can pull down both JPH1 and JPH2 from microsomes (Nakada et al., 2018).

In addition to RyR and LTCC, junctophilins were found to bind to the plasma membrane-localized ion channels TRPC3 and SK2 and the integral plasma membrane protein caveolin-3. JPH2, but not JPH1, was found to co-immunoprecipitate with TRPC3 from primary mouse skeletal myotubes (Woo et al., 2008). TRPC3 is a non-selective cation channel that allows Ca^{2+} and Na^{+} ions into the cell. Woo and colleagues generated recombinant GST-JPH2 constructs and found that JPH2 aa 143-234 in the joining region was able to find TRPC3, and that binding requires JPH2 residue E227, which is located in the joining region (Woo et al., 2009). Coimmunoprecipitation from mouse heart tissue and H9C2 rat cardiomyoblasts showed that JPH2 binds the small conductance calcium-activated potassium channel SK2 (Fan et al., 2018; Luo et al., 2020). Transient transfection of HEK293 cells and co-immunoprecipitation suggests that this interaction is direct (Fan et al., 2018). GST-JPH2 fusion protein pull down of mouse heart lysate and transfected HEK293 cells suggests that the JPH2 N-terminus interacts with the SK2 C-terminus (Fan et al., 2018; Luo et al., 2020). Coimmunoprecipitation showed that caveolin-3 binds JPH1 and JPH2 in mouse skeletal muscle (Golini et al., 2011) and heart (Minamisawa et al., 2004), respectively. Caveolins are integral membrane proteins involved in the formation of caveolae, 60- to 80-nm flask-shaped infoldings of the plasma membrane (Yang et al., 2020). Several plasma membrane ion channels, including L-type calcium channels, localize to cardiac caveolae (Balijepalli and Kamp, 2008).

Lastly, JPH1 and JPH2 were found to form homo- and heterodimers, which was demonstrated by coimmunoprecipitation in transfected HEK293T cells (Rossi et al., 2019). This interaction occurs via the transmembrane domain, as demonstrated by biomolecular fluorescence complementation in primary rat myotubes, and the joining region, shown by GST-JPH1 and JPH2 fusion protein pulldowns of mouse skeletal microsomes.

Junctophilins facilitate localization of ER- and PM-localized channels

The co-localization of ER- and PM-localized channels is essential for effective crosstalk between channels. Junctophilins are required for the localization of these channels, and the binding of the channels by junctophilin likely plays a role their correct positioning. In C2C12 myotubes, JPH1+JPH2 dual knockdown causes DHPR and RyR localization to change from punctate to diffuse (Golini et al., 2011). Interestingly, RyR localizes to muscle triads in rat cardiomyocytes before JPH2 (Ziman et al., 2010), raising the possibility that junctophilin is only required to maintain RyR localization. In cardiomyocytes from JPH2 heart-specific knockdown mice, there is less co-localization of VGCC and RyR2 (Van Oort et al., 2011). The best evidence demonstrating that junctophilin directs channel localization by binding comes from work by Nakada and colleagues. Corroborating the work by Golini and colleagues, Nakada and colleagues show that JPH1+JPH2 KD in C2C12 myotubes changes CaV1.1 and RyR localization from punctate to diffuse (Nakada et al., 2018). A CaV1.1 point mutant unable to bind JPH1 or JPH2 shows a diffuse localization in GLT myotubes, highlighting the critical role junctophilin binding plays in CaV1.1 localization. Furthermore, expressing a mis-localized JPH1 lacking the transmembrane domain causes mis-localization of CaV1.1 in GLT myotubes and mouse FDB muscle.

Junctophilin is also required for the co-localization of the Na^+/Ca^{2+} exchanger NCX and RyR. Cardiomyocytes from inducible JPH2 heart-specific knockdown mice have reduced NCX and RyR2 co-localization, visualized by super-resolution microscopy (Wang et al., 2014). Lastly, cell surface biotinylation studies suggest that JPH2 is required for SK2 cell surface localization (Fan et al., 2018; Luo et al., 2020).

Junctophilins couple ER- and PM-localized calcium channels

The ER-PM tethering and binding of ion channels by junctophilins allows the positioning of ER- and PM-localized ion channels for efficient inter-membrane coupling. In skeletal muscle, depolarization of the PM causes DHPR, through physical linkage, to trigger opening of RyR to release calcium from SR stores into the cytoplasm and allow muscle filament contraction. In heart muscle, PM depolarizations opens L-type calcium channels and calcium enters the cell, triggering the opening of RyR and releasing additional calcium from the SR. In both skeletal and heart muscle, coupling of PM-localized LTCC and SR-localized RyR is crucial for effective conversion of PM depolarization to SR calcium release to allow muscle contraction, in a process known as excitation-contraction coupling.

Since the discovery of junctophilins, numerous experimental models have shown that junctophilins are essential for excitation-contraction coupling. This was observed in the first study on junctophilins by Takeshima and colleagues. Unlike wild type embryonic cardiomyocytes, which have spontaneous rhythmic cytosolic calcium oscillations that can be visualized by the fluorescent calcium indicator Fluo-3 AM, JPH2 knockouts exhibited random unsynchronized calcium transients (Takeshima et al., 2000). This occurred even in the absences of extracellular calcium, indicating that calcium release from the SR had been uncoupled from calcium entry through LTCC. As JPH2 knockout is embryonic lethal, subsequent studies were performed using JPH2 knockdown models and showed similar results. In cardiomyocytes isolated from inducible heart-specific JPH2 knockdown mice, depolarization stimulates normal calcium influx through LTCC, measured by whole-cell patch clamp, but smaller cytosolic transients, measured by the fluorescent calcium indicator Fluo-4 AM (Van Oort et al., 2011). This indicates that JPH2 does not affect entry of extracellular calcium, but is required for the amplification of this signal by the

release of SR calcium. In cardiomyocytes isolated from a constitutive heart-specific JPH2 knockdown mice, electric field stimulation induces calcium transients, measured by Fluo-4 AM, that rise more slowly and have a smaller amplitude, indicating an uncoupling between depolarization and cytosolic calcium levels (Reynolds et al., 2013). Calcium imaging was also performed in intact hearts loaded with the fluorescent calcium indicator Rhod-2 AM and showed similar results to the isolated cardiomyocytes (Chen et al., 2013). Irregular calcium transients were observed in JPH2 knockdown hearts that were beating autonomously or electrically stimulated, and calcium transients rose more slowly and had smaller amplitudes. In the HL-1 immortalized mouse cardiomyocyte cell line, JPH2 knockdown reduces the amplitude of spontaneous calcium oscillations, measured by Fluo-4 AM (Landstrom et al., 2011). The oscillations in the JPH2 knockdown cells were minimally affected by LTCC activators (BayK and FPL) or a blocker (nifedipine), indicating uncoupling between LTCC and SR calcium release. Lastly, effective calcium-induced calcium release, assessed by voltage-induced cytosolic calcium rise as a percentage of SR calcium capacity, does not occur in mice until P15, which is after JPH2 arrival on P10, further supporting the role for JPH2 in excitation-contraction coupling (Ziman et al., 2010). The same role for junctophilin in excitation-contraction coupling is seen in skeletal muscle. JPH1 knockout mice die within a day of birth, likely due to defective suckling. Skeletal muscle from neonatal JPH1 knockout mice has weaker contractile force when electrically stimulated at low frequency but the same contractile force at tetanus as wild type, indicating that JPH1 is required for efficient excitation-contraction coupling (Ito et al., 2001).

The most compelling evidence comes from Nakada and colleagues. A point mutation in Cav1.1 that prevents binding to JPH1 or JPH2 caused Cav1.1 localization to become more diffuse in GLT myotubes, without affecting Cav1.1 protein level or membrane expression or RyR, JPH1,

or JPH2 localization (Nakada et al., 2018). Fewer myotubes produced calcium transients in response to electric field stimulation, and those that did had smaller amplitudes measured by Fluo-4 AM. These results indicate that junctophilins bind to LTCC to direct their localization to membrane contact sites, thus facilitating coupling of extracellular calcium entry through LTCC and release of SR calcium through RyR. In further support of this, expressing a mis-localized JPH1 lacking its transmembrane domain caused mis-localization of CaV1.1 and reduced calcium amplitude at tetanus, measured by Fluo-4 AM, and reduced contraction strength in mouse FDB muscle.

JPH2 directly gate calcium channels

A growing body of evidence suggests that JPH2 not only tethers membrane and couples ER- and PM-localized channels but also directly gates the RyR calcium channel. In the seminal 2000 paper reporting the discovery of junctophilins, the authors reported that JPH2 knockout mouse embryonic cardiomyocytes exhibit random non-rhythmic calcium transients (Takeshima et al., 2000). These persist even in the absence of extracellular calcium, indicating that they are independent of calcium entry through LTCC. The transients are abolished by dual treatment with caffeine and ryanodine to lock open RyR, demonstrating that the transients are caused by RyR.

Subsequent studies found that JPH2-deficient mice have spontaneous calcium transients more frequently or of greater volume, suggesting mis-regulation of RyR gating. Cardiomyocytes from inducible JPH2 knockdown mouse hearts have more frequent spontaneous calcium release events (Van Oort et al., 2011) and larger calcium transients (Wang et al., 2014) with no change in RyR2 levels. Cardiomyocytes from pseudoknock-in mice with a JPH2 E169K mutation, which decreases JPH2 – RyR2 binding, also have more frequent spontaneous calcium release events

(Beavers et al., 2013). A 25aa JPH2-derived peptide, flanking residue E169, abolishes spontaneous calcium release in permeabilized cardiomyocytes from JPH2 knockdown mice. This suggests that JPH2-binding stabilizes RyR2-mediated SR calcium release, although the authors do not actually show that the 25aa peptide binds RyR2. One counterexample has been reported: wild-type HL-1 cells have random calcium transients in the absence of extracellular calcium while JPH2 knockdown cells do not, with no change to LTCC or RyR2 levels (Landstrom et al., 2011).

The most direct evidence for RyR gating by JPH2 come from *in vitro* single-channel recordings. In these experiments, microsomes are extracted from mouse hearts and reconstituted in planar lipid bilayers. RyR from inducible JPH2 knockdown mouse hearts have higher open probability than RyR from wild-type mice, suggesting that JPH2 prevents RyR opening (Wang et al., 2014). The 25aa JPH2-derived peptide mentioned earlier reduces RyR2 opening probability to wild-type levels, providing further evidence that JPH2-binding controls RyR gating (Beavers et al., 2013).

Future work will be required to determine if JPH1, JPH3, or JPH4 also gate RyR in their respective tissues, and what affects this may have on calcium signaling.

1.5 Functional studies of junctophilins in neurons

JPH3 and JPH4 are broadly expressed in neurons of the brain and nervous system (Nishi et al., 2003, 2000; Takeshima et al., 2000). A growing body of evidence suggest that JPH3 and JPH4 have overlapping roles mediating learning and motor control through the regulation of intracellular calcium signaling in neurons. JPH3 knockout (KO) mice exhibit no apparent abnormalities in learning or memory at 3 months of age but have slight impairments in balance and motor coordination (Nishi et al., 2002). 6- and 9-month old JPH3 KO mice show progressive defects in balance, motor coordination, and neuromuscular strength (Seixas et al., 2012). JPH4 expression in the brain largely overlaps with JPH3 (Kakizawa et al., 2007). 2-month old JPH4 KO mice have balance and motor coordination defects similar to JPH3 KO mice (Kakizawa et al., 2007).

The overlapping expression patterns and similar phenotypes of JPH3 and JPH4 KO mice suggest that these genes have redundant functions. Indeed, JPH3/4 double knockout (JPH DKO) mice exhibit more severe defects in balance and locomotion than JPH3 or JPH4 KO mice (Kakizawa et al., 2007). In addition, JPH3/4 DKO mice also exhibit poor learning and memory and reduced exploratory activity (Moriguchi et al., 2006). JPH DKO mice die 3-4 weeks after birth (Moriguchi et al., 2006). Interestingly, this can be prevented by switching their food from dry pellets to a wet paste, suggesting that they have defects in the circuitry controlling saliva secretion. The molecular basis for these neurological defects may lie in a role for junctophilin in coupling calcium channels to produce slow afterhyperpolarization (sAHP) currents. The depolarization and repolarization phases of an action potential are followed by afterhyperpolarization, where the neuron's membrane potential falls below the normal resting potential. The length of afterhyperpolarization can range from fast (fAHP) to slow (sAHP) and can determine action

potential frequency (Andrade et al., 2012). Purkinje cells obtained from JPH DKO mice have impaired sAHP, an effect also seen with inhibitors of ER-localized RyR calcium channels and PM-localized small conductance calcium-activated potassium (SK) channels (Kakizawa et al., 2007). Importantly, these inhibitors have no effect on the impaired sAHP in JPH DKO Purkinje cells. Although global calcium changes were not detected, these results suggest that junctophilin is required for communication between RyR and SK channels to generate a sAHP current. Supporting this hypothesis, sAHP was rescued in JPH DKO Purkinje cells by the addition of the SK channel enhancer EBIO. This result indicates that SK channels are functional and localized where they can produce a sAHP current, but suggests they lack a calcium source. This calcium could be provided by ER calcium release through RyR, which may normally be linked to SK channels by junctophilin.

JPH DKO mice show a similar impairment of sAHP in hippocampal CA1 neurons (Moriguchi et al., 2006). Inhibitors of PM-localized NMDA receptor cation channels, ER-localized RyR, and PM-localized SK channels impair sAHP in wild-type neurons but have no effect on JPH DKO neurons, suggesting junctophilin is required for communication between these three channels. Super-resolution microscopy shows that junctophilin is required to maintain the co-assembly of PM-localized CaV1.3 voltage-gated calcium channels, RyRs, and PM-localized calcium-activated potassium KCa3.1 channels in hippocampal CA1 neurons, and that disruption of this co-assembly leads to impaired sAHP and more frequent action potentials (Sahu et al., 2019). These results suggest that junctophilin is required to couple PM-localized cation channels (e.g. NMDA receptor, CaV1.3), ER-localized calcium-activated calcium channels (i.e. RyR), and PM-localized calcium-activated potassium channels (e.g. SK channels, KCa3.1) for intracellular communication to link membrane depolarization to sAHP current generation and ultimately

control action potential frequency. Further study is required to determine exactly which channels are associated by junctophilin in each neuron type.

JPH DKO neurons have an abnormal response to input signals, which may be explained by their defect in sAHP. Hippocampal CA1 neurons obtained from JPH DKO mice demonstrate impaired high-frequency-stimulation-induced long-term potentiation (LTP) (Moriguchi et al., 2006). Conjunctive stimulation of two neurons that input on a Purkinje cell normally results in long-term depression (LTD); however, in JPH DKO this instead induces LTP (Kakizawa et al., 2007). Wild-type cells first treated with a SK channel inhibitor to reduce sAHP and then conjunctively stimulated also exhibit LTP, suggesting that the reduced sAHP in JPH DKO animals causes this "reversed LTD". It has been demonstrated that reduced sAHP leads to increased action potential frequency (Sahu et al., 2019), and it is conceivable that in this context a stimulus that normally causes LTD could instead induce LTP. The abnormal LTP and LTD seen in JP DKO mice may explain their impairments in learning, memory, and locomotion, although so far no studies have shown a causative link.

JPH3 KO and JPH DKO mice have no overt changes to brain morphology and normal Purkinje cell excitatory circuitry (Kakizawa et al., 2007; Moriguchi et al., 2006; Nishi et al., 2002). Unlike in muscle, where JPH1 and JPH2 are necessary for formation of skeletal muscle triads or heart muscle dyads, JPH3 KO and JPH DKO mice had no discernible disruption to ER-PM membrane contact sites examined by electron microscopy (Kakizawa et al., 2007; Moriguchi et al., 2006; Nishi et al., 2002) Although these phenotypes have not been examined in JPH4 KO mice, the results from JPH3 KO and JPH DKO mice suggest that in neurons, junctophilin is not a critical component of ER-PM tethers and is more important for channel localization.

These studies support the role of neuronal junctophilins to couple PM- and ER-localized channels for efficient intracellular calcium signaling to produce sAHP currents that are required for regulating action potential frequency. Despite JPH3 and JPH4's broad expression in the brain, detailed studies have only been performed in hippocampal CA1 neurons and cerebellar Purkinje cells. It remains unclear exactly which channels junctophilins couple in each neuron type, as there are multiple channel combinations proposed even within the same neuron type (Moriguchi et al., 2006; Sahu et al., 2019). Furthermore, direct changes to calcium levels in JPH KO mice remain to be shown, although detecting local calcium perturbations may be technically challenging. While it is plausible that decreased sAHP in JPH DKO mice leads to increased action potential frequency causing abnormal LTP/LTD, this has not been definitively shown. It is also unknown if the abnormal LTP/LTD is causative for the neurological defects of JPH DKO mice. A more detailed study of JPH DKO in multiple neuron types will be required to determine if neuronal junctophilins have any cellular roles other than regulating sAHP.

References

Andrade R, Foehring RC, Tzingounis A V. 2012. The calcium-activated slow AHP: Cutting through the Gordian Knot. *Front Cell Neurosci* **6**:1–38. doi:10.3389/fncel.2012.00047

Balijepalli RC, Kamp TJ. 2008. Caveolae, ion channels and cardiac arrhythmias. *Prog Biophys Mol Biol* **98**:149–160. doi:10.1016/j.pbiomolbio.2009.01.012

Beavers DL, Wang W, Ather S, Voigt N, Garbino A, Dixit SS, Landstrom AP, Li N, Wang Q, Olivotto I, Dobrev D, Ackerman MJ, Wehrens XHT. 2013. Mutation E169K in junctophilin-2 causes atrial fibrillation due to impaired RyR2 stabilization. *J Am Coll Cardiol* **62**:2010–2019. doi:10.1016/j.jacc.2013.06.052

Bennett HJ, Davenport JB, Collins RF, Trafford AW, Pinali C, Kitmitto A. 2013. Human junctophilin-2 undergoes a structural rearrangement upon binding PtdIns(3,4,5)P3 and the S101R mutation identified in hypertrophic cardiomyopathy obviates this response. *Biochem J* **456**:205–217. doi:10.1042/BJ20130591

Chen B, Guo A, Zhang C, Chen R, Zhu Y, Hong J, Kutschke W, Zimmerman K, Weiss RM, Zingman L, Anderson ME, Wehrens XHT, Song LS. 2013. Critical roles of junctophilin-2 in T-tubule and excitation-contraction coupling maturation during postnatal development. *Cardiovasc Res* **100**:54–62. doi:10.1093/cvr/cvt180

Chung J, Torta F, Masai K, Lucast L, Czapla H, Tanner LB, Narayanaswamy P, Wenk MR, Nakatsu F, De Camilli P. 2015. PI4P/phosphatidylserine countertransport at ORP5- and ORP8-mediated ER - Plasma membrane contacts. *Science (80-)* **349**:428–432. doi:10.1126/science.aab1370

Fan HK, Luo TX, Zhao WD, Mu YH, Yang Y, Guo WJ, Tu HY, Zhang Q. 2018. Functional interaction of Junctophilin 2 with small- conductance Ca 2+ -activated potassium channel subtype 2(SK2) in mouse cardiac myocytes. *Acta Physiol* **222**. doi:10.1111/apha.12986

Fernández-Chacón R, Königstorfer A, Gerber SH, García J, Matos MF, Stevens CF, Brose N, Rizo J, Rosenmund C, Südhof TC. 2001. Synaptotagmin I functions as a calcium regulator of release probability. *Nature* **410**:41–49. doi:10.1038/35065004

Franzini-Armstrong C, Pincon-Raymond M, Rieger F. 1991. Muscle fibers from dysgenic mouse in vivo lack a surface component of peripheral couplings. *Dev Biol* **146**:364–376. doi:10.1016/0012-1606(91)90238-X

Gallo A, Vannier C, Galli T. 2016. Endoplasmic Reticulum-Plasma Membrane Associations:Structures and Functions. *Annu Rev Cell Dev Biol* **32**:279–301. doi:10.1146/annurev-cellbio-111315-125024

Garbino A, Van Oort RJ, Dixit SS, Landstrom AP, Ackerman MJ, Wehrens XHT. 2009. Molecular evolution of the junctophilin gene family. *Physiol Genomics* **37**:175–186. doi:10.1152/physiolgenomics.00017.2009

Geppert M, Goda Y, Hammer RE, Li C, Rosahl TW, Stevens CF, Südhof TC. 1994. Synaptotagmin I: A major Ca2+ sensor for transmitter release at a central synapse. *Cell* **79**:717–727. doi:10.1016/0092-8674(94)90556-8

Giordano F, Saheki Y, Idevall-Hagren O, Colombo SF, Pirruccello M, Milosevic I, Gracheva EO, Bagriantsev SN, Borgese N, De Camilli P. 2013. PI(4,5)P2-Dependent and Ca2+-Regulated ER-PM interactions mediated by the extended synaptotagmins. *Cell* **153**:1494–1509. doi:10.1016/j.cell.2013.05.026

Golini L, Chouabe C, Berthier C, Cusimano V, Fornaro M, Bonvallet R, Formoso L, Giacomello E, Jacquemond V, Sorrentino V. 2011. Junctophilin 1 and 2 proteins interact with the L-type Ca 2+ channel dihydropyridine receptors (DHPRs) in skeletal muscle. *J Biol Chem* **286**:43717–43725. doi:10.1074/jbc.M111.292755

Guo A, Zhang X, Iyer VR, Chen B, Zhang C, Kutschke WJ, Weiss RM, Franzini-Armstrong C, Song LS. 2014. Overexpression of junctophilin-2 does not enhance baseline function but attenuates heart failure development after cardiac stress. *Proc Natl Acad Sci U S A* **111**:12240–12245. doi:10.1073/pnas.1412729111

Hirata Y, Brotto M, Weisleder N, Chu Y, Lin P, Zhao X, Thornton A, Komazaki S, Takeshima H, Ma J, Pan Z. 2006. Uncoupling store-operated Ca2+ entry and altered Ca2+ release from sarcoplasmic reticulum through silencing of junctophilin genes. *Biophys J* **90**:4418–4427. doi:10.1529/biophysj.105.076570

Hogan PG, Rao A. 2015. Store-operated calcium entry: Mechanisms and modulation. *Biochem Biophys Res Commun* **460**:40–49. doi:10.1016/j.bbrc.2015.02.110

Idevall-Hagren O, Lü A, Xie B, De Camilli P. 2015. Triggered Ca 2+ influx is required for extended synaptotagmin 1-induced ER -plasma membrane tethering . *EMBO J* **34**:2291–2305. doi:10.15252/embj.201591565

Ikemoto T, Komazaki S, Takeshima H, Nishi M, Noda T, Iino M, Endo M. 1997. Functional and morphological features of skeletal muscle from mutant mice lacking both type 1 and type 3 ryanodine receptors. *J Physiol* **501**:305–312. doi:10.1111/j.1469-7793.1997.305bn.x

Ito K, Komazaki S, Sasamoto K, Yoshida M, Nishi M, Kitamura K, Takeshima H. 2001. Deficiency of triad junction and contraction in mutant skeletal muscle lacking junctophilin type 1. *J Cell Biol* **154**:1059–1067. doi:10.1083/jcb.200105040

Jayasinghe ID, Baddeley D, Kong CHT, Wehrens XHT, Cannell MB, Soeller C. 2012. Nanoscale organization of junctophilin-2 and ryanodine receptors within peripheral couplings of rat ventricular cardiomyocytes. *Biophys J* **102**:L19–L21. doi:10.1016/j.bpj.2012.01.034

Jayasinghe ID, Munro M, Baddeley D, Launikonis BS, Soeller C. 2014. Observation of the molecular organization of calcium release sites in fast- and slowtwitch skeletal muscle with nanoscale imaging. *J R Soc Interface* **11**. doi:10.1098/rsif.2014.0570

Jean S, Mikryukov A, Tremblay MG, Baril J, Guillou F, Bellenfant S, Moss T. 2010. Extended-synaptotagmin-2 Mediates FGF receptor endocytosis and ERK activation in vivo. *Dev Cell* **19**:426–439. doi:10.1016/j.devcel.2010.08.007

Jones LR, Zhang L, Sanborn K, Jorgensen AO, Kelley J. 1995. Purification, primary structure, and immunological characterization of the 26-kDa calsequestrin binding protein (junctin) from cardiac junctional sarcoplasmic reticulum. *J Biol Chem* **270**:30787–30796. doi:10.1074/jbc.270.51.30787

Kakizawa S, Kishimoto Y, Hashimoto K, Miyazaki T, Furutani K, Shimizu H, Fukaya M, Nishi M, Sakagami H, Ikeda A, Kondo H, Kano M, Watanabe M, Iino M, Takeshima H. 2007. Junctophilin-mediated channel crosstalk essential for cerebellar synaptic plasticity. *EMBO J* **26**:1924–1933. doi:10.1038/sj.emboj.7601639

Kakizawa S, Moriguchi S, Ikeda A, Iino M, Takeshima H. 2008. Functional crosstalk between cell-surface and intracellular channels mediated by junctophilins essential for neuronal functions. *Cerebellum* **7**:385–391. doi:10.1007/s12311-008-0040-1

Knudson CM, Stang KK, Moomaw CR, Slaughter CA, Campbell KP. 1993. Primary structure and topological analysis of a skeletal muscle-specific junctional sarcoplasmic reticulum glycoprotein (triadin). *J Biol Chem* **268**:12646–12654.

Kopec KO, Alva V, Lupas AN. 2010. Homology of SMP domains to the TULIP superfamily of lipid-binding proteins provides a structural basis for lipid exchange between ER and mitochondria. *Bioinformatics* **26**:1927–1931. doi:10.1093/bioinformatics/btq326

Landstrom AP, Kellen CA, Dixit SS, Van Oort RJ, Garbino A, Weisleder N, Ma J, Wehrens XHT, Ackerman MJ. 2011. Junctophilin-2 expression silencing causes cardiocyte hypertrophy and abnormal intracellular calcium-handling. *Circ Hear Fail* **4**:214–223. doi:10.1161/CIRCHEARTFAILURE.110.958694

Li L, Pan ZF, Huang X, Wu BW, Li T, Kang MX, Ge RS, Hu XY, Zhang YH, Ge LJ, Zhu DY, Wu YL, Lou YJ. 2016. Junctophilin 3 expresses in pancreatic beta cells and is required for glucose-stimulated insulin secretion. *Cell Death Dis* **7**:1–10. doi:10.1038/cddis.2016.179

Luo T, Li L, Peng Y, Xie R, Yan N, Fan H, Zhang Q. 2020. The MORN domain of Junctophilin2 regulates functional interactions with small-conductance Ca2+-activated potassium channel subtype2 (SK2). *BioFactors* 1–11. doi:10.1002/biof.1608

Manford AG, Stefan CJ, Yuan HL, MacGurn JA, Emr SD. 2012. ER-to-Plasma Membrane Tethering Proteins Regulate Cell Signaling and ER Morphology. *Dev Cell* **23**:1129–1140. doi:10.1016/j.devcel.2012.11.004

Min SW, Chang WP, Südhof TC. 2007. E-Syts, a family of membranous Ca2+-sensor proteins with multiple C2 domains. *Proc Natl Acad Sci U S A* **104**:3823–3828. doi:10.1073/pnas.0611725104

Minamisawa S, Oshikawa J, Takeshima H, Hoshijima M, Wang Y, Chien KR, Ishikawa Y, Matsuoka R. 2004. Junctophilin type 2 is associated with caveolin-3 and is down-regulated in the hypertrophic and dilated cardiomyopathies. *Biochem Biophys Res Commun* **325**:852–856. doi:10.1016/j.bbrc.2004.10.107

Moriguchi S, Nishi M, Komazaki S, Sakagami H, Miyazaki T, Masumiya H, Saito SY, Watanabe M, Kondo H, Yawo H, Fukunaga K, Takeshima H. 2006. Functional uncoupling between Ca2+ release and afterhyperpolarization in mutant hippocampal neurons lacking junctophilins. *Proc Natl Acad Sci U S A* **103**:10811–10816. doi:10.1073/pnas.0509863103

Nakada T, Kashihara T, Komatsu M, Kojima K, Takeshita T, Yamada M. 2018. Physical interaction of junctophilin and the CaV1.1 C terminus is crucial for skeletal muscle contraction. *Proc Natl Acad Sci U S A* **115**:4507–4512. doi:10.1073/pnas.1716649115

Nalefski EA, Falke JJ. 1996. The C2 domain calcium-binding motif: Structural and functional diversity. *Protein Sci* **5**:2375–2390. doi:10.1002/pro.5560051201

Nishi M, Mizushima A, Nakagawara K ichi, Takeshima H. 2000. Characterization of human junctophilin subtype genes. *Biochem Biophys Res Commun* **273**:920–927. doi:10.1006/bbrc.2000.3011

Nishi M, Sakagami H, Komazaki S, Kondo H, Takeshima H. 2003. Coexpression of junctophilin type 3 and type 4 in brain. *Mol Brain Res* **118**:102–110. doi:10.1016/S0169-328X(03)00341-3

Nishi M, Takeshima H, Hashimoto K, Kano M, Hashimoto K, Kano M, Kuriyama K, Komazaki S, Shibata S. 2002. Motor discoordination in mutant mice lacking junctophilin type 3. *Biochem Biophys Res Commun* **292**:318–324. doi:10.1006/bbrc.2002.6649

Phillips MJ, Voeltz GK. 2016. Structure and function of ER membrane contact sites with other organelles. *Nat Rev Mol Cell Biol* **17**:69–82. doi:10.1038/nrm.2015.8

Phimister AJ, Lango J, Eun HL, Ernst-Russell MA, Takeshima H, Jianjie M, Allen PD, Pessah IN. 2007. Conformation-dependent stability of junctophilin 1 (JP1) and Ryanodine Receptor Type 1 (RyR1) channel complex is mediated by their hyper-reactive thiols. *J Biol Chem* **282**:8667–8677. doi:10.1074/jbc.M609936200

Porter KR, Palade GE. 1957. STUDIES ON THE ENDOPLASMIC RETICULUM III. Its Form and Distribution in Striated Muscle Cells. *J Biophys Biochem Cytol* **3**:269–300.

Prinz WA, Toulmay A, Balla T. 2020. The functional universe of membrane contact sites. *Nat Rev Mol Cell Biol* **21**:7–24. doi:10.1038/s41580-019-0180-9

Pritchard HAT, Griffin CS, Yamasaki E, Thakore P, Lane C, Greenstein AS, Earley S. 2019. Nanoscale coupling of junctophilin-2 and ryanodine receptors regulates vascular smooth muscle cell contractility. *Proc Natl Acad Sci U S A* **116**:21874–21881. doi:10.1073/pnas.1911304116

Reynolds JO, Chiang DY, Wang W, Beavers DL, Dixit SS, Skapura DG, Landstrom AP, Song LS, Ackerman MJ, Wehrens XHT. 2013. Junctophilin-2 is necessary for T-tubule maturation during mouse heart development. *Cardiovasc Res* **100**:44–53. doi:10.1093/cvr/cvt133

Rossi D, Scarcella AM, Liguori E, Lorenzini S, Pierantozzi E, Kutchukian C, Jacquemond V, Messa M, De Camilli P, Sorrentino V. 2019. Molecular determinants of homo- And heteromeric interactions of Junctophilin-1 at triads in adult skeletal muscle fibers. *Proc Natl Acad Sci U S A* **116**:15716–15724. doi:10.1073/pnas.1820980116

Saeki T, Suzuki Y, Yamamura H, Takeshima H, Imaizumi Y. 2019. A junctophilin-caveolin interaction enables efficient coupling between ryanodine receptors and BKCa channels in the Ca2+ microdomain of vascular smooth muscle. *J Biol Chem* **294**:13093–13105. doi:10.1074/jbc.RA119.008342

Saheki Y, Bian X, Schauder CM, Sawaki Y, Surma MA, Klose C, Pincet F, Reinisch KM, De Camilli P. 2016. Control of plasma membrane lipid homeostasis by the extended synaptotagmins. *Nat Cell Biol* **18**:504–515. doi:10.1038/ncb3339

Sahu G, Wazen RM, Colarusso P, Chen SRW, Zamponi GW, Turner RW. 2019. Junctophilin Proteins Tether a Cav1-RyR2-KCa3.1 Tripartite Complex to Regulate Neuronal Excitability. *Cell Rep* **28**:2427-2442.e6. doi:10.1016/j.celrep.2019.07.075

Schauder CM, Wu X, Saheki Y, Narayanaswamy P, Torta F, Wenk MR, De Camilli P, Reinisch KM. 2014. Structure of a lipid-bound extended synaptotagmin indicates a role in lipid transfer. *Nature* **510**:552–555. doi:10.1038/nature13269

Schulz TA, Creutz CE. 2004. The Tricalbin C2 Domains: Lipid-Binding Properties of a Novel, Synaptotagmin-Like Yeast Protein Family. *Biochemistry* **43**:3987–3995. doi:10.1021/bi036082w

Sclip A, Bacaj T, Giam LR, Südhof TC. 2016. Extended Synaptotagmin (ESyt) triple knock-out mice are viable and fertile without obvious endoplasmic reticulum dysfunction. *PLoS One* **11**:1–17. doi:10.1371/journal.pone.0158295

Seixas AI, Holmes SE, Takeshima H, Pavlovich A, Sachs N, Pruitt JL, Silveira I, Ross CA, Margolis RL, Rudnicki DD. 2012. Loss of junctophilin-3 contributes to huntington disease-like 2 pathogenesis. *Ann Neurol* **71**:245–257. doi:10.1002/ana.22598

Silverthorn DU. 2013. Human Physiology: An Integrated Approach, 6th ed. Pearson.

Südhof TC, Rizo J. 1996. Synaptotagmins: C2-domain proteins that regulate membrane traffic. *Neuron* **17**:379–388. doi:10.1016/S0896-6273(00)80171-3

Takeshima H, Komazaki S, Nishi M, Iino M, Kangawa K. 2000. Junctophilins: A novel family of junctional membrane complex proteins. *Mol Cell* **6**:11–22. doi:10.1016/s1097-2765(00)00003-4

Takeshima H, Shimuta M, Komazaki S, Ohmi K, Nishi M, Uno M, Miyata A, Kangawa K. 1998. Mitsugumin29, a novel synaptophysin family member from the triad junction in skeletal muscle. *Biochem J* **331**:317–322. doi:10.1042/bj3310317

Tremblay MG, Moss T. 2016. Loss of all 3 Extended Synaptotagmins does not affect normal mouse development, viability or fertility. *Cell Cycle* **15**:2360–2366. doi:10.1080/15384101.2016.1203494

Van Meer G, Voelker DR, Feigenson GW. 2008. Membrane lipids: Where they are and how they behave. *Nat Rev Mol Cell Biol* **9**:112–124. doi:10.1038/nrm2330

Van Oort RJ, Garbino A, Wang W, Dixit SS, Landstrom AP, Gaur N, De Almeida AC, Skapura DG, Rudy Y, Burns AR, Ackerman MJ, Wehrens XHT. 2011. Disrupted junctional membrane complexes and hyperactive ryanodine receptors after acute junctophilin knockdown in mice. *Circulation* **123**:979–988. doi:10.1161/CIRCULATIONAHA.110.006437

Wang W, Landstrom AP, Wang Q, Munro ML, Beavers D, Ackerman MJ, Soeller C, Wehrens XHT. 2014. Reduced junctional Na+/Ca2+-exchanger activity contributes to sarcoplasmic reticulum Ca2+ leak in junctophilin-2-deficient mice. *Am J Physiol - Hear Circ Physiol* **307**:H1317–H1326. doi:10.1152/ajpheart.00413.2014

Wei S, Guo A, Chen B, Kutschke W, Xie YP, Zimmerman K, Weiss RM, Anderson ME, Cheng H, Song LS. 2010. T-tubule remodeling during transition from hypertrophy to heart failure. *Circ Res* **107**:520–531. doi:10.1161/CIRCRESAHA.109.212324

Woo JS, Hwang JH, Ko JK, Kim DH, Ma J, Lee EH. 2009. Glutamate at position 227 of junctophilin-2 is involved in binding to TRPC3. *Mol Cell Biochem* **328**:25–32. doi:10.1007/s11010-009-0070-0

Woo JS, Kim DH, Allen PD, Lee EH. 2008. TRPC3-interacting triadic proteins in skeletal muscle. *Biochem J* **411**:399–405. doi:10.1042/BJ20071504

Woo JS, Srikanth S, Nishi M, Ping P, Takeshima H, Gwack Y. 2016. Junctophilin-4, a component of the endoplasmic reticulum-plasma membrane junctions, regulates Ca2+ dynamics in T cells. *Proc Natl Acad Sci U S A* **113**:2662–2767. doi:10.1073/pnas.1524229113

Wu CYC, Chen B, Jiang YP, Jia Z, Martin DW, Liu S, Entcheva E, Song LS, Lin RZ. 2014. Calpain-dependent cleavage of junctophilin-2 and T-tubule remodeling in a mouse model of reversible heart failure. *J Am Heart Assoc* **3**:1–18. doi:10.1161/JAHA.113.000527

Yang W, Geng C, Yang Z, Xu B, Shi W, Yang Y, Tian Y. 2020. Deciphering the roles of caveolin in neurodegenerative diseases: The good, the bad and the importance of context. *Ageing Res Rev* **62**:101116. doi:10.1016/j.arr.2020.101116

Yu H, Liu Y, Gulbranson DR, Paine A, Rathore SS, Shen J. 2016. Extended synaptotagmins are Ca2+-dependent lipid transfer proteins at membrane contact sites. *Proc Natl Acad Sci U S A* **113**:4362–4367. doi:10.1073/pnas.1517259113

Ziman AP, Gómez-Viquez NL, Bloch RJ, Lederer WJ. 2010. Excitation-contraction coupling changes during postnatal cardiac development. *J Mol Cell Cardiol* **48**:379–386. doi:10.1016/j.yjmcc.2009.09.016

Chapter 2:

Differential roles of ER-PM contact sites in axon regeneration

Abstract

The mechanisms underlying axon regeneration in mature neurons are relevant to the understanding of normal nervous system maintenance and for developing therapeutic strategies for injury. Here, I investigate the role of ER-plasma-membrane membrane contact site components using the *C. elegans* mechanosensory neuron axotomy model. I find that individually mutating membrane contact site components often has little effect on axon regeneration – for example, all four *obr* genes must be mutated to significantly hinder axon regeneration – hinting at functional redundancy among membrane contact site components. I show that the *ok2823* mutation, which affects the sole *C. elegans* junctophilin *jph-1*, reduces axon regrowth after injury. Interestingly, *jph-1(ok2823)* also enhances axon-axon fusion, dependent on the fusogen EFF-1. I find that the extended-synaptotagmin ESYT-2 in the axon responds to injury by rapidly condensing into puncta, suggesting that membrane contact sites may undergo restructuring following axon injury. These results suggest that changes to membrane contact sites may be among the cellular processes that occur during axon injury, and highlight a role for the membrane contact site protein junctophilin in the subsequent regeneration process.

Introduction

Axon regeneration after injury is an important and conserved biological process in many animals, involving a large number of genes and pathways (He and Jin, 2016; Mahar and Cavalli, 2018; Tedeschi and Bradke, 2017). Upon axonal injury, distal axon segments degenerate and segments proximal to the cell body remain alive and can in certain cases regenerate (Chen et al., 2007; Mcquarrie and Grafstein, 1973; Neumann and Woolf, 1999). Axon regeneration after injury requires rapid sealing of the damaged plasma membrane (PM) and subsequent formation of growth cones, leading to regrowth and extension from damaged proximal axons. These cellular changes involve numerous molecular pathways, starting with rapid calcium influx at injury sites (Ghosh-Roy et al., 2010; Rishal and Fainzilber, 2014; Wolf et al., 2001), retrograde injury signaling, transcriptional reprogramming to re-structuring of the cytoskeleton and re-organization of the extracellular matrix (ECM) (Blanquie and Bradke, 2018). In the adult mammalian central nervous system (CNS), axon regeneration is limited, due to the combination of a repressive glial environment and a lower intrinsic growth capacity of CNS neurons (He and Jin, 2016). The lack of axonal regrowth after CNS injuries, therefore, impairs functional recovery.

Many approaches have been proposed and tested to promote axon regeneration over the past decades (David and Aguayo, 1981; He and Jin, 2016; Park et al., 2008). Yet, mechanistic understanding of how damaged axons regenerate in a permissive environment remains fragmented. Since the discovery of functional axon regeneration in the nematode *Caenorhabditis elegans* (Yanik et al., 2004), several function-based genetic screens have revealed conserved axon regeneration genes and pathways, notably the highly conserved MAPKKK DLK-1 signaling cascade (Chen et al., 2011; Hammarlund et al., 2009; Nix et al., 2014; Yan et al., 2009). Previous work from our lab reported a distinct set of genes identified from a genetic screen of 654 genes in

mechanosensory axon regeneration (Chen et al., 2011). For example, regulators of microtubule (MT) dynamics play a rate-limiting role in axon regrowth, consistent with findings from other animal models (Bradke et al., 2012; Hur et al., 2012). Additional studies revealed other conserved pathways include the RNA-binding protein CELF/UNC-75 (Chen et al., 2016), the miRNA and piRNA pathway (Kyung Won Kim et al., 2018; Zou et al., 2013), the fusogen EFF-1 (Ghosh-Roy et al., 2010; Neumann et al., 2015), and the apoptotic pathway (Pinan-Lucarre et al., 2012). Importantly, the findings from *C. elegans* were echoed in similar screening in mammalian neurons (Sekine et al., 2018; Zou et al., 2015). These discoveries validate *C. elegans* as a system to investigate previously unexplored pathways to determine if they have roles in axon regeneration.

Membrane contact sites (MCSs) are regions where membranes from two organelles or an organelle and the PM are held together by protein tethers, most of which are conserved from yeast to mammals (Phillips and Voeltz, 2016; Saheki et al., 2016). MCSs can coordinate activities such as calcium entry or lipid transfer between membranes. Calcium entry via voltage-gated calcium channels in the PM is critical for PLM axon regeneration (Ghosh-Roy et al., 2010). Additionally, MCSs between the PM and ER might be involved in lipid addition to the PM during rapid extension of regrowing axons (Hausott and Klimaschewski, 2016).

Here, I examined mutants affecting conserved ER-PM MCS components including junctophilin, extended-synaptotagmin (E-Syt), anoctamins, and OxySterol Binding Proteins (OSBP). I find that most ER-PM MCS components exhibit functional redundancy in axon regeneration. An exception to this is the junctophilin mutant *jph-1(ok2823)*, which enhances axon-axon fusion while at the same time reducing the regrowth of unfused axons. I also show that extended-synaptotagmin ESYT-2 rapidly relocalizes following axonal injury. Together, my

findings highlight the differential roles of ER-PM MCS proteins and provide a genetic framework for a more comprehensive understanding of MCS proteins in axon regeneration.

Materials and Methods

Experimental model

The nematode Caenorhabditis elegans was used as the experimental model for this study. All experiments were performed with hermaphrodite animals; males were used only for crosses. Unless otherwise indicated, all experiments were carried out with L4 stage animals. Strains were maintained under standard conditions on Nematode Growth Media (NGM) plates seeded with *E. coli* OP50 bacteria unless mentioned. Wild type was the N2 Bristol strain (Brenner, 1974). New strains were constructed using standard procedures and all genotypes confirmed by PCR or sequencing. Extrachromosomal array transgenic lines were generated as described (Mello et al., 1991).

Laser microsurgery of axons (axotomy)

We cut PLM axons and quantified the length of regrown axons as previously described (Wu et al., 2007). Briefly, GFP-labeled PLM axons of L4 animals were cut 40 µm anterior to the cell body by a femtosecond laser on a spinning-disk confocal microscope. Animals were recovered onto seeded NGM plates and the regrown axon was imaged 24 hours later on a Zeiss LSM510 or LSM800 confocal microscope.

CRISPR-Cas9 gene editing

We generated the *esyt-2(ju1409)* deletion allele using two CRISPR RNAs (crRNAs): 5'-GGTTTCAGTAATTGTGGGCT-3' and 5'-GTGCACTTACGGGTTGTAGG-3' (Integrated DNA Technologies) targeting upstream of the *esyt-2* start codon and downstream of the *esyt-2* stop codon, respectively. The crRNAs were injected into wild-type hermaphrodites with purified Cas9

(MacroLabs, University of California, Berkeley), trans-activating crRNA (tracrRNA) and *dpy-10* crRNA, as described (Paix et al., 2015). We isolated animals with CRISPR modifications based on dumpy (Dpy) and roller (Rol) phenotypes. We identified *ju1409* as a deletion in *esyt-2* by PCR genotyping with flanking primers YJ12052 5'- TAAAGTAACAGCCGCGCCAA-3' and YJ12053 5'- CGTCCTACTTCTCGTTGCCA-3'.

Confocal imaging with Airyscan

L4 stage animals were immobilized using 2.5 mM levamisole in M9 buffer on 5% agar pads. PLM mechanosensory neuron cell bodies were imaged using a Zeiss LSM800 equipped with Airyscan. Z-stack planes were taken at 0.2 µm intervals in both mKate2 and GFP channels using Airyscan.

Axotomy imaging with MicroPoint laser

L4 stage animals were immobilized using 2.5 mM levamisole in M9 buffer on 5% agar pads. Using a MicroPoint laser on an Andor spinning disk confocal unit (CSU-W1) with Leica DMi8 microscope, laser axotomy was performed on the PLM axon ~45 µm away from the cell body. Images were taken immediately before and immediately after axotomy (0.81 s) with iXon ultra 888 EMCCD camera.

Quantification and statistical analysis

We used Prism (GraphPad Software) for all statistical analysis except for Fisher's exact test, for which we used the online tool QuickCalcs (Graphpad Software). To compare regrowth between experiments with different control means, we normalized each experimental data point

by dividing it by its control means. Statistical tests and sample sizes are indicated in Figures or Figure legends.

Results

To investigate the roles of ER-PM MCS in axon regeneration, I examined mutants affecting conserved ER-PM MCS proteins. Junctophilins are localized to ER-PM contacts in excitable cells, where they couple PM- and ER-localized calcium channels (Landstrom et al., 2014). Junctophilins are characterized by eight N-terminal MORN (Membrane Occupation and Recognition Nexus) repeats that bind to the plasma membrane and a C-terminal transmembrane domain that anchors the protein in the ER. JPH-1 is the sole junctophilin in *C. elegans* (Yoshida et al., 2001) (Figure 1A). I observed that *jph-1(ok2823)* mutants exhibited a significantly increased rate of reconnection or fusion between the regrowing axon and distal fragment (Figure 1B). Axons that did not reconnect in *jph-1* mutants exhibited reduced axon regeneration, compared to controls (Figure 2). As reconnected axons were not measured for regrowth analysis, the reduced regrowth in *jph-1* mutants might be due to an overrepresentation of poorly growing axons. Axon-axon fusion requires the fusogen EFF-1 (Ghosh-Roy et al., 2010; Pérez-Vargas et al., 2014) and a phosphoserine-mediated apoptotic cell engulfment pathway (Neumann et al., 2015). I analyzed *eff-1; jph-1* double mutants and found that the enhanced reconnection in *jph-1* was greatly reduced (Figure 1B). These observations suggest that the mutant JPH-1(ok2823) enhances axon-axon fusion, dependent on *eff-1*.

Extended-synaptotagmins (E-Syt) are a family of proteins containing multiple C2 domains that have been shown to tether the ER to the PM (Giordano et al., 2013) and are implicated in membrane lipid transfer (Saheki et al., 2016; Yu et al., 2016). Mammals have three E-Syts that differ in the number of C2 domains. E-Syt1 contains five tandem C2 domains while E-Syt2 and E-Syt3 contain three C2 domains (Figure 3A). All E-Syts contain a SMP (Synaptotagmin-like Mitochondrial and lipid-binding Protein) domain, which is hypothesized to harbour lipids

(Schauder et al., 2014), and an N-terminal hydrophobic hairpin that anchors the protein in the ER (Giordano et al., 2013).

ESYT-2 is the sole E-Syt in *C. elegans* and has a domain structure that most closely resembles human E-Syt2 and E-Syt3 (Figure 3A). I found that *esyt-2* showed wide expression in the nervous system (Figure 3B). In the mechanosensory neuron cell body, full-length GFP-ESYT-2 showed a punctate pattern, colocalizing with an ER marker PISY-1 (Rolls et al., 2002) at the peripheral ER, suggesting it localizes to ER-PM contact sites (Figure 3C). In uninjured axons, ESYT-2 was distributed intermittently (Figure 4A; top panel). Strikingly, upon axon injury, axonal ESYT-2 condensed into small puncta almost immediately (Figure 4A; lower panels). Axon injury triggers a wave of axonal calcium that starts at the cut site and propagates in both directions along the axon (Ghosh-Roy et al., 2010). I observed that ESYT-2 puncta formation begins near the cut site and rapidly spreads along the axon. Due to the similar timing of the calcium wave and ESYT-2 puncta formation, I speculate that the injury-induced calcium transient triggers ESYT-2 relocalization to axonal ER-PM contact sites. This is consistent with the observation that vertebrate E-Syt1 can localize to ER-PM contact sites following an increase in cytosolic calcium (Giordano et al., 2013; Idevall-Hagren et al., 2015).

To determine if *esyt-2* plays a role in axon regeneration, I generated *esyt-2* null mutants by genome editing (Figure 3A). These mutant animals were indistinguishable from wild-type animals in growth rate, body morphology, and exhibited normal axon development and regrowth (Figure 2). Thus, while ESYT-2 undergoes temporal changes in response to axon injury, it does not appear to be essential for axon regrowth.

The Anoctamin protein family function as tethers at ER-PM contact sites in yeast (Manford et al., 2012; Wolf et al., 2012). C. elegans has two orthologs, ANOH-1 and ANOH-2. ANOH-1 is

expressed in mechanosensory neurons and acts together with the apoptotic factor CED-7 to promote phosphatidylserine exposure in the removal of necrotic cells (Li et al., 2015). *ced-7(0)* reduces PLM axon regrowth (Neumann et al., 2015). However, I found that loss of function in *anoh-1* or *anoh-2*, or the *anoh-1; anoh-2* double mutant, did not affect PLM axon regeneration (Figure 2).

The eukaryotic OSBP and OSBP-related (ORP) family of MCS-localized lipid transfer proteins includes multiple members. ORP5/8 act as tethers at ER-PM MCSs where they mediate PI4P/Phosphatidylserine counter-transport, while OSBP and the other ORPs function at different MCSs (Chung et al., 2015). We tested the four *C. elegans* homologs individually as well as a quadruple mutant. Each *obr* single mutant displayed normal regeneration, and the quadruple mutant displayed a significant decrease in axon regrowth (Figure 2). While the expression pattern and action site of these OBR proteins remain to be determined, our finding is consistent with the known redundancy within the OBR family (Kobuna et al., 2010).

Altogether, the above analysis echoes a recent study in yeast where elimination of multiple MCS components did not impair ER-PM sterol exchange (Quon et al., 2018), highlighting the challenge to tease apart the functional redundancy of MCS proteins in biological processes.

Discussion

ER-PM MCSs play key roles in calcium signaling and lipid transfer, making them candidates to regulate axon regeneration (Gallo et al., 2016). Here, I report that mutating individual ER-PM MCS proteins does not have a strong effect on axon regeneration, likely due to functional redundancy between MCS proteins. I show that an exception is the junctophilin mutant *jph-1(ok2823),* which reduces axon regrowth after injury. Strikingly, *jph-1(ok2823)* also increases regenerative axon-axon fusion. While several mutants have been identified that increase axon regrowth after injury (Chen et al., 2011; K.W. Kim et al., 2018), only axon fusion has been shown to restore function to severed PLM axons (Abay et al., 2017). PLM axon fusion requires the fusogen EFF-1, likely to mediate membrane fusion between the regrowing axon and the severed fragment (Ghosh-Roy et al., 2010; Neumann et al., 2015). The increased axon fusion caused by *jph-1(ok2823)* also requires *eff-1*, suggesting that fusion occurs via the same mechanism as spontaneous axon-axon fusion. The nature of the *jph-1(ok2823)* mutation and how it may enhance axon fusion is explored further in Chapter 3.

While loss of the extended-synaptotagmin *esyt-2* does not affect axon regrowth length, I observed that ESYT-2 rapidly condenses into puncta following axon injury. As E-Syts localize to ER-PM MCSs, this suggests that axon injury may cause MCSs to undergo rapid restructuring. After injury, axons experience a wave of calcium influx that drives microtubule depolarization, cleavage of the submembranous cytoskeletal component spectrin, and ultimately collapse of the plasma membrane at the cut site (Bradke et al., 2012). Due to the similar timescale of calcium wave propagation and ESYT-2 puncta formation, it is conceivable that the calcium influx causes MCS restructuring. However, what role MCS restructuring plays in axon regeneration, if any, is still unclear.

Acknowledgements

I thank my lab members for valuable discussions and Laura Toy for assistance in strain construction. I thank Dr. S Mitani and National Bioresource Project of Japan, and the *Caenorhabditis* Genetics Center (funded by NIH Office of Research Infrastructure Programs P40 OD010440) for strains. This work was supported by NIH R01 grants to YJ, and ADC (NS057317 and NS093588).

Chapter 2, in large part, is a reprint of the material as it appears in Kim KW, Tang NH, Piggott CA, Andrusiak MG, Park S, Zhu M, Kurup N, Cherra SJ, Wu Z, Chisholm AD, Jin Y. 2018. Expanded genetic screening in caenorhabditis elegans identifies new regulators and an inhibitory role for NAD + in axon regeneration. *Elife* 7:e39756. The dissertation author was a co-author of this material.

Figures

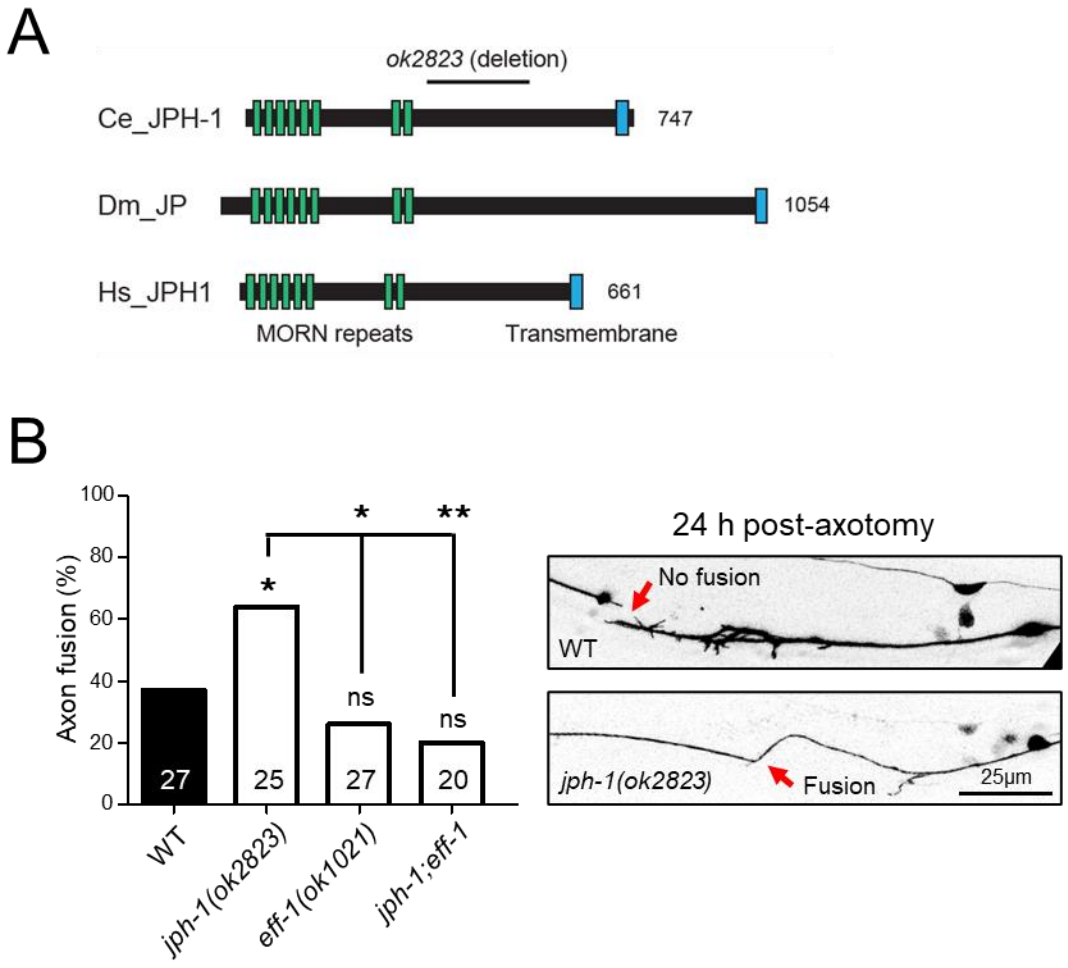

Figure 1. *jph-1(ok2823)* enhances axon fusion after injury
A) Junctophilin-1 protein structure. From top to bottom: *C. elegans* JPH-1 (NP_492193.2), its *Drosophila* ortholog (NP_523525.2), and human ortholog JPH1 (NP_065698.1). Junctophilins contain N-terminal MORN (Membrane Occupation and Recognition Nexus) repeats (green) and a C-terminal transmembrane domain (blue). *C. elegans* deletion allele is indicated above (*ok2823*).
B) Percentage of axons that exhibit fusion between the regrowing axon and distal fragment 24 h post-axotomy. *eff-1(ok1021)* is a loss-of-function mutation. Upper image shows a regrowing axon that has not fused with the distal fragment in a wild-type animal. Lower image shows fusion between the regrowing axon and the distal fragment in a *jph-1(ok2823)* animal. Fisher's exact test. *p<0.05; **p<0.01.

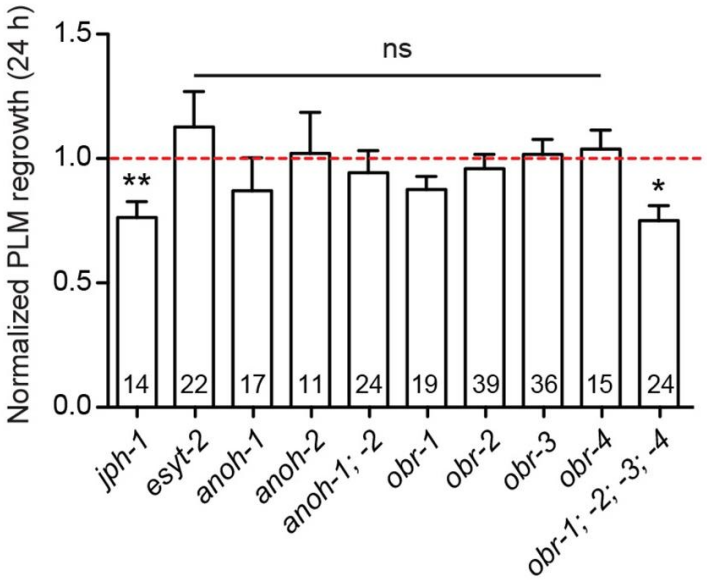

Figure 2. Select ER-PM membrane contact site proteins are required for axon regeneration
Normalized regrowth 24 h post-axotomy in mutants of selected genes encoding ER-PM MCS proteins. Data are shown as mean ± SEM. n, number of animals shown within columns. Student's *t*-test with same day controls. ns, not significant; *p<0.05; **p<0.01.

Figure 3. ESYT-2 localizes to membrane contact sites in neurons

A) E-Syt protein structure. From top to bottom: *C. elegans* ESYT-2 and its human orthologs E-Syt2, E-Syt3, and E-Syt1 (NP_065779.1, NP_114119.2, NP_056107.1, respectively). Amino acid length is indicated to the right of each protein. E-Syt proteins contain N-terminal hydrophobic regions (blue), SMP (Synaptotagmin-like Mitochondrial and lipid-binding Protein) domains (yellow), and C-terminal C2 domains (red). *C. elegans* deletion allele is indicated above (*ju1409*).

B) Confocal images of P*esyt-2*::GFP transcriptional reporter showing widespread expression in the nervous system of L4 stage animals, including in head ganglia, ventral nerve cord, and tail ganglia. Maximum intensity projection.

C) Images of the PLM cell body and surrounding neurites. Left, GFP::PISY-1 ER marker; Middle, mKate2::ESYT-2 driven by the *mec-4* promoter; Right, Image overlays. Images show single slices taken at 1 µm intervals.

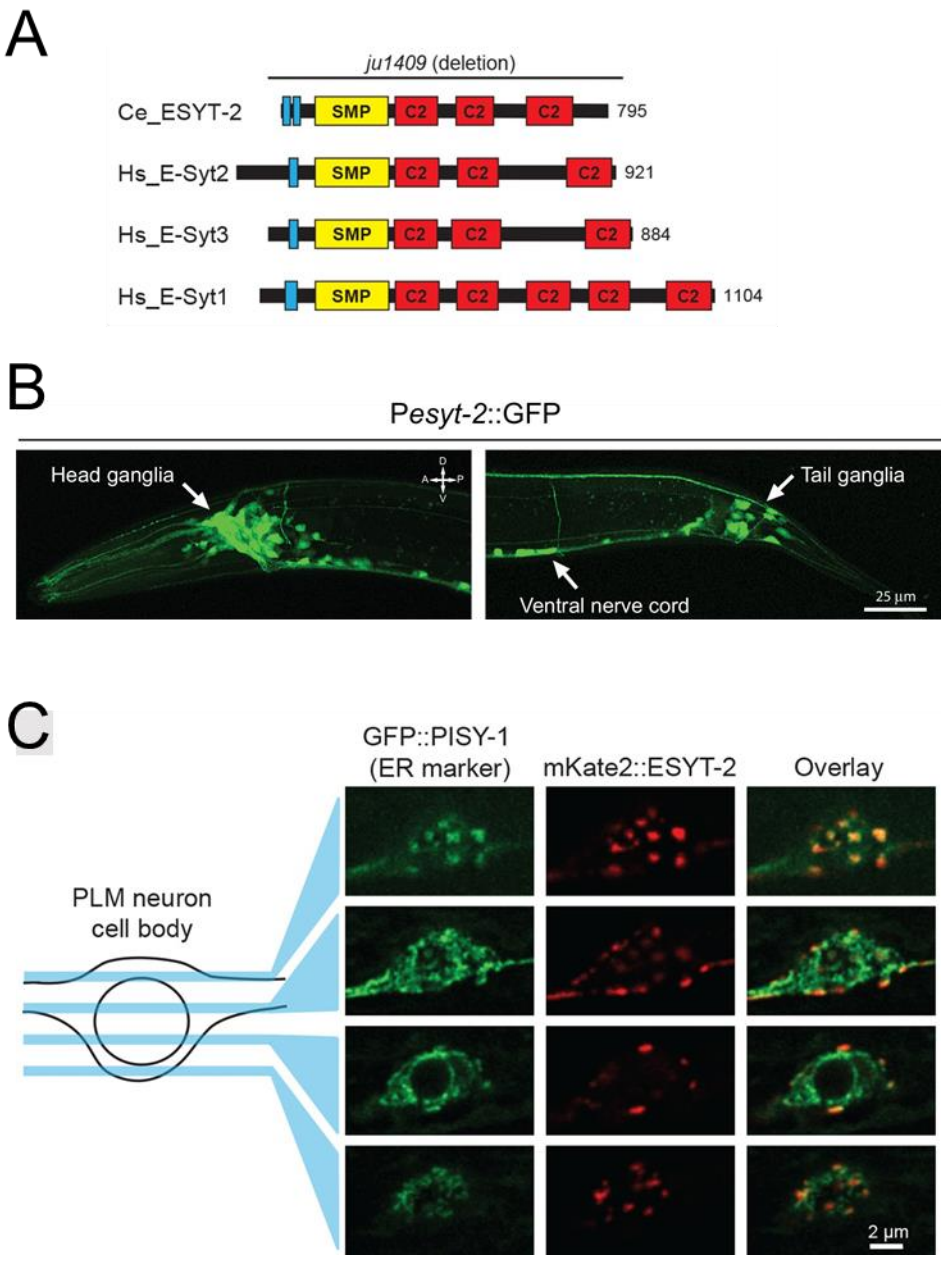
A
ju1409 (deletion)
Ce_ESYT-2
SMP
C2
C2
C2
795
Hs_E-Syt2
SMP
C2
C2
C2
921
Hs_E-Syt3
SMP
C2
C2
C2
884
Hs_E-Syt1
SMP
C2
C2
C2
C2
C2
1104
B
Pesyt-2::GFP
Head ganglia
Tail ganglia
Ventral nerve cord
25 µm
C
GFP::PISY-1
(ER marker)
mKate2::ESYT-2
Overlay
PLM neuron
cell body
2 µm

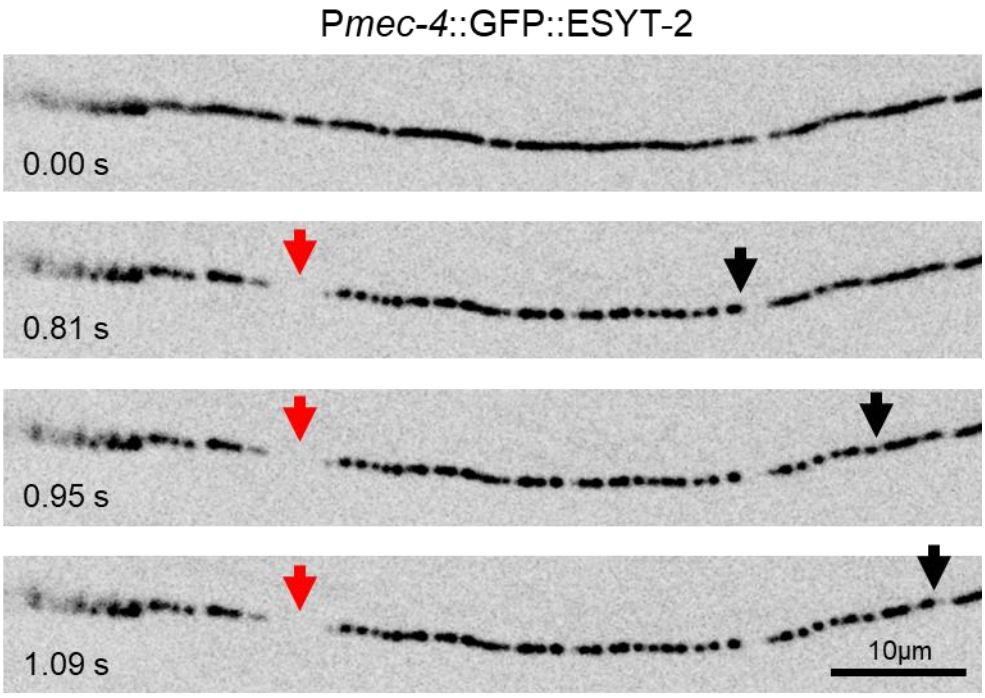

Figure 4. ESYT-2 is sensitive to axon injury
Image sequence of GFP::ESYT-2 in the axon of the PLM neuron before (0.00 s) and immediately after axotomy. Inverted grayscale images. Site of laser axotomy indicated by red arrow; furthest extend of puncta formation indicated by black arrow. The PLM cell body is out of frame to the left of the image.

References

Abay ZC, Wong MYY, Teoh JS, Vijayaraghavan T, Hilliard MA, Neumann B. 2017. Phosphatidylserine save-me signals drive functional recovery of severed axons in Caenorhabditis elegans. *Proc Natl Acad Sci U S A* **114**:E10196–E10205. doi:10.1073/pnas.1703807114

Blanquie O, Bradke F. 2018. Cytoskeleton dynamics in axon regeneration. *Curr Opin Neurobiol* **51**:60–69. doi:10.1016/j.conb.2018.02.024

Bradke F, Fawcett JW, Spira ME. 2012. Assembly of a new growth cone after axotomy: The precursor to axon regeneration. *Nat Rev Neurosci* **13**:183–193. doi:10.1038/nrn3176

Brenner S. 1974. The genetics of Caenorhabditis elegans. *Genetics* **77**:71–94.

Chen L, Liu Z, Zhou B, Wei C, Zhou Y, Rosenfeld MG, Fu XD, Chisholm AD, Jin Y. 2016. CELF RNA binding proteins promote axon regeneration in C. elegans and mammals through alternative splicing of syntaxins. *Elife* **5**:1–26. doi:10.7554/eLife.16072

Chen L, Wang Z, Ghosh-Roy A, Hubert T, Yan D, O'Rourke S, Bowerman B, Wu Z, Jin Y, Chisholm AD. 2011. Axon Regeneration Pathways Identified by Systematic Genetic Screening in C. elegans. *Neuron* **71**:1043–1057. doi:10.1016/j.neuron.2011.07.009

Chen ZL, Yu WM, Strickland S. 2007. Peripheral regeneration. *Annu Rev Neurosci* **30**:209–233. doi:10.1146/annurev.neuro.30.051606.094337

Chung J, Torta F, Masai K, Lucast L, Czapla H, Tanner LB, Narayanaswamy P, Wenk MR, Nakatsu F, De Camilli P. 2015. PI4P/phosphatidylserine countertransport at ORP5- and ORP8-mediated ER - Plasma membrane contacts. *Science (80-)* **349**:428–432. doi:10.1126/science.aab1370

David S, Aguayo A. 1981. Axonal elongation into peripheral nervous system "bridges" after central nervous system injury in adult rats. *Science (80-)* **214**:931–933. doi:10.1126/science.6171034

Gallo A, Vannier C, Galli T. 2016. Endoplasmic Reticulum-Plasma Membrane Associations:Structures and Functions. *Annu Rev Cell Dev Biol* **32**:279–301. doi:10.1146/annurev-cellbio-111315-125024

Ghosh-Roy A, Wu Z, Goncharov A, Jin Y, Chisholm AD. 2010. Calcium and cyclic AMP promote axonal regeneration in Caenorhabditis elegans and require DLK-1 kinase. *J Neurosci* **30**:3175–3183. doi:10.1523/JNEUROSCI.5464-09.2010

Giordano F, Saheki Y, Idevall-Hagren O, Colombo SF, Pirruccello M, Milosevic I, Gracheva EO, Bagriantsev SN, Borgese N, De Camilli P. 2013. PI(4,5)P2-Dependent and Ca2+-Regulated ER-PM interactions mediated by the extended synaptotagmins. *Cell* **153**:1494–1509. doi:10.1016/j.cell.2013.05.026

Hammarlund M, Nix P, Hauth L, Jorgensen EM, Bastiani M. 2009. Axon Regeneration Requires a Conserved MAP Kinase Pathway. *Science (80-)* **323**:802–806. doi:10.1126/science.1165527

Hausott B, Klimaschewski L. 2016. Membrane turnover and receptor trafficking in regenerating axons. *Eur J Neurosci* **43**:309–317. doi:10.1111/ejn.13025

He Z, Jin Y. 2016. Intrinsic Control of Axon Regeneration. *Neuron* **90**:437–451. doi:10.1016/j.neuron.2016.04.022

Hur EM, Saijilafu, Zhou FQ. 2012. Growing the growth cone: Remodeling the cytoskeleton to promote axon regeneration. *Trends Neurosci* **35**:164–174. doi:10.1016/j.tins.2011.11.002

Idevall-Hagren O, Lü A, Xie B, De Camilli P. 2015. Triggered Ca 2+ influx is required for extended synaptotagmin 1-induced ER -plasma membrane tethering . *EMBO J* **34**:2291–2305. doi:10.15252/embj.201591565

Kim Kyung Won, Tang NH, Andrusiak MG, Wu Z, Chisholm AD, Jin Y. 2018. A Neuronal piRNA Pathway Inhibits Axon Regeneration in C. elegans. *Neuron* **97**:511-519.e6. doi:10.1016/j.neuron.2018.01.014

Kim K.W., Tang NH, Piggott CA, Andrusiak MG, Park S, Zhu M, Kurup N, Cherra SJ, Wu Z, Chisholm AD, Jin Y. 2018. Expanded genetic screening in caenorhabditis elegans identifies new regulators and an inhibitory role for NAD^+ in axon regeneration. *Elife* **7**. doi:10.7554/eLife.39756

Kobuna H, Inoue T, Shibata M, Gengyo-Ando K, Yamamoto A, Mitani S, Arai H. 2010. Multivesicular body formation requires OSBP-related proteins and cholesterol. *PLoS Genet* **6**. doi:10.1371/journal.pgen.1001055

Landstrom AP, Beavers DL, Wehrens XHT. 2014. The junctophilin family of proteins: From bench to bedside. *Trends Mol Med* **20**:353–362. doi:10.1016/j.molmed.2014.02.004

Li Z, Venegas V, Nagaoka Y, Morino E, Raghavan P, Audhya A, Nakanishi Y, Zhou Z. 2015. Necrotic Cells Actively Attract Phagocytes through the Collaborative Action of Two Distinct PS-Exposure Mechanisms. *PLoS Genet* **11**:1–26. doi:10.1371/journal.pgen.1005285

Mahar M, Cavalli V. 2018. Intrinsic mechanisms of neuronal axon regeneration. *Nat Rev Neurosci* **19**:323–337. doi:10.1038/s41583-018-0001-8

Manford AG, Stefan CJ, Yuan HL, MacGurn JA, Emr SD. 2012. ER-to-Plasma Membrane Tethering Proteins Regulate Cell Signaling and ER Morphology. *Dev Cell* **23**:1129–1140. doi:10.1016/j.devcel.2012.11.004

Mcquarrie IG, Grafstein B. 1973. Axon Outgrowth Enhanced by a Previous Nerve Injury. *Arch Neurol* **29**:53–55. doi:10.1001/archneur.1973.00490250071008

Mello CC, Kramer JM, Stinchcomb D, Ambros V. 1991. Efficient gene transfer in C.elegans: Extrachromosomal maintenance and integration of transforming sequences. *EMBO J* **10**:3959–3970. doi:10.1002/j.1460-2075.1991.tb04966.x

Neumann B, Coakley S, Giordano-Santini R, Linton C, Lee ES eun., Nakagawa A, Xue D, Hilliard MA. 2015. EFF-1-mediated regenerative axonal fusion requires components of the apoptotic pathway. *Nature* **517**:219–222. doi:10.1038/nature14102

Neumann S, Woolf CJ. 1999. Regeneration of dorsal column fibers into and beyond the lesion site following adult spinal cord injury. *Neuron* **23**:83–91. doi:10.1016/S0896-6273(00)80755-2

Nix P, Hammarlund M, Hauth L, Lachnit M, Jorgensen EM, Bastiani M. 2014. Axon regeneration genes identified by RNAi screening in C. elegans. *J Neurosci* **34**:629–645. doi:10.1523/JNEUROSCI.3859-13.2014

Paix A, Folkmann A, Rasoloson D, Seydoux G. 2015. High efficiency, homology-directed genome editing in Caenorhabditis elegans using CRISPR-Cas9ribonucleoprotein complexes. *Genetics* **201**:47–54. doi:10.1534/genetics.115.179382

Park KK, Liu K, Hu Y, Smith PD, Wang C, Cai B, Xu B, Connolly L, Kramvis I, Sahin M, He Z. 2008. Promoting Axon Regeneration in the Adult CNS by Modulation of the PTEN/mTOR Pathway. *Science (80-)* **322**:963–966. doi:10.1126/science.1161566

Pérez-Vargas J, Krey T, Valansi C, Avinoam O, Haouz A, Jamin M, Raveh-Barak H, Podbilewicz B, Rey FA. 2014. Structural basis of eukaryotic cell-cell fusion. *Cell* **157**:407–419. doi:10.1016/j.cell.2014.02.020

Phillips MJ, Voeltz GK. 2016. Structure and function of ER membrane contact sites with other organelles. *Nat Rev Mol Cell Biol* **17**:69–82. doi:10.1038/nrm.2015.8

Pinan-Lucarre B, Gabel C V., Reina CP, Hulme SE, Shevkoplyas SS, Slone RD, Xue J, Qiao Y, Weisberg S, Roodhouse K, Sun L, Whitesides GM, Samuel A, Driscoll M. 2012. The core apoptotic executioner proteins CED-3 and CED-4 promote initiation of neuronal regeneration in caenorhabditis elegans. *PLoS Biol* **10**. doi:10.1371/journal.pbio.1001331

Quon E, Sere YY, Chauhan N, Johansen J, Sullivan DP, Dittman JS, Rice WJ, Chan RB, Di Paolo G, Beh CT, Menon AK. 2018. Endoplasmic reticulum-plasma membrane contact sites integrate sterol and phospholipid regulation, PLoS Biology. doi:10.1371/journal.pbio.2003864

Rishal I, Fainzilber M. 2014. Axon-soma communication in neuronal injury. *Nat Rev Neurosci* **15**:32–42. doi:10.1038/nrn3609

Rolls MM, Hall DH, Victor M, Stelzer EH, Rapoport TA. 2002. Targeting of Rough Endoplasmic Reticulum Membrane Proteins and Ribosomes in Invertebrate Neurons. *Mol Biol Cell* **13**:1778–1791. doi:10.1091/mbc.01

Saheki Y, Bian X, Schauder CM, Sawaki Y, Surma MA, Klose C, Pincet F, Reinisch KM, De Camilli P. 2016. Control of plasma membrane lipid homeostasis by the extended synaptotagmins. *Nat Cell Biol* **18**:504–515. doi:10.1038/ncb3339

Schauder CM, Wu X, Saheki Y, Narayanaswamy P, Torta F, Wenk MR, De Camilli P, Reinisch KM. 2014. Structure of a lipid-bound extended synaptotagmin indicates a role in lipid transfer. *Nature* **510**:552–555. doi:10.1038/nature13269

Sekine Y, Lin-Moore A, Chenette DM, Wang X, Jiang Z, Cafferty WB, Hammarlund M, Strittmatter SM. 2018. Functional Genome-wide Screen Identifies Pathways Restricting Central Nervous System Axonal Regeneration. *Cell Rep* **23**:415–428. doi:10.1016/j.celrep.2018.03.058

Tedeschi A, Bradke F. 2017. Spatial and temporal arrangement of neuronal intrinsic and extrinsic mechanisms controlling axon regeneration. *Curr Opin Neurobiol* **42**:118–127. doi:10.1016/j.conb.2016.12.005

Wolf JA, Stys PK, Lusardi T, Meaney D, Smith DH. 2001. Traumatic axonal injury induces calcium influx modulated by tetrodotoxin-sensitive sodium channels. *J Neurosci* **21**:1923–1930. doi:10.1523/JNEUROSCI.21-06-01923.2001

Wolf W, Kilic A, Schrul B, Lorenz H, Schwappach B, Seedorf M. 2012. Yeast Ist2 recruits the endoplasmic reticulum to the plasma membrane and creates a ribosome-free membrane microcompartment. *PLoS One* **7**. doi:10.1371/journal.pone.0039703

Wu Z, Ghosh-Roy A, Yanik MF, Zhang JZ, Jin Y, Chisholm AD. 2007. Caenorhabditis elegans neuronal regeneration is influenced by life stage, ephrin signaling, and synaptic branching. *Proc Natl Acad Sci U S A* **104**:15132–15137. doi:10.1073/pnas.0707001104

Yan D, Wu Z, Chisholm AD, Jin Y. 2009. The DLK-1 Kinase Promotes mRNA Stability and Local Translation in C. elegans Synapses and Axon Regeneration. *Cell* **138**:1005–1018. doi:10.1016/j.cell.2009.06.023

Yanik MF, Cinar H, Cinar HN, Chisholm AD, Jin Y, Ben-Yakar A. 2004. Functional regeneration after laser axotomy. *Nature* **432**:822. doi:10.1038/432822a

Yoshida M, Sugimoto A, Ohshima Y, Takeshima H. 2001. Important role of junctophilin in nematode motor function. *Biochem Biophys Res Commun* **289**:234–239. doi:10.1006/bbrc.2001.5951

Yu H, Liu Y, Gulbranson DR, Paine A, Rathore SS, Shen J. 2016. Extended synaptotagmins are Ca2+-dependent lipid transfer proteins at membrane contact sites. *Proc Natl Acad Sci U S A* **113**:4362–4367. doi:10.1073/pnas.1517259113

Zou Y, Chiu H, Zinovyeva A, Ambros V, Chuang C-F, Chang C. 2013. Developmental Decline in Neuronal Regeneration by the Progressive Change of Two Intrinsic Timers. *Science (80-)* **340**:372–376. doi:10.1126/science.1231321

Zou Y, Stagi M, Wang X, Yigitkanli K, Siegel CS, Nakatsu F, Cafferty WBJ, Strittmatter SM. 2015. Gene-silencing screen for mammalian axon regeneration identifies Inpp5f (Sac2) as an endogenous suppressor of repair after spinal cord injury. *J Neurosci* **35**:10429–10439. doi:10.1523/JNEUROSCI.1718-15.2015

Chapter 3:

Caenorhabditis elegans junctophilin has tissue-specific functions and regulates neurotransmission with extended-synaptotagmin

Abstract

The junctophilin family of proteins tether together plasma membrane (PM) and endoplasmic reticulum (ER) membranes, and couple PM- and ER-localized calcium channels. Understanding in vivo functions of junctophilins is of great interest for dissecting the physiological roles of ER-PM contact sites. Here, we show that the sole *C. elegans* junctophilin JPH-1 localizes to discrete membrane contact sites in neurons and muscles and has important tissue-specific functions. *jph-1* null mutants display slow growth and development due to weaker contraction of pharyngeal muscles, leading to reduced feeding. In the body wall muscle, JPH-1 co-localizes with the PM-localized EGL-19 voltage-gated calcium channel and ER-localized UNC-68/RyR calcium channel, and is required for animal movement. We also find an unexpected cell non-autonomous effect of *jph-1* in axon regrowth after injury. In neurons, JPH-1 co-localizes with the membrane contact site protein Extended-SYnaptoTagmin 2 (ESYT-2) and modulates neurotransmission. Interestingly, *jph-1* and *esyt-2* null mutants display mutual suppression in their response to aldicarb, suggesting that JPH-1 and ESYT-1 have antagonistic roles in neuromuscular synaptic transmission. Our genetic double mutant analysis also reveals that *jph-1* functions in overlapping pathways with two PM-localized voltage-gated calcium channels, *egl-19* and *unc-2*, and *unc-68*/RyR for animal health and development. Finally, we show that *unc-68*/RyR is required for JPH-1 localization to ER-PM puncta. Our data demonstrate important roles for junctophilin in cellular physiology, and also provide insights into how junctophilin functions together with other calcium channels in vivo.

Introduction

Membrane contact sites (MCSs) are regions of close contact, generally within 10 to 30 nm between organelles or between an organelle and the plasma membrane (PM). MCSs were first described between the endoplasmic reticulum (ER) and PM in muscle cells by electron microscopy over 60 years ago (Porter and Palade, 1957). MCSs have now been found for most organelles in many organisms (Lang et al., 2015; Valm et al., 2017). MCSs are maintained by protein tethers that bind to opposing membranes simultaneously and hold them in close proximity. Different types of MCSs are organized by distinct protein tethers, many of which are conserved from yeast to mammals (Phillips and Voeltz, 2016). Recent studies have begun to uncover their functions. For example, oxysterol-binding proteins (OSBPs) facilitate exchange of PM-localized phosphatidylinositol 4-phosphate (PI4P) for ER-localized cholesterol (Mesmin et al., 2013), and binding of ER-localized calcium sensor Stim1 to PM-localized calcium channel Orai1 triggers the entry of extracellular calcium to the ER to replenish calcium stores (Hirve et al., 2018). Genetic analysis suggests many MCS tethering proteins act redundantly. For example, studies of ER-PM contact sites in yeast showed that full separation of the ER from the PM is only achieved when six genes encoding MCS proteins are deleted (Manford et al., 2012). Similarly, in *C. elegans*, enlarged lysosomes and endosomes were observed only when knocking out all four *obr* genes encoding OSBP homologs (Kobuna et al., 2010). It is thus necessary to identify new experimental models or paradigms to tease apart the functions of individual MCS proteins and to dissect their interaction network *in vivo*.

The junctophilin (JPH) family of proteins were first identified based on their localization to muscle ER-PM contact sites in a screen using monoclonal antibodies raised against ER vesicles enriched for ER-PM junctions(Takeshima et al., 2000). Junctophilins are characterized by a N-

terminal domain consisting of eight membrane occupation and recognition nexus (MORN) motifs, which bind to the PM, and a C-terminal transmembrane domain, which anchors the protein to the ER. Mammals have four junctophilins (JPH1 through 4) that are differentially expressed in excitable cells. JPH1 and JPH2 are expressed in skeletal and cardiac muscle (Nishi et al., 2000; Takeshima et al., 2000) and the smooth muscle surrounding arteries (Pritchard et al., 2019; Saeki et al., 2019). JPH3 and JPH4 are broadly expressed in neurons of the brain and many parts of the nervous system (Nishi et al., 2003, 2000; Takeshima et al., 2000). Studies of genetic knockout mice have provided some evidence for their functions. Cardiomyocytes from JPH2 knockout mice have fewer ER-PM contacts, and skeletal muscle from JPH1 knockout mice have abnormal ER morphology and fewer ER-PM contacts (Ito et al., 2001; Takeshima et al., 2000). In addition to tethering together ER and PM membranes, junctophilins bind to ER- and PM-localized calcium channels and facilitate their co-localization at ER-PM contact sites in mouse cardiomyocytes, skeletal muscle, and cultured hippocampal neurons (Nakada et al., 2018; Sahu et al., 2019; Van Oort et al., 2011). Junctophilin-mediated ER-PM coupling is reported to promote efficient excitation-contraction in heart and skeletal muscle (Ito et al., 2001; Nakada et al., 2018; Takeshima et al., 2000; Van Oort et al., 2011) and regulate action potential frequency in neurons (Kakizawa et al., 2007; Moriguchi et al., 2006; Sahu et al., 2019). Unlike mammals, invertebrates have a single junctophilin (Garbino et al., 2009). In *D. melanogaster*, the sole junctophilin was shown to have roles in muscle contraction and neural development (Calpena et al., 2018).

C. elegans has a single junctophilin gene named *jph-1* (Garbino et al., 2009; Yoshida et al., 2001). Here we show that JPH-1 protein localizes to punctate structures in muscles and neurons. In muscles, JPH-1 puncta co-localize with the ER-localized UNC-68/RyR calcium channel and PM-localized EGL-19/Cav1 calcium channel. In neurons JPH-1 puncta co-localize with the ER-

PM contact site protein extended-synaptotagmin 2 (ESYT-2). Through characterization of *jph-1* null mutants and tissue-specific rescue experiments, we defined tissue-specific roles of *jph-1*. In the pharynx muscle, *jph-1* is required for the pumping that drives animal feeding and contributes to animal growth. In the body wall muscle, *jph-1* is required for animal movement. We observed a cell non-autonomous effect of *jph-1* in axon regeneration after injury. Additionally, *jph-1* modulates synaptic transmission, and can balance the effects of *esyt-2*. Genetic double mutant analyses reveal differential interactions between *jph-1* and the ER-localized *unc-68*/RyR calcium channel and two PM-localized voltage-gated calcium channels (VGCCs) for animal development and health. Lastly, we show that precise localization of JPH-1 in both neurons and muscles depends on *unc-68*. These data support critical roles of junctophilin in cellular function and animal development.

Materials and Methods

C. elegans genetics

Wild-type *C. elegans* is the N2 Bristol variant (Brenner, 1974). Strains were maintained under standard conditions on Nematode Growth Media (NGM) plates seeded with *E. coli* OP50 bacteria. New strains were constructed using standard procedures, based on a combination of visual identification of phenotypes, such as uncoordinated (Unc) movement, and genotyping for specific alleles. Strains and primers for genotyping are shown in the reagents tables (**Tables 1, 4-6**).

Molecular biology and transgenesis

We cloned *jph-1* cDNAs from wild-type N2 mRNAs, first using primers YJ12558 5'-GACGTAGGTGTGTCAGCAG-3' and YJ12559 5'- CCTGAGGAGAAGTGTGTCTG-3' in the 5'UTR and 3'UTR of *jph-1,* followed by a second round of amplification using primers YJ12560 5′-ATGAATGGAGGCAGATTTGAC-3′ and YJ12561 5'-CTACGAAGAAGACTTCTTCTTCTTC-3′ targeting the start and stop codons. We obtained two amplified products, which were cloned into pCR8 vectors. Sanger sequencing analysis of these clones revealed a 2.2 kb cDNA encoding JPH-1 isoform A, and a 2.4 kb cDNA encoding JPH-1 isoform B. The coding region of JPH-1B was then amplified using primers YJ12560 5′-ATGAATGGAGGCAGATTTGAC-3′ and YJ12562 5′-CTAATATGTGAGGGTGTGTACCG-3′ and cloned into a pCR8 vector. The 4.5 kb *jph-1* promoter was amplified from wild-type genomic DNA using the primers YJ12563 5′-TGTTCTGCCATTACCAGCCCG-3′ and YJ12564 5′- TTCCCATTTGCCGTACTGCTG -3′. All expression constructs were generated either by Gateway recombination (Invitrogen / Thermo Fisher

Scientific), Gibson assembly (New England Biolabs), or restriction enzyme digest and ligation. All expression clones were sequenced to ensure sequence fidelity.

We generated transgenic lines by microinjection, as described (Mello et al., 1991). Plasmids, fosmids, co-injection markers, and injection concentrations are listed in the reagents tables (**Tables 2,3**).

Single-copy insertion transgenes with *ju* designation were generated on Chromosome IV at cxTi10882, following a previously published protocol (Andrusiak et al., 2019). Briefly, we injected N2 hermaphrodites with four plasmids, one containing GFP-cDNA flanked by homology arms and expressing a hygromycin resistance gene (HygR), pCZGY2750 expressing Cas9 and an sgRNA targeting cxTi10882, and pCFJ90 Pmyo-2-mCherry (Addgene plasmid 19327) and pCFJ104 Pmyo-3-mCherry (Addgene plasmid 19328)(Frøkjær-Jensen et al., 2008) as co-injection markers. F1 animals from injected P0 parents were treated with hygromycin (Hyg). Among the survivors, we looked for the absence of co-injections markers to identify animals with genomic insertion, which was further verified by PCR genotyping using primers YJ10503, YJ10504, and YJ10686 (wild type 562 bp, insertion 744 bp). Single-copy insertion transgene *nuTi144* was generated by using a modified Mos1 transposon, following a previously published protocol (Frøkjær-Jensen et al., 2014).

CRISPR-Cas9 gene editing

We generated the *jph-1(ju1683)* and *jph-1(ju1684)* deletion alleles using two CRISPR RNAs (crRNAs): 5'-CCGTCCGGTAACACCTATCA-3' and 5'-ACGACGTTGACCAGCAAGAC-3' (Integrated DNA Technologies) targeting *jph-1* exon 1 and exon 9, respectively. The crRNAs were injected into wild-type hermaphrodites with purified Cas9

(MacroLabs, University of California, Berkeley), trans-activating crRNA (tracrRNA) and *dpy-10* crRNA, as described (Paix et al., 2015). We selected small and slow-growing Unc animals resembling *jph-1(ok2823)* mutants, as we were unable to isolate animals based on Dpy or Rol phenotypes, possibly because the *jph-1* crRNA was more efficient than the *dpy-10* crRNA. We identified *ju1683* and *ju1684* as deletions in *jph-1* by PCR genotyping with flanking primers YJ12565 5'-GACGACGGCGGAACCTATG-3' and YJ12566 5'-TCAGGTACGTTCTAGTCGGT-3'.

GFP11 knock-in alleles *unc-68(nu664)* and *egl-19(nu674)* were generated by injecting wild-type hermaphrodites with 75 ng/µl pDD162 expressing Cas9, 36 ng/µl pRB1017-derived guide RNA, and 75ng/ul of a PCR product of 7 copies of GFP11 flanked by 1 kb of wild-type sequence 5' and 3' of the cut site. Guide RNAs were selected using the CRISPR guide RNA selection tool (http://genome.sfu.ca/crispr/). A gRNA targeting *unc-58* (pGW28) 36 ng/µl and repair oligo (AF-JA-76) were also injected as a co-conversion marker (El Mouridi et al., 2017).

Animal growth assessment

Adult hermaphrodite animals were placed on seeded NGM plates and allowed to lay eggs for two hours, after which they were removed. The plates were kept at 20°C and observed daily to determine the time it took the offspring to reach the fourth larval (L4) stage.

Brood size assay

L4 hermaphrodite animals were individually placed on seeded NGM plates and moved to new plates daily. Two days after a parent animal was placed on a plate, the number of hatched

offspring were counted. This was continued until parent animals laid no more eggs or died. The number of hatched offspring produced per parent animal was totaled to calculate brood size.

Fluorescence microscopy

Animals were immobilized in a drop of M9 solution with or without 30 mM muscimol or 10 mM levamisole on a 4% agar pad or 10% agarose pad. Most confocal fluorescence images were collected using a Zeiss LSM800 confocal microscope with Z-stacks taken at 0.5 or 1 µm intervals between planes for most images, with the exception of 0.21 µm intervals for GFP::JPH-1A in *unc-68(0)* (**Figure 16A,B**). P*jph-1*-GFP in the head and tail (**Figure 8A**) were imaged using a Zeiss LSM710 confocal microscope, and GFP::JPH-1A in the PLM neuron (**Figure 13B**) was imaged using an Andor spinning disk confocal unit (CSU-W1) with a Leica DMi8 microscope. All confocal fluorescence images were taken at 63x magnification. Maximum intensity projections were prepared using Fiji (ImageJ).

Images of GFP-labeled touch neurons [P*mec-7*-GFP(*muIs32*)] in wild-type and *jph-1(0)* animals were taken on a Zeiss Axio Imager A2 compound scope at 10x magnification under identical settings.

Brightfield microscopy

Images depicting gross body morphology (**Figure 5C**) were taken by immobilizing animals in a drop of M9 solution on a 10% agarose pad and imaging on a Leica DMi8 microscope under brightfield settings at 10x magnification with an Andor iXon Ultra camera. Images depicting

animal movement crawling on NGM petri plates (**Figure 10A**) were taken on a Zeiss M2 stereodissecting microscope with a Nikon DS-Qi1Mc camera.

Pharyngeal pumping assays

To count pumping rate, day-1 adult animals on seeded plates were observed through dissection stereomicroscopes. We counted the number of grinder movements in 20 seconds twice per animal and took the average. Counting was done while animals were on the OP50 bacterial lawn to prevent variations in pumping rate caused by food availability.

To measure pumping strength, we adapted a published protocol that used serotonin to stimulate pumping in immobilized animals (Trojanowski and Fang-Yen, 2015). We prepared 8% agarose pads with 8mM serotonin (H7752, Sigma Aldrich), placed animals in an M9 drop on the pad, and immediately placed a cover slip on top. We began imaging when animals started pumping (about 0-10 minutes after animals were placed in the M9 drop). Imaging was performed on a Leica DMi8 microscope at 40x magnification. 20 second videos were taken at 100 ms/frame for a total of 200 frames per animal. Videos were then analyzed in Fiji (ImageJ). The distance from the grinder to an arbitrary point on the pharyngeal lumen was measured in the frame immediately preceding pump initiation (**Figure 9B, left image**). The distance from the grinder to the same point was measured in the frame when the grinder had moved to its fullest extent (**Figure 9B, right image**). The difference between these two measurements is the distance moved by the grinder in one pump. We took the average of the first five pumps in each video, although in three instances wild-type animals only pumped three or four times during the video. The distance moved by the

grinder was divided by the length of the pharynx (**Figure 9B, left image**) to normalize to animal size.

Thrashing assay

Individual L4 animals were placed in 1 µl drops of M9 on a glass dissection plate. We counted the number of thrashes performed by the animal in one minute. We considered a single thrash to be one sufficiently large movement of the animal's head or tail back and forth, with the head or tail not necessarily crossing the centre of mass.

Aldicarb and levamisole assays

To test aldicarb sensitivity, 15 day-1 adult animals were transferred to fresh plates containing 0.5 mM or 1 mM aldicarb. Animals were scored for paralysis every 30 minutes by gently touching the animal with a platinum wire. For levamisole sensitivity, 15 day-1 adult animals were transferred to fresh plates containing 1 mM levamisole. Animals were scored for paralysis every 15 minutes by gently touching the animal with a platinum wire. Final sample size for each assay was 13-15 animals due to some animals crawling off the plate. Drug sensitivity was quantified from three independent experiments.

Laser axotomy of PLM axons

We cut PLM axons and quantified the length of regrown axons as previously described (Wu et al., 2007). Briefly, GFP-labeled PLM axons [P*mec-7*-GFP(*muIs32*)] of L4 animals were

cut 40 µm anterior to the cell body by a femtosecond laser on a spinning-disk confocal microscope. Animals were recovered onto seeded NGM plates and the regrown axon was imaged 24 hours later on a Zeiss LSM510 or LSM800 confocal microscope.

Statistical analysis

We used Prism (GraphPad Software) for all statistical analysis except for Fisher's exact test, for which we used the online tool QuickCalcs (Graphpad Software). To compare regrowth between experiments with different control means, we normalized each experimental data point by dividing it by its control means. Statistical tests and sample sizes are indicated in Figures or Figure legends.

Results

jph-1 expresses two isoforms

A previous study described a *jph-1* cDNA that encodes a 747 amino acid protein (Yoshida et al., 2001). In the process of obtaining *jph-1* cDNA for our own study, we obtained two cDNAs of 2.2 kb and 2.4 kb in size, amplified using primers flanking the start and stop codons (**Figure 5A**). The 2.2 kb cDNA matches the previously reported *jph-1* cDNA, which we designated isoform A (Yoshida et al., 2001). The 2.4 kb cDNA retains the intron between exon 7 and exon 8 and would encode a protein with the C-terminal 138 amino acids of the previously reported *jph-1* cDNA replaced by a different 35 amino acid sequence (**Figure 5B**). We designated this shorter protein isoform B. The C-terminal 35 amino acids do not contain a predicted transmembrane domain, nor conserved domains or low complexity regions. A BLASTp search of all published *Caenorhabditis* genomes found no significant hits for the 35 amino acid sequence, suggesting that it is not conserved. Furthermore, a BLASTn search showed that although the intron is conserved in 10 out of 26 published *Caenorhabditis* genomes (**Figure 6A**), the translated sequences have low amino acid conservation and highly variable sequence length due to intronic stop codons (**Figure 6B**). The absence of conserved motifs and the lack of conservation between species suggests that these 35 amino acids may not be important for the function of *jph-1*. JPH-1 isoform A shares between 39% and 42% overall sequence identity with human JPH1 through 4, with higher sequence homology in the MORN repeats, which target junctophilin to the PM (Takeshima et al., 2000).

jph-1 is required for normal development

To define the function of *jph-1*, we generated two null *(0)* alleles, *ju1683* and *ju1684*, using CRISPR-Cas9 editing. Both alleles delete the entire coding sequence of both *jph-1* isoforms (**Figure 5A**). These two alleles show indistinguishable phenotypes in all analyses; therefore, we generally present the quantification data for *ju1683* (**Table 7**). By gross body morphology, *jph-1(0)* mutant animals are smaller and thinner than stage-matched wild-type animals (**Figure 5C**). *jph-1(0)* mutants develop more slowly compared to wild-type animals (**Table 7**). *jph-1(0)* mutants have reduced fertility, with a brood size (52 ± 25, n = 12) about 20% of that in wild-type animals (279 ± 19, n = 10). Transgenic expression of a fosmid containing the entire *jph-1* locus rescued the developmental defects (**Table 7**). These observations indicate that *jph-1* is necessary for proper animal development.

jph-1 is expressed in muscles and neurons, and its function requires the transmembrane domain

A previously reported *jph-1* transcriptional reporter showed expression in most muscles and some neurons in the head (Yoshida et al., 2001). We made a similar transcriptional reporter using a 4.5 kb *jph-1* promoter to control GFP expression (**Figure 7A**). We confirmed GFP expression in all hermaphrodite muscle types, including body wall, pharyngeal, vulval, uterine, stomatointestinal, anal sphincter and anal depressor muscles, with the exception of the contractile gonadal sheath (**Figure 7A**). We also observed expression in many neurons from head to tail.

All developmental defects of *jph-1(0)* were rescued by expression of N-terminally GFP-tagged JPH-1A under the control of the 4.5 kb *jph-1* promoter (**Figure 7B**) as either a multicopy extrachromosomal array or a single copy insertion line (**Table 7, Figure 5C**). This result indicates

that GFP-tagged JPH-1A can perform the developmental functions of *jph-1* and that the 4.5 kb promoter provides sufficient tissue specificity for *jph-1* function. In contrast, transgenic expression of GFP::JPH-1B, the truncated isoform lacking the transmembrane domain, under the same promoter, did not show rescuing activity (**Figure 7C, Table 7**). This analysis supports a conclusion that the transmembrane domain is necessary for the function of JPH-1.

JPH-1A localizes to subcellular puncta and co-localizes with the ER-PM contact site protein ESYT-2 in neurons

We observed that the functional GFP-tagged JPH-1A showed a punctate subcellular pattern in muscles and neurons. In body wall muscle, GFP::JPH-1A localizes to rows of puncta that follow the obliquely striated pattern of the muscle (**Figure 8A,B**). In the pharyngeal muscle, JPH-1A localizes to puncta radiating from the pharyngeal lumen and lining the pharynx periphery (**Figure 8A**). We observed broad expression in neurons in the head and tail, including the bundled neuronal processes of the nerve ring, the ventral cord neurons, and touch receptor neurons (**Figure 8A-E**). In neuronal cell bodies of the head ganglia (**Figure 8C**), tail ganglia (**Figure 8D**), and ventral nerve cord (**Figure 8E**), GFP::JPH-1A shows a reticulate localization pattern and forms bright puncta near the periphery of the cell body. This localization is observed in newly hatched L1 animals and adults, suggesting that the localization is established prior to hatching and maintained into adulthood (**Figure 7B**).

Junctophilins generally function to couple calcium channels between the ER and PM, including ER-localized ryanodine receptors (RyRs) and PM-localized L-type calcium channels (Landstrom et al., 2014). In *C. elegans*, *unc-68* encodes the RyR and *egl-19* encodes the Cav1 VGCC α1-subunit. We generated split-GFP knock-in lines for both *unc-68* and *egl-19* and

visualized their subcellular localization by expressing muscle GFP1-10 and mKate2::JPH-1A expressed under the *jph-1* promoter. In the body wall muscle, both UNC-68 and EGL-19 localize to rows of puncta, which nearly completely overlap with JPH-1A puncta (**Figure 8F-K**). JPH-1A co-localization with both the ER-localized UNC-68 and PM-localized EGL-19 is consistent with targeting to ER-PM contact sites in muscle cells.

To determine if the neuronal puncta of JPH-1A represent MCSs, we analyzed animals co-expressing GFP::JPH-1A with a reporter line expressing mKate2::ESYT-2 in touch receptor neurons. E-Syt (extended-synaptotagmin) proteins are conserved tethering proteins at ER-PM contact sites (Giordano et al., 2013). We showed previously that *C. elegans* ESYT-2 is expressed broadly in neurons and co-localizes with an ER marker at the cell periphery (Kim et al., 2018). In the PLM soma, GFP::JPH-1A puncta co-localize with mKate2::ESYT-2 (**Figure 8L-P**), suggesting that JPH-1A clusters at ER-PM contact sites in neuronal cell bodies. We also examined GFP-tagged JPH-1B and observed a mostly diffuse localization in the muscles and neurons (**Figure 7C**), consistent with the transmembrane domain being critical for JPH-1 subcellular localization. The lack of *jph-1(0)* rescuing activity by JPH-1B suggests that the transmembrane domain is important for its localization and function.

jph-1 regulates pharyngeal muscle contraction

The gross phenotypes of *jph-1(0)* mutants broadly resemble those of mutants with feeding defects in that they are small, thin, pale, and take longer to reach adulthood than wild-type animals (Avery, 1993; Avery and Horvitz, 1989). Our observation that *jph-1* is expressed in the pharynx suggests that the *jph-1(0)* phenotype may be due to defects in feeding related function. *C. elegans* eat by drawing bacteria into their mouth using pharynx pumping and crushing the bacteria with

their grinder (Avery and You, 2012). We measured pumping rate by counting grinder movements and found that *jph-1(0)* mutants had a lower pumping rate than wild-type animals (**Figure 9A**). Pharyngeal muscle contraction is regulated by glutamatergic transmission. Loss of function in *eat-4*, encoding the sole glutamate transporter, causes reduced pumping rate (Lee et al., 1999). We found that *jph-1(0)* mutants had a similar pumping rate to *eat-4(ky5)* mutants (**Figure 9A**). However, since *eat-4(ky5)* animals are not as small as *jph-1(0)* mutants (**Table 7**), reduced pumping rate alone cannot account for the starved appearance of *jph-1(0)* mutants. We next quantified pumping strength by measuring the distance moved by the grinder in one pump (**Figure 9B, Materials and Methods**). *jph-1(0)* mutants had significantly weaker pumping strength than either wild type or *eat-4* mutants (**Figure 9C**). To test if reduced pharynx muscle activity was causing the starved appearance of *jph-1(0)* mutants, we expressed JPH-1A specifically in the pharynx muscle using the *myo-2* promoter. Pharyngeal muscle expression of JPH-1A restored pumping strength to wild-type levels (**Figure 9C**). Importantly, it also rescued the small body size and delayed development of *jph-1(0)* mutants (**Table 7, Figure 9C**). These observations indicate that JPH-1A is required for proper pharyngeal muscle function which ultimately impacts gross organismal development.

jph-1 is required in the body wall muscle for locomotion

On solid surfaces, wild-type *C. elegans* crawl by sinusoidal body undulations (**Figure 10A**). In contrast, *jph-1(0)* mutants adopt unusual extended or curled postures during locomotion, move slowly, and are frequently immobile, consistent with previous observations of *jph-1* RNAi treated animals (Yoshida et al., 2001). When placed in liquid, *C. elegans* swim by moving their entire bodies side-to-side to produce alternating C-shaped conformations (Gjorgjieva et al., 2014), which

can be quantitated by counting thrashing frequency. We observed that *jph-1(0)* mutants exhibit far fewer thrashes per minute than wild-type animals (**Figure 10B**). Furthermore, *jph-1(0)* mutants would often thrash only the heads without moving the tail. The failure of muscle contraction to propagate to the tail suggested that *jph-1* might be required for transmission of the signal for muscle contraction. A fosmid containing genomic *jph-1* fully rescued locomotion on both solid surfaces and in liquid (**Table 7, Figure 10B**). JPH-1A driven by the *jph-1* promoter rescued locomotion defects and thrashing frequency, although not as well as the fosmid transgene (**Figure 10B**). JPH-1B did not discernably improve movement on solid surfaces, supporting the importance of the transmembrane domain for JPH-1 function. Expression of JPH-1A in body wall muscle, but not pharyngeal muscle or neurons, restored full-body thrashing in liquid and sinusoidal movement on solid surfaces (**Figure 10B**). These data indicate that *jph-1* is required in the body wall muscle for animal movement and suggest that it may be involved in both muscle contraction and propagation of a signal for contraction between muscle cells.

jph-1 promotes axon regeneration cell non-autonomously

We previously characterized a different *jph-1* mutation, *jph-1(ok2823)*, for its role in axon regeneration. *jph-1(ok2823)* is a small deletion removing part of the fourth intron to the sixth exon (**Figure 5A**). By analyzing cDNA isolated from *jph-1(ok2823)* animals, we found that *jph-1(ok2823)* would generate a protein truncated after the seventh MORN repeat. The gross morphology and movement of *jph-1(ok2823)* animals are similar to *jph-1(0)*, and these defects are fully rescued by the *jph-1* fosmid transgene (**Table 7**). We had observed that PLM axons of *jph-1(ok2823)* animals display reduced axon regeneration and enhanced axon-axon fusion after laser-induced axon injury (Kim et al., 2018). We tested if PLM axon regeneration is similarly affected

in *jph-1(0)* mutants. Like *jph-1(ok2823)* animals, touch receptor neurons of *jph-1(0)* mutants have normal morphology (**Figure 11A**), indicating that *jph-1* is not required for axon outgrowth during development. After laser injury, *jph-1(0)* mutants exhibited strongly reduced axon regeneration, significantly different from both wild type and *jph-1(ok2823)* (**Figure 12A,B**). Expression of JPH-1A under the *jph-1* promoter fully rescued the regeneration defect, indicating that *jph-1* is required for axon regrowth after injury. Expression of JPH-1A in pharyngeal muscle, which rescued the growth and size of the animal (**Table 7**), also rescued axon regrowth (**Figure 12B**), suggesting that nutrient intake may influence axon regeneration. While *jph-1* is expressed in PLM neurons (**Figure 8**), expression of JPH-1A specifically in touch neurons did not rescue axon regrowth (**Figure 12B**). Furthermore, knocking down GFP:JPH-1A specifically in touch neurons of *jph-1(0)* animals through Degron-mediated degradation of GFP-JPH-1 (Wang et al., 2017) did not reduce axon regeneration (**Figure 11B**). Together, these data indicate that *jph-1* regulates axon regeneration cell non-autonomously.

While we were able to replicate the increased axon fusion of *jph-1(ok2823)* mutants, we did not observe an increase in axon fusion in injured PLM axons in *jph-1(0)* mutants (**Figure 11C**). We considered if the enhanced axon fusion observed in *jph-1(ok2823)* animals might be caused by the production of an abnormal protein. To test this, we made a construct fusing GFP to *jph-1* cDNA isolated from *jph-1(ok2823)* animals, named GFP::JPH-1(ok2823). In contrast to the subcellular punctate pattern of full-length JPH-1A, GFP::JPH-1(ok2823) was found in the nucleus of many neurons and body wall muscles (**Figure 11D**). Therefore, two explanations can be made for the increased axon fusion of *jph-1(ok2823)* mutants: either that *jph-1(ok2823)* is a partial loss of function and that fusion is more likely when axon regrowth is only mildly impaired, or that *jph-1(ok2823)* produces a protein with altered activity that enhances axon fusion.

jph-1 contributes to neuromuscular synaptic transmission

Junctophilins are required for proper regulation of cytosolic calcium levels in cell types such as mouse cardiomyocytes, HL-1 immortalized mouse cardiomyocytes, and C2C12 myotubes (Chen et al., 2013; Landstrom et al., 2011; Nakada et al., 2018; Reynolds et al., 2013; Takeshima et al., 2000; Van Oort et al., 2011). We observed broad expression of *jph-1* in neurons. Within the ventral nerve cord, we found that cholinergic motor neurons express *jph-1* (**Figure 13A**). JPH-1A is present at the presynaptic terminal of touch receptor neurons (**Figure 13B**). To examine if *jph-1* plays a role in synaptic transmission, we focused our study on the neuromuscular junction, where pharmacological assays can assess neuromuscular transmission. Release of acetylcholine from ventral cord motor neurons stimulates body wall muscle contraction in *C. elegans* (Von Stetina et al., 2006). Two pharmacological responses are widely used to assess neuromuscular transmission. Levamisole is an agonist of acetylcholine receptors expressed on the body wall muscle (Lewis et al., 1980). Upon exposure to 1 mM levamisole, *jph-1(0)* mutants paralyzed at the same rate as wild-type animals (**Figure 14A**), suggesting that *jph-1* is not required for muscle responses to acetylcholine. The acetylcholinesterase inhibitor aldicarb causes the accumulation of acetylcholine at the neuromuscular junction, which leads to muscle hypercontraction and paralysis (Miller et al., 1996). Nearly all wild-type animals were paralyzed after 2 hours of exposure to 1 mM aldicarb (**Figure 15A**). In contrast, 70-80% of *jph-1(0)* mutants were still moving, suggesting that these animals may have decreased acetylcholine release. Aldicarb resistance was confirmed using a second *jph-1(0)* allele (**Figure 14B**) and expression of a fosmid containing *jph-1* genomic DNA rescued the aldicarb resistance of *jph-1(0)* mutants (**Figure 15A**). Altogether, these results indicate that *jph-1* contributes to neuromuscular synaptic transmission.

As we had observed co-localization between JPH-1 and ESYT-2 in neurons, we tested the response of *esyt-2(0)* mutants to aldicarb. We found that *esyt-2(0)* mutants are aldicarb resistant, suggesting that they are also involved in neuromuscular synaptic transmission (**Figure 15B**). A transgene containing the whole *esyt-2* genomic locus rescued the aldicarb resistance of *esyt-2(0)* (**Figure 15B**). Remarkably, the *jph-1(0)*;*esyt-2(0)* double mutant paralyzed at a similar rate to wild-type – in effect, the *jph-1(0)* and *esyt-2(0)* mutations cancel each other out (**Figure 15C**). We tested second alleles of *jph-1(0)* and *esyt-2(0)* and observed the same result (**Figure 14C**). A transgene containing the *esyt-2* genomic locus in the *jph-1(0)*;*esyt-2(0)* double mutant restored aldicarb resistance, indicating that the wild-type aldicarb response is due to loss of *esyt-2* (**Figure 15D**). While *esyt-2(0)* animals are superficially wild-type, *jph-1(0)*;*esyt-2(0)* mutants resemble *jph-1(0)* in growth and locomotion, suggesting that the *esyt-2* mutation does not compensate for the loss of *jph-1* in muscles. Taken together, these results suggest that while loss of *jph-1* or *esyt-2* alone disrupts neurotransmission, loss of both restores neurotransmission to wild-type levels.

esyt-2(0) mutants displayed a slight resistance to levamisole that was not observed in *jph-1(0)* or *jph-1(0)*;*esyt-2(0)* mutants (**Figure 14D**). A non-wild type response to levamisole typically suggests a role in the muscle response to acetylcholine. However, as we had previously shown that a *esyt-2* promoter::GFP transgene is expressed exclusively in the nervous system (Kim et al., 2018), this hints that the role of *esyt-2* in neurotransmission may be more complex.

jph-1 promotes animal health and development in parallel with *unc-68*/RyR and voltage-gated calcium channels

Our observation that JPH-1A co-localizes with UNC-68/RyR and the VGCC α1-subunit EGL-19 raises the possibility of direct interaction between them. We thus next investigated genetic interactions between *jph-1* and calcium channels in *C. elegans*.

Like *jph-1(0)* mutants, *unc-68(e540)* null mutants are small, slow growing, and show incomplete flaccid paralysis (Maryon et al., 1996). However, *unc-68(0)* mutants have darker pigmentation and grow more quickly than *jph-1(0)* mutants (**Table 8**), suggesting that they have less severe defects in nutrient intake (Avery, 1993). We found that *jph-1(0); unc-68(0)* double mutants grew even slower than either *jph-1(0)* or *unc-68(0)* single mutants (**Table 8**). Expressing JPH-1A under the *jph-1* promoter in *jph-1(0); unc-68(0)* double mutants partially restored animal growth to more closely resemble *unc-68(0)* single mutants. The exacerbated slow growth of the *jph-1(0); unc-68(0)* double mutant indicates that *jph-1* has functions independent of *unc-68* and suggests that *jph-1* may couple other ER and PM components.

egl-19 is expressed in both muscles and neurons, and *egl-19* null mutants are embryonic lethal (Lee et al., 1997). We therefore used a partial loss-of-function mutation, *egl-19(ad1006lf)*, to test genetic interactions with *jph-1*. Animals homozygous for the *egl-19(ad1006lf)* mutation are long, thin, and flaccid, move slowly, and display weak pumping (Lee et al., 1997). We were unable to obtain viable *jph-1(0)*; *egl-19(lf)* double mutants, suggesting that *jph-1* becomes crucial when *egl-19* function is impaired. We also constructed double mutants of *jph-1(0)* with the gain-of-function mutation *egl-19(ad695gf)*. Animals with *egl-19(ad695gf)* are short due to body wall muscle hypercontraction (Lainé et al., 2014) but otherwise appear normal in overall growth rate and movement. We found that *jph-1(0); egl-19(gf)* animals lived to adulthood, but grew more

slowly than *jph-1(0)* single mutants (**Table 8**). Overall, these observations suggest that when *egl-19* activity is impaired or altered, *jph-1* activity becomes more important.

The non-L-type VGCC α1-subunit *unc-2*, orthologous to CACNA1A, is predominantly expressed in neurons and localizes to presynaptic terminals (Mathews et al., 2003; Saheki and Bargmann, 2009). *unc-2(e55)* null mutants exhibit sluggish movement but normal development and growth (Mathews et al., 2003; Schafer et al., 1996). We found that *jph-1(0); unc-2(0)* double mutants grew substantially more slowly than *jph-1(0)* single mutants and were sterile as adults (**Table 8**). The *unc-2(zf35gf)* gain-of-function mutation causes the channel to open at a lower membrane potential, causing hyperactive locomotion but otherwise normal growth and development (Huang et al., 2019). *jph-1(0); unc-2(gf)* double mutants displayed significantly slower growth than *jph-1* single mutants (**Table 8**). These results suggest that *jph-1* and *unc-2* function cooperatively in neurons.

Altogether, our analysis of genetic interactions supports a conclusion that *jph-1* acts together with RyR and VGCC channels for animal development, where they are not in completely overlapping pathways but may have some overlapping roles.

JPH-1A subcellular localization depends on *unc-68*/RyR

Evidence from other cell types suggest that junctophilins and their interacting partners may depend on each other to be localized to MCS (Golini et al., 2011; Nakada et al., 2018). We thus tested if JPH-1A localization depends on calcium channels and *esyt-2*. In the body wall muscle of wild type animals, JPH-1A localizes to longitudinal rows of puncta (**Figure 16A**). In *unc-68* mutants, JPH-1A puncta were less distinct and often connected to neighbouring puncta. (**Figure 16A**). In wild-type neurons, JPH-1A has a reticulate pattern with bright puncta in the cell periphery

(**Figure 16B**). In *unc-68* mutants, while the reticulate pattern of JPH-1 remained, the bright puncta were absent (**Figure 16B**). The lack of puncta in both muscles and neurons of *unc-68* animals suggests that *unc-68* is required for anchoring JPH-1A in puncta. JPH-1A localization was unchanged from wild type in *unc-2* and *esyt-2* mutants (**Figure 16, Figure 17A-B**), indicating that these genes are not required for JPH-1A localization.

Discussion

Junctophilins play key roles in excitation-contraction coupling in heart and skeletal muscles (Ito et al., 2001; Nakada et al., 2018; Takeshima et al., 2000; Van Oort et al., 2011). In particular, junctophilins couple PM- and ER-localized calcium channels to efficiently trigger calcium release from the ER following membrane depolarization (Chen et al., 2013; Nakada et al., 2018; Reynolds et al., 2013; Van Oort et al., 2011). Here, we report that the *C. elegans* junctophilin JPH-1 is expressed in pharyngeal muscle, body wall muscle, and neurons, and performs important functions in each tissue. We show that in the pharyngeal muscle, *jph-1* is required for robust pumping and timely growth and development. The stunted development of *jph-1(0)* mutants is likely due to reduced food intake caused by weak pumping, as their slow growth and starved appearance is seen in other mutants with defects in feeding related function (Avery, 1993; Avery and Horvitz, 1989). In the body wall muscle, we find that *jph-1* is required for body movement and locomotion. *jph-1(0)* mutants move slowly and display flaccid paralysis, suggesting that the body wall muscle lacks contraction strength. Our tissue-specific rescue experiments indicate that muscle contraction in both pharyngeal and body wall muscle requires *jph-1*. In flies, knockdown or overexpression of the sole junctophilin was shown to cause muscular deficits and cardiac dysfunction (Calpena et al., 2018). Skeletal muscle from neonatal JPH-1 knockout mice have weaker electrically-stimulated contractile force, indicating that JPH-1 is required for excitation-contraction coupling (Ito et al., 2001). Thus, the role for junctophilin in muscle contraction is conserved from *C. elegans* pharyngeal and body wall muscle to vertebrates.

The role of calcium regulation in axon regeneration in *C. elegans* has been widely demonstrated (Ghosh-Roy et al., 2010). *unc-68*/RyR promotes axon regeneration, and is required for localized calcium release from the ER following axon injury (Sun et al., 2014). We previously

reported that *jph-1(ok2823)* mutants have decreased axon regeneration (Kim et al., 2018). Here, we extended our analysis to the genetic null alleles of *jph-1* and uncovered a surprising role of *jph-1* in promoting axon regeneration in a cell non-autonomous manner. The observation that the regeneration defects could be rescued by expressing *jph-1* in the pharyngeal muscle implies that PLM axon regeneration may be influenced by nutrient uptake or through substances released by the pharynx. This finding raises an intriguing possibility that gut nutrients may impact neuronal injury response, a theme that shares similarities to emerging findings on the gut-brain axis in other axon regeneration studies (Kigerl et al., 2020). Additionally, despite *jph-1(ok2823)* animals resembling *jph-1(0)* in all gross phenotypes, our data suggest that the increased fusion in *jph-1(ok2823)* is likely due to an altered activity associated with the truncated protein JPH-1(ok2823) that localizes to the nucleus. Interestingly, a study in mouse found that heart stress induces cleavage of JPH-2, with the N-terminal JPH-2 fragment translocating to the nucleus where it alters transcription (Guo et al., 2018). Therefore, it is conceivable that the mutant protein produced in *jph-1(ok2823)* alters neuronal transcription to enhance axon fusion after injury.

Our finding that *jph-1(0)* mutants are resistant to the acetylcholinesterase inhibitor aldicarb suggests that *jph-1* modulates neurotransmission at the neuromuscular junction. The fact that *jph-1(0)* mutants showed a normal response to the acetylcholine receptor agonist levamisole suggests that *jph-1* modulates neurotransmission by functioning in neurons. In JPH-3/4 double knockout mice, paired-pulse stimulation of climbing fibres elicits normal depression in Purkinje cells, but paired-pulse stimulation of parallel fibres elicits reduced facilitation in Purkinje cells, leading the authors of the study to conclude that JPH-3/4 may play a subtle role in mammalian synaptic transmission (Kakizawa et al., 2007). Our work suggests that *jph-1* may have a role in synaptic transmission that has largely been overlooked in studies on neuronal junctophilins in mammals. In

hippocampal neurons, junctophilins couple PM-localized CaV1.3 VGCCs, ER-localized RyR2 Ca^{2+}-gated Ca^{2+} channels, and PM-localized KCa3.1 Ca^{2+}-activated K^+ channels (Sahu et al., 2019). This coupling generates the slow afterhyperpolarization current, which regulates action potential frequency. Unlike mammalian neurons, which generate voltage-gated Na^+ channel-dependent action potentials, *C. elegans* neurons mostly rely on a calcium current for membrane depolarization (Goodman et al., 1998). Therefore, while junctophilins likely regulate calcium-induced calcium release in both *C. elegans* and mammalian neurons, the physiological consequences of losing junctophilin depend on neuronal properties.

Our data further uncovers intriguing genetic interactions between *jph-1* and *esyt-2* in synaptic transmission. Extended-synaptotagmin was shown to have a presynaptic role in neurotransmission in *Drosophila* (Kikuma et al., 2017). Consistently, we found that *esyt-2* null mutants were aldicarb resistant. Strikingly, we found that *jph-1(0)*; *esyt-2(0)* double mutants had a wild-type response to aldicarb. This mutual suppression suggests that when either *jph-1* or *esyt-2* is mutated, neurotransmission is unbalanced; when the other is also mutated, the balance is restored. As we do not yet know whether *jph-1* and *esyt-2* function pre- or postsynaptically, the mechanism is unclear. However, as both proteins are ER-PM tethers, the mechanism likely involves ER calcium release. It would be of future interest to determine the exact nature of how *jph-1* regulates neurotransmission.

Finally, our genetic double mutant analysis sheds light on the importance of JPH-1 mediated ER-PM calcium channel coupling. Many studies on junctophilins have focused on their roles in coupling the ER-localized RyR with PM-localized channels in muscles and neurons. In *C. elegans*, RyR is encoded by *unc-68*. Early studies showed using both *unc-68* promoter::GFP and anti-UNC-68 immunostaining that *unc-68* is expressed in muscles and neurons, but absent in the

anterior pharynx (Maryon et al., 1998). *unc-68* null mutants are aldicarb resistant, and electrophysiological studies have shown that *unc-68* has a pre-synaptic role in synaptic transmission (Liu et al., 2005; Maryon et al., 1998). We observed *jph-1* expression in the entire pharynx. Close comparison of *jph-1* and *unc-68* null mutants showed that they have similar movement and growth phenotypes, but *jph-1(0)* exhibited more severe growth retardation. Moreover, *jph-1(0); unc-68(0)* double mutants exhibit more severe growth defects than *unc-68* or *jph-1* single mutants. This analysis suggests that JPH-1 has additional RyR-independent roles. Possibilities include the generation of ER-PM contact sites, regulation of store-operated calcium entry (Hirata et al., 2006; Li et al., 2010), and coupling other ER components to the PM. Previous studies have shown that junctophilins are required for the co-localization of ER- and PM-localized calcium channels in isolated mouse cardiomyocytes, mouse skeletal muscle, and cultured hippocampal neurons (Nakada et al., 2018; Sahu et al., 2019; Van Oort et al., 2011). In rat cardiomyocytes, RyR localizes to muscle triads before JPH-2 arrives (Ziman et al., 2010), suggesting that the targeting of junctophilins by RyR may be conserved. Junctophilins and RyRs have been shown to directly interact (Beavers et al., 2013; Golini et al., 2011; Nakada et al., 2018; Phimister et al., 2007; Van Oort et al., 2011; Woo et al., 2008). We found that JPH-1 localization depends on *unc-68*/RyR. It is possible that junctophilin targeting may involve directly binding to RyR already localized at MCSs.

In conclusion, our study shows that *C. elegans jph-1*, similar to vertebrate homologs, has broad functions in excitable cells. Our data uncover new roles of junctophilins in synaptic transmission and axon regeneration, and the requirement for RyR in junctophilin localization. The conservation in function between mammalian and *C. elegans* junctophilins presents the opportunity for *C. elegans* to be used for further investigations of junctophilins.

Acknowledgements

We thank our lab members for discussion and comments. This work was supported by grants from NIH (R01 NS093588 to ADC and YJ, R01 GM054657 (ADC), R01 NS32196 to JMK, and R37 NS 035546 to YJ).

Chapter 3, in full, has been submitted for publication as it may appear in Piggott CA, Wu Z, Nurrish S, Xu S, Kaplan JM, Chisholm AD, Jin Y. 2020. *Caenorhabditis elegans* junctophilin has tissue-specific functions and regulates neurotransmission with extended-synaptotagmin. The dissertation author was the primary investigator and author of this material.

Figures

Figure 5. *jph-1* expresses two isoforms that differ at their C-termini and is required for animal development

A) Illustration of *jph-1* spliced isoforms and deletion alleles. Exons are dark grey boxes, introns are black lines, and UTRs are light grey boxes. *ok2823* is a 637 bp deletion, *ju1683* is a 3891 bp deletion, and *ju1684* is a 3858 bp deletion with a 13 bp insertion.

B) Illustration of *C. elegans* JPH-1 proteins predicted from isolated cDNA sequences in comparison to human JPH proteins. Dark grey boxes indicate membrane occupation and recognition nexus (MORN) repeats and white boxes indicate transmembrane domains. The striped box at the C-terminus of JPH-1B indicates the 35 amino residues predicted from the cDNA. These 35 amino acids are not predicted to form a transmembrane region or low-complexity domain using Pfam (El-Gebali et al., 2019), the TMHMM Server v 2.0 (http://www.cbs.dtu.dk/services/TMHMM/), or SMART (Letunic and Bork, 2018). A BLASTp search of these 35 amino acids against all published *Caenorhabditis* genomes (Caenorhabditis.org) also revealed no significant hits with a low e-value threshold of 1.0. Gene accession numbers are: JPH-1A (NP_492193.2), Human JPH1 (NP_001304759.1), JPH2 (NP_065166.2), JPH3 (NP_065706.2), and JPH4 (NP_001139500.1). Pairwise sequence alignments were performed between *C. elegans* JPH-1A and human JPH1, JPH2, JPH3, and JPH4 using MUSCLE (Madeira et al., 2019) and the Percent Identity Matrix was viewed to find percent identity. To determine conservation between MORN repeats, we concatenated all eight 14 amino acid MORN repeats into one sequence for each protein and then performed pairwise sequence alignments using MUSCLE. Sequence identity ranges from 69% to 77% when comparing only MORN sequences in *C. elegans* JPH-1A and human JPH1 through 4.

C) Bright field images of L4 stage animals of genotypes indicated. Compared to wild type animals *jph-1(ju1683)* animals are small, thin, and pale, all of which was rescued by transgenic expression of a fosmid containing genomic *jph-1* (*juEx3390*), JPH-1A expressed under the *jph-1* promoter [P*jph-1*-GFP::JPH-1A(*juSi387*)], or JPH-1A expressed in the pharyngeal muscle [P*myo-2*-GFP::JPH-1A(*juEx8041*)]. Scale bar 100 µm.

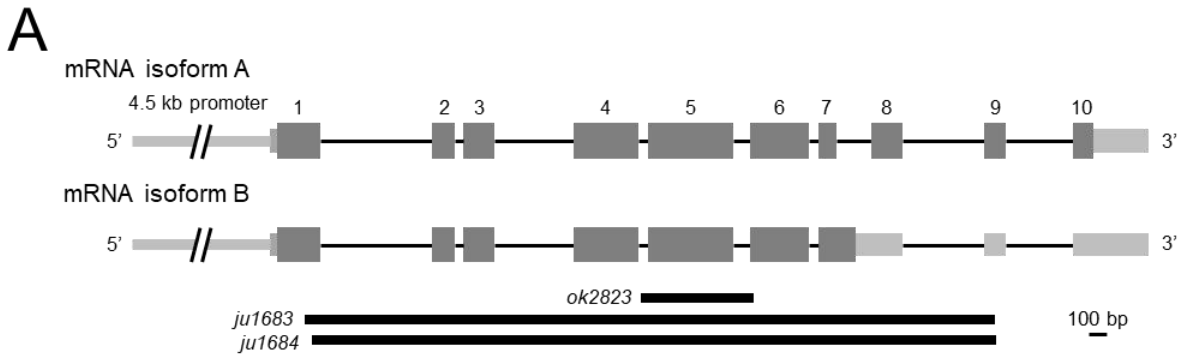
A
mRNA isoform A
4.5 kb promoter
1
2
3
4
5
6
7
8
9
10
5'
3'
mRNA isoform B
5'
3'
ok2823
ju1683
ju1684
100 bp


B
C. elegans
MORN repeats
Transmembrane
JPH-1A
747
JPH-1B
644
Human
JPH1
661
JPH2
696
JPH3
748
JPH4
628

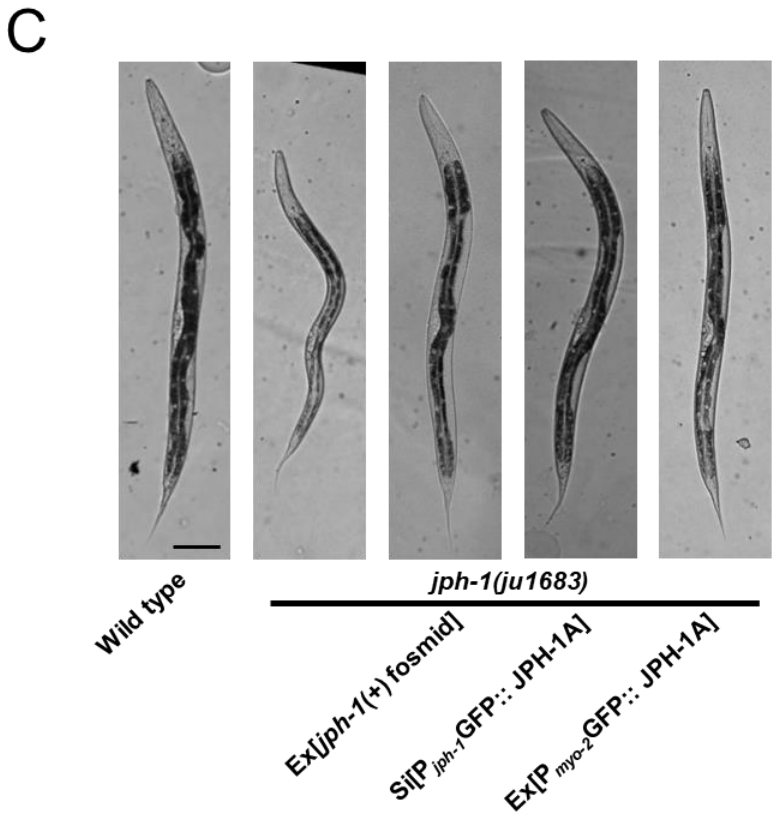
C
jph-1(ju1683)
Wild type
Ex[jph-1(+) fosmid]
Si[P jph-1 GFP:: JPH-1A]
Ex[P myo-2 GFP:: JPH-1A]

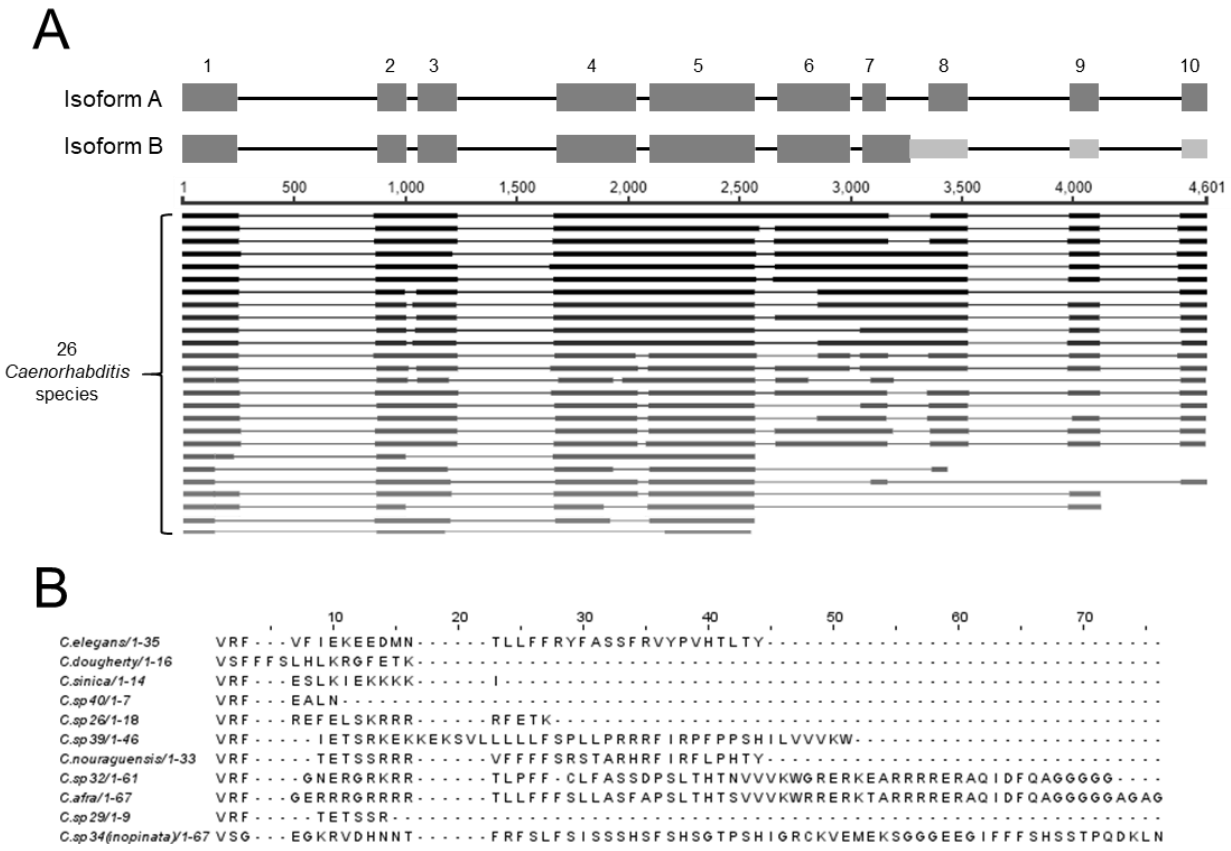

Figure 6. Comparison of genomic sequences concerning the intron retained in JPH-1B.
A) Top: Exon-intron diagrams for *C. elegans jph-1* isoform A and B.
Bottom: We performed a BLASTn search of *C. elegans jph-1* against 26 *Caenorhabditis* genomes published on Caenorhabditis.org. Aligned sequences are thick black lines and unaligned sequences are thin black lines. Darker lines indicate stronger hits. Boundaries between aligned and unaligned regions often match up with exon-intron boundaries. 10 *Caenorhabditis* sequences align with the intron retained in JPH-1B.
B) We translated the introns of these 10 species in the same reading frame as *C. elegans jph-1* and aligned the amino acid sequences using MUSCLE (Madeira et al., 2019). The sequences vary in length because most encounter stop codons, except for sister species *C. sp32* and *C. afra*, which have no stop codons in the intron and are in frame with the following exon. Beyond the first three amino acids there is little amino acid conservation between sequences.

Figure 7. Expression pattern of a *jph-1* transcriptional reporter and a JPH-1B translational fusion reporter.

A) *jph-1* is expressed in neurons and most muscles. Top: Illustration of *jph-1* promoter::GFP expression construct [P*jph-1*-GFP(*juEx8013* and *juEx8014*)]. Bottom: GFP expression was seen in head ganglia neurons and pharyngeal, body wall, vulval, uterine, stomatointestinal, anal sphincter, and anal depressor muscles. The large fluorescent circle marked by an asterisk is a coelomocyte labeled by the coinjection marker [P*unc-122*-RFP].

B) *jph-1* localization in an L1 stage animal. Top: Illustration of expression construct [P*jph-1*-GFP::JPH-1A(*juSi387*)]. Bottom: Confocal images of an L1 stage animal. A plane near the surface of the animal shows expression in the body wall muscle, while a plane taken through the middle of the animal shows expression in the pharyngeal muscle and head ganglia neurons.

C) JPH-1B has a diffuse localization. Top: Illustration of construct expressing *jph-1b* cDNA under the *jph-1* promoter [P*jph-1*-GPF::JPH-1B(*juEx8038*)]. Bottom: Confocal projection of an L4 stage animal head shows a diffuse localization in neurons and muscles.

Scale bars 20 μm.

A

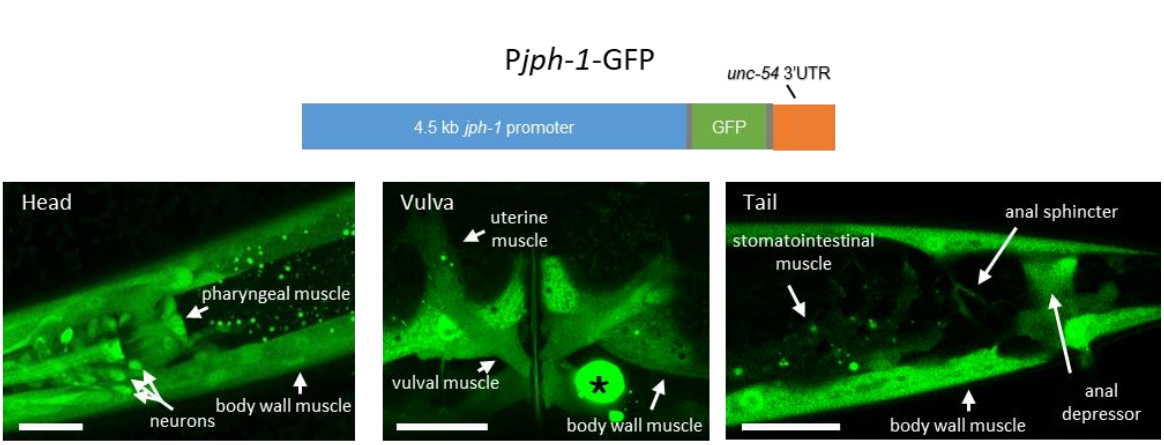
Pjph-1-GFP
unc-54 3'UTR
4.5 kb jph-1 promoter
GFP
Head
pharyngeal muscle
neurons
body wall muscle
Vulva
uterine muscle
vulval muscle
body wall muscle
Tail
anal sphincter
stomatointestinal muscle
body wall muscle
anal depressor

B

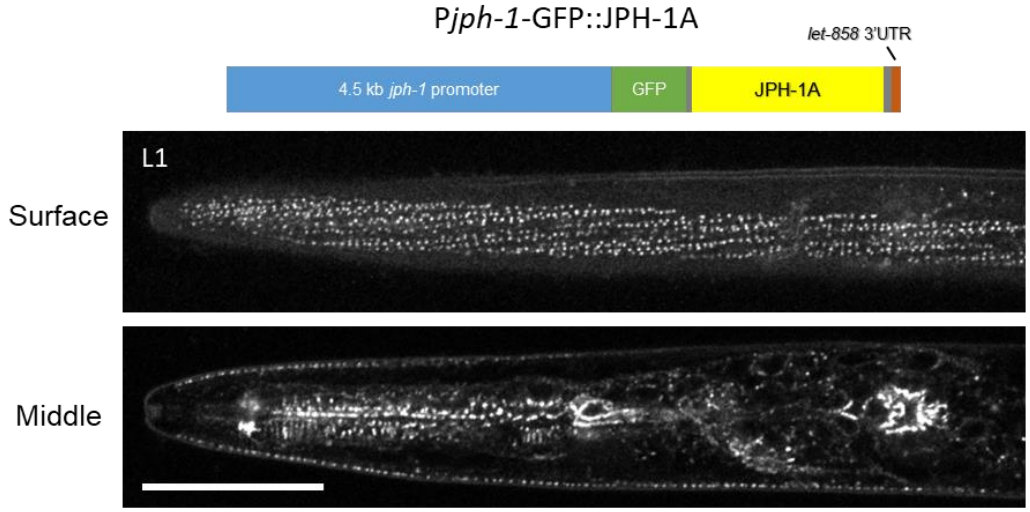
Pjph-1-GFP::JPH-1A
let-858 3'UTR
4.5 kb jph-1 promoter
GFP
JPH-1A
L1
Surface
Middle

C

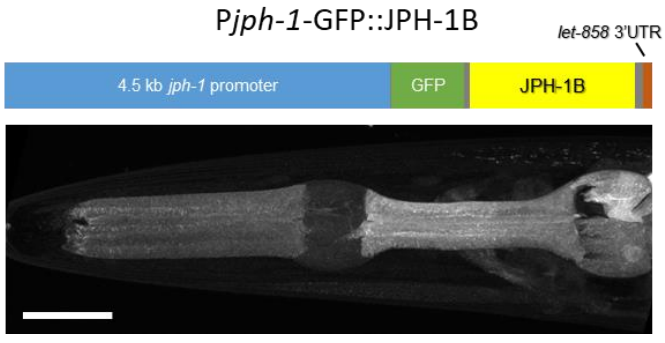
Pjph-1-GFP::JPH-1B
let-858 3'UTR
4.5 kb jph-1 promoter
GFP
JPH-1B

Figure 8. JPH-1A co-localizes with calcium channels UNC-68 and EGL-19 in muscles and MCS protein ESYT-2 in neurons.

A-D: Confocal images of GFP::JPH-1A expressed under the *jph-1* promoter as a single copy insertion [P*jph-1*-GFP::JPH-1A(*juSi387*)] in L4 stage animals.

A) Maximum intensity projection of the head showing GFP::JPH-1A expression in body wall muscle, pharynx muscle, and neurons. Arrow indicates nerve ring.

B) Single plane image of body wall muscle. JPH-1A localizes to rows of dots that run parallel to muscle striations.

C) Single plane image of head ganglia neurons. JPH-1A in neuronal cell bodies is excluded from the nucleus and is concentrated in puncta. Arrowheads indicate some of the neurons expressing GFP::JPH-1A.

D) Single plane image of tail ganglia. Arrowheads indicate neurons expressing GFP::JPH-1A. Arrow indicates PLM cell body. Asterisks mark body wall muscle.

E) Maximum intensity projection of GFP::JPH-1A [P*jph-1*-GFP::JPH-1A(*juEx7999*)] in the ventral nerve cord in an L4 stage *jph-1(ju1683)* animal. Arrowheads indicate neuronal cell bodies. Fluorescent blobs outside the cells are autofluorescent particles in the gut.

F-H: JPH-1A co-localizes with UNC-68 in body wall muscle. Single plane confocal images of an L4 stage animal with split-GFP knock-in *unc-68* (*nu664*) expressing muscle GFP1-10 [P*myo-3*-GFP1-10(*nuSi144*)] and mKate2::JPH-1A expressed under the *jph-1* promoter [P*jph-1*-mKate2::JPH-1A(*juEx8103*)].

I-K: JPH-1A co-localizes with EGL-19. Single plane confocal images of an L4 stage animal with split-GFP knock-in *egl-19* (*nu674*) expressing muscle GFP1-10 [P*myo-3*-GFP1-10(*nuSi144*)] and mKate2::JPH-1A expressed under the *jph-1* promoter [P*jph-1*-mKate2::JPH-1A(*juEx8103*)].

L-N: JPH-1A localizes to ER-PM contact sites labeled by ESYT-2 in the cell body. Single plane confocal images of an L4 animal expressing mKate2-tagged ESYT-2 under the *mec-4* touch neuron specific promoter [P*mec-4*-mKate2::ESYT-2(*juIs540*)] and GFP::JPH-1A under the *jph-1* promoter [P*jph-1*-GFP::JPH-1A(*juSi387*)]. PLM cell body outlined by dashed line.

O) Close-up of panel N showing partial colocalization of JPH-1A and ESYT-2 in the PLM cell body.

P) Close up of the box in Panel N shows that both ESYT-2 and JPH-1A are in the PLM axon. In all images, anterior is to the left, dorsal is up. Scale bars, 5 μm.

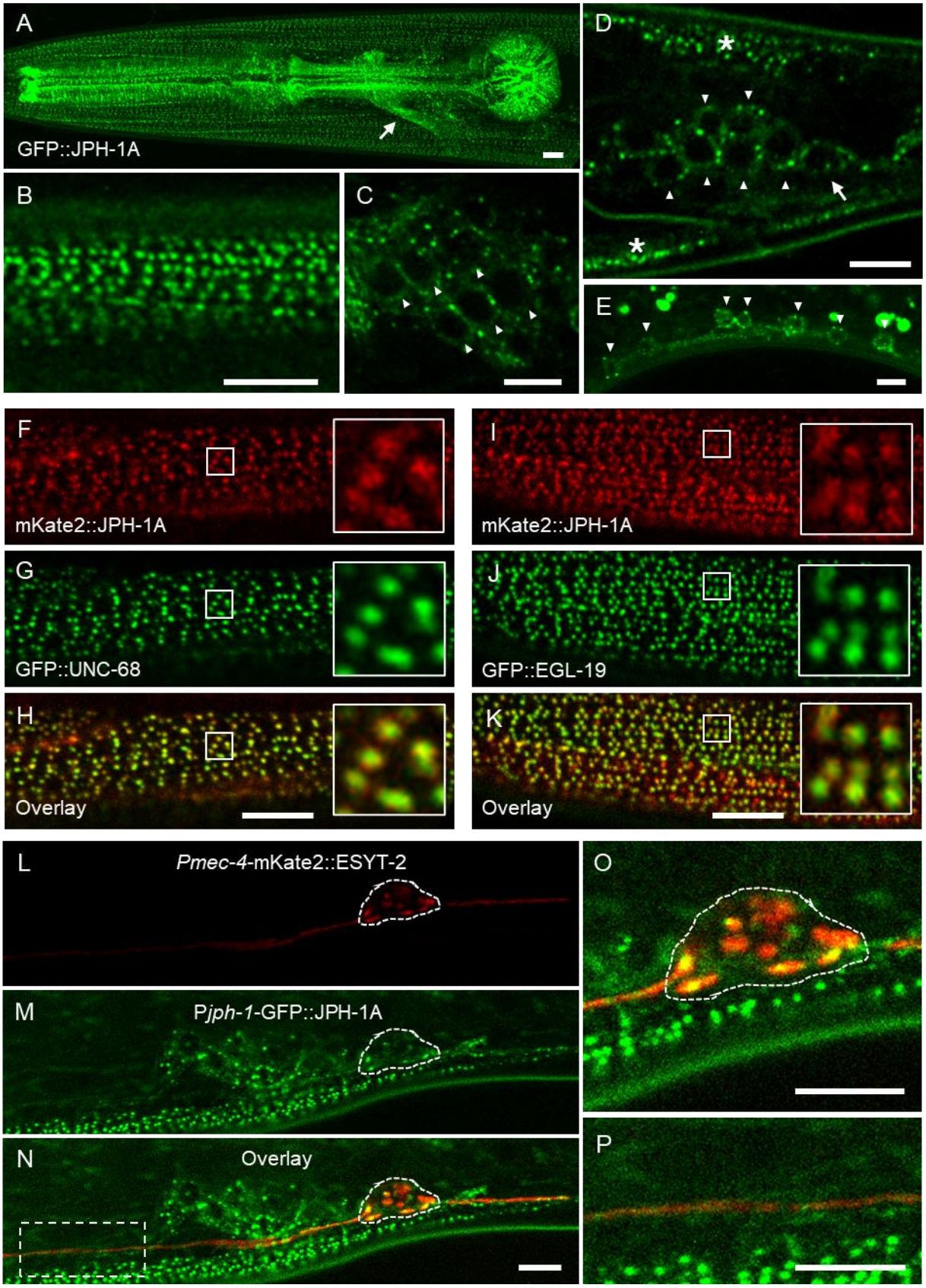
A
GFP::JPH-1A
B
C
D
E
F
mKate2::JPH-1A
I
mKate2::JPH-1A
G
GFP::UNC-68
J
GFP::EGL-19
H
Overlay
K
Overlay
L
Pmec-4-mKate2::ESYT-2
M
P*jph-1*-GFP::JPH-1A
N
Overlay
O
P

Figure 9. *jph-1* is required in the pharyngeal muscle for normal rate and strength of pumping.
A) *jph-1* is required for normal pharyngeal pumping rate. *jph-1(ju1683)* mutants had reduced pumping rate, which was rescued by expression of JPH-1A by the *jph-1* promoter [P*jph-1*-GFP::JPH-1A(*juSi387*)] but not by expression in the pharyngeal muscle [P*myo-2*-GFP::JPH-1A(*juEx8041*)]. e*at-4(ky5)* loss-of-function mutants had reduced pumping rate, as previously reported (Lee et al., 1999). Number of animals per genotype indicated above X-axis tick marks. Data are shown as individual data points and mean±SEM. Statistics: Non-parametric Kruskal-Wallis test with Dunn's multiple comparison test. ns not significant, *p<0.05, **p<0.01.
B) Pumping strength was determined by the distance moved by the grinder. The image on the left shows the head of the animal just before the pump is initiated, with the grinder position indicated by the arrow. The image on the right shows the animal mid-pump when the grinder has moved to its fullest extent. The distance moved by the grinder between the two images was normalized to the total length of the pharynx to quantify pumping strength. Scale bar, 25 µm.
C) Quantification of pharyngeal pumping strength. *jph-1(ju1683)* mutants had substantially reduced grinder movement, which was rescued by expression of JPH-1A by the *jph-1* promoter [P*jph-1*-GFP::JPH-1A(*juSi387*)] or in the pharyngeal muscle [P*myo-2*-GFP::JPH-1A(*juEx8041*)]. Number of animals per genotype indicated below X-axis tick marks. Data are shown as individual data points and mean±SEM. Statistics: One-way ANOVA with Tukey's post-test. ns not significant, ***p<0.001.

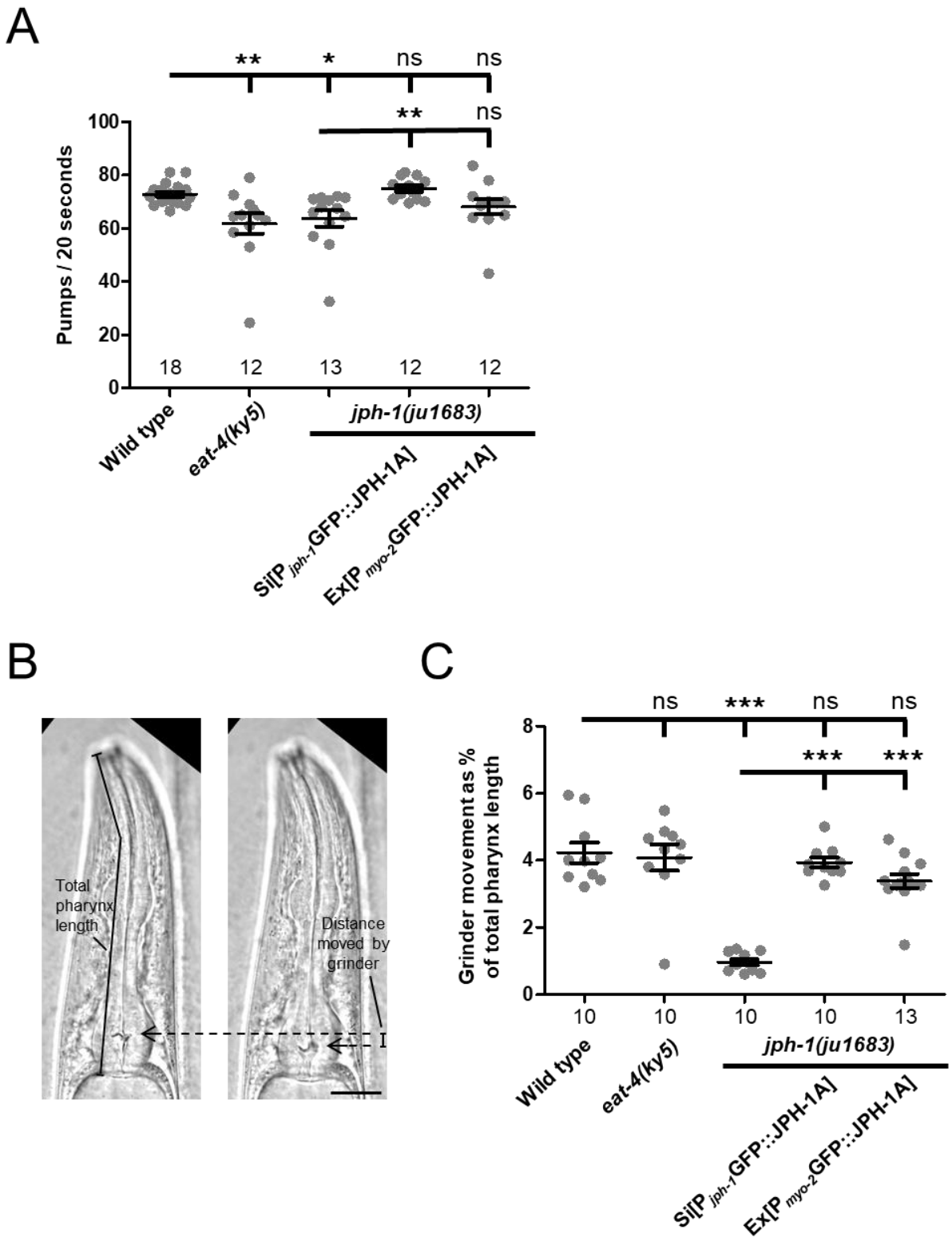
A
**
*
ns
ns
**
ns
Pumps / 20 seconds
100
80
60
40
20
0
18
12
13
12
12
jph-1(ju1683)
Wild type
eat-4(ky5)
Si[P jph-1 GFP::JPH-1A]
Ex[P myo-2 GFP::JPH-1A]
B
Total pharynx length
Distance moved by grinder
C
ns
***
ns
ns
***
***
Grinder movement as % of total pharynx length
8
6
4
2
0
10
10
10
10
13
jph-1(ju1683)
Wild type
eat-4(ky5)
Si[P jph-1 GFP::JPH-1A]
Ex[P myo-2 GFP::JPH-1A]

Figure 10. *jph-1* is required in the body wall muscle for locomotion.
A) L4 stage wild type animals exhibit smooth sinusoidal movement and posture while *jph-1(ju1683)* animals assume unusually straight body positions (shown here) and unusually tight sinusoidal or curled positions. Scale bar, 100 µm.
B) *jph-1(ju1683)* null mutants thrash less frequently than wild-type N2 animals. Thrashing rate was rescued by expression of a fosmid containing *jph-1* (*juEx3390*) and partially rescued by expression of JPH-1A by the *jph-1* promoter [P*jph-1*-GFP::JPH-1A(*juSi387*)]. Expression of JPH-1A in body wall muscle [P*myo-3*-GFP::JPH-1A(*juEx8023*)] rescued thrashing rate, but expression in neurons [P*rab-3*-GFP::JPH-1A(*juSi389*)] did not. Expression of JPH-1A in the pharyngeal muscle [P*myo-2*-GFP::JPH-1A(*juEx8041*)] slightly decreased thrashing rate. Number of animals per genotype indicated below X-axis tick marks. Data are shown as individual data points and mean±SEM. Statistics: One-way ANOVA with Tukey's post-test. ns not significant, ***p<0.001.

A

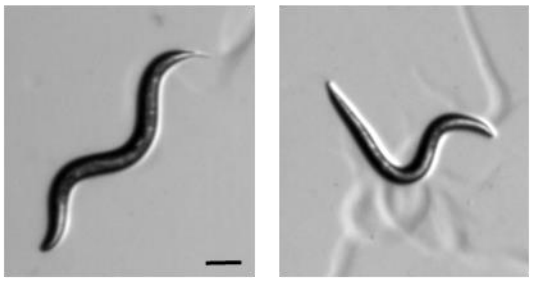

Wild type *jph-1(ju1683)*

B

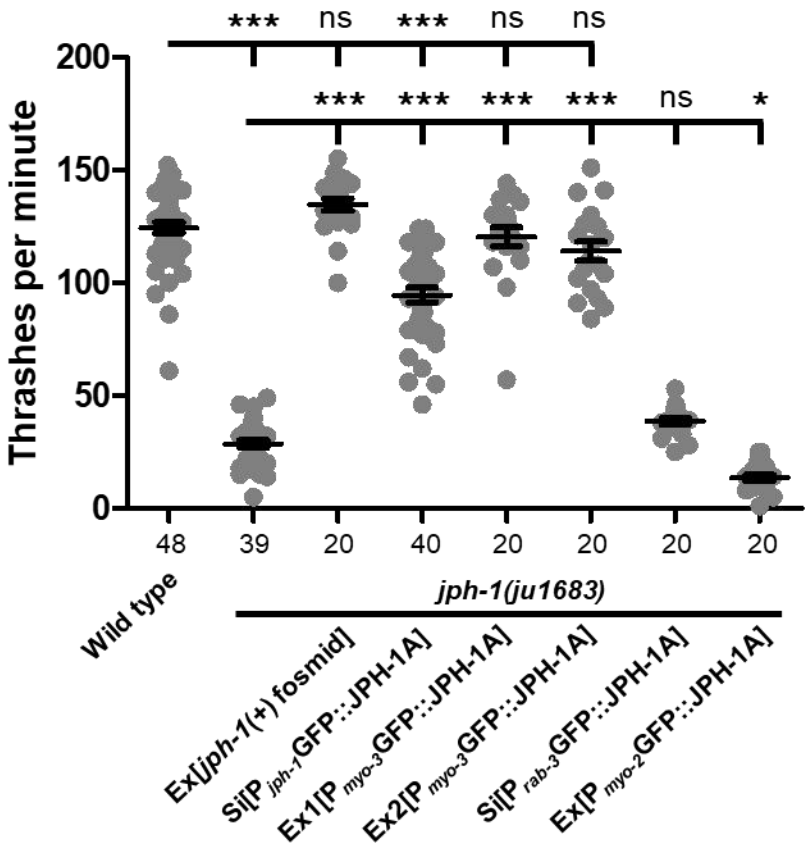

Figure 11. *jph-1(0)* mutants do not alter touch neuron morphology or enhance axon fusion after injury.

A) Touch neuron morphology is normal in *jph-1(ju1683)* animals. Representative images of wild-type and *jph-1(ju1683)* day-1 adult animals expressing the touch neuron marker P*mec-7*-GFP(*muIs32*). Labels indicate ALM, PLM, AVM, and PVM neuron cell bodies. The bright spot below the *jph-1(ju1683)* ALM cell body is likely fluorescence from the ALM on the opposite side of the body. Scale bar, 100 µm.

B) Distance regrown by PLM axon 24h post-injury. Control animals expressed GFP Degron in the touch neurons. *jph-1(ju1683)* animals expressing GFP-tagged JPH-1A under the *jph-1* promoter [P*jph-1*-GFP::JPH-1A(*juSi387*)] also expressed GFP Degron in the touch neurons, predicted to degrade GFP::JPH-1 specifically in touch neurons. There was no statistically significant difference between groups. Number of animals per genotype indicated below X-axis tick marks. Data are shown as individual data points and mean±SEM. Statistics: Student's t-test. ns not significant.

C) Percentage of animals with axon-axon fusion 24h post-injury. *jph-1(ok2823)* mutants had increased axon fusion while null mutants *ju1683* and *ju1684* exhibited wild-type levels of axon fusion. Number of animals per genotype indicated below X-axis tick marks. Statistics: Fisher's exact test performed pairwise. ns not significant, **p<0.01.

D) JPH-1(*ok2823*) localizes to the nucleus. Top: Illustration of construct expressing *jph-1(ok2823)* cDNA from original start to stop codon under the *jph-1* promoter [P*jph-1*-GFP::JPH-1(*ok2823*)(*juEx8035)*]. A premature stop codon in the middle of JPH-1(*ok2823*) truncates the C-terminal two-thirds of the protein. Bottom: Confocal projection of L4-stage animal tail with arrows indicating neuronal nuclei labeled by JPH-1(ok2823). Scale bar, 20 µm.

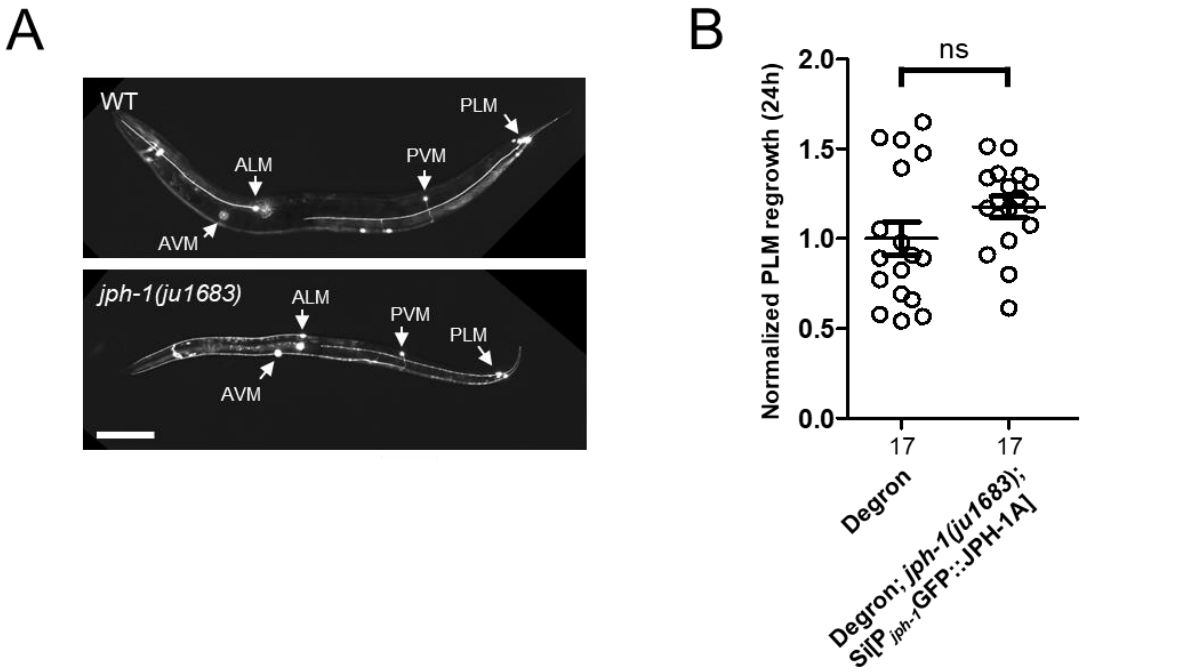
A
WT
PLM
ALM
PVM
AVM
jph-1(ju1683)
ALM
PVM
PLM
AVM
B
ns
Normalized PLM regrowth (24h)
2.0
1.5
1.0
0.5
0.0
17
17
Degron
Degron; jph-1(ju1683); Si[P jph-1 GFP::JPH-1A]
C
Axon fusion (%)
100
80
60
40
20
0
**
ns
ns
64
26
43
22
Wild type
jph-1(ok2823)
jph-1(ju1683)
jph-1(ju1684)
D
Pjph-1-GFP-JPH-1(ok2823)
let-858 3'UTR
4.5 kb jph-1 promoter
GFP
JPH-1(ok2823)
STOP

Figure 12. *jph-1* promotes touch neuron PLM axon regeneration cell non-autonomously.
A) Representative confocal images of PLM axon regrowth 24 h post-axotomy in animals expressing the touch neuron marker P*mec-7*-GFP(*muIs32*). Genotype in the bottom image is *jph-1(ju1683);* P*jph-1*-GFP::JPH-1A(*juSi387*). Anterior is to the left, dorsal is up. Arrows indicate the site of axon injury. Scale bar, 20 μm.
B) *jph-1* is required in the pharyngeal muscle for touch neuron axon regeneration. Distance regrown by PLM axon 24 h post-injury, normalized to wild-type regrowth. *jph-1(ok2823)* axon regrowth was not significantly different from wild type [P*mec-7*-GFP(*muIs32*)]. *jph-1(ju1683)* animals had significantly reduced regrowth. Expression of JPH-1A by the *jph-1* promoter [P*jph-1*-GFP::JPH-1A(*juSi387*)] or in the pharyngeal muscle [P*myo-2*-GFP::JPH-1A(*juEx8041*)] rescued the reduced regrowth of *jph-1(ju1683)* mutants. Expression of JPH-1A in the touch receptor neurons [P*mec-4*-GFP::JPH-1A(*juSi388*)] did not rescue axon regeneration. Number of animals per genotype indicated below X-axis tick marks. Data are shown as individual data points and mean±SEM. Statistics: Non-parametric Kruskal-Wallis test with Dunn's multiple comparison test. ns not significant, ***p<0.001.

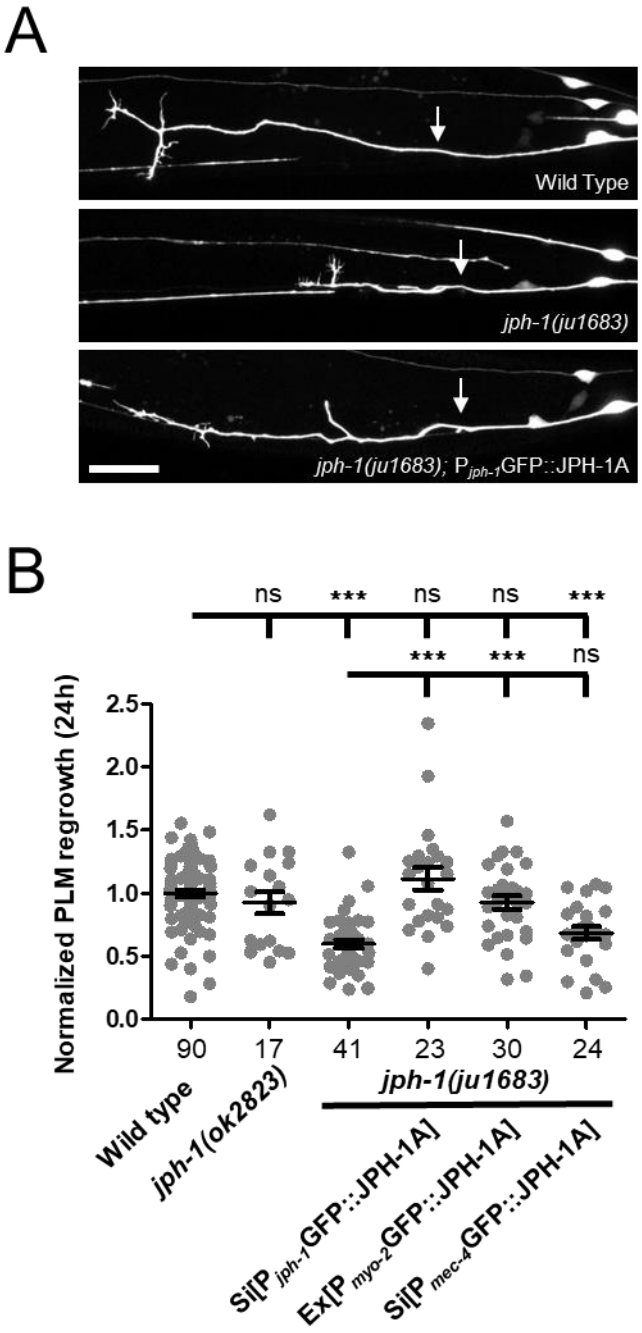
A
Wild Type
jph-1(ju1683)
jph-1(ju1683); Pjph-1GFP::JPH-1A
B
ns
***
ns
ns
***
***
***
ns
Normalized PLM regrowth (24h)
2.5
2.0
1.5
1.0
0.5
0.0
90
17
41
23
30
24
jph-1(ju1683)
Wild type
jph-1(ok2823)
Si[Pjph-1GFP::JPH-1A]
Ex[Pmyo-2GFP::JPH-1A]
Si[Pmec-4GFP::JPH-1A]

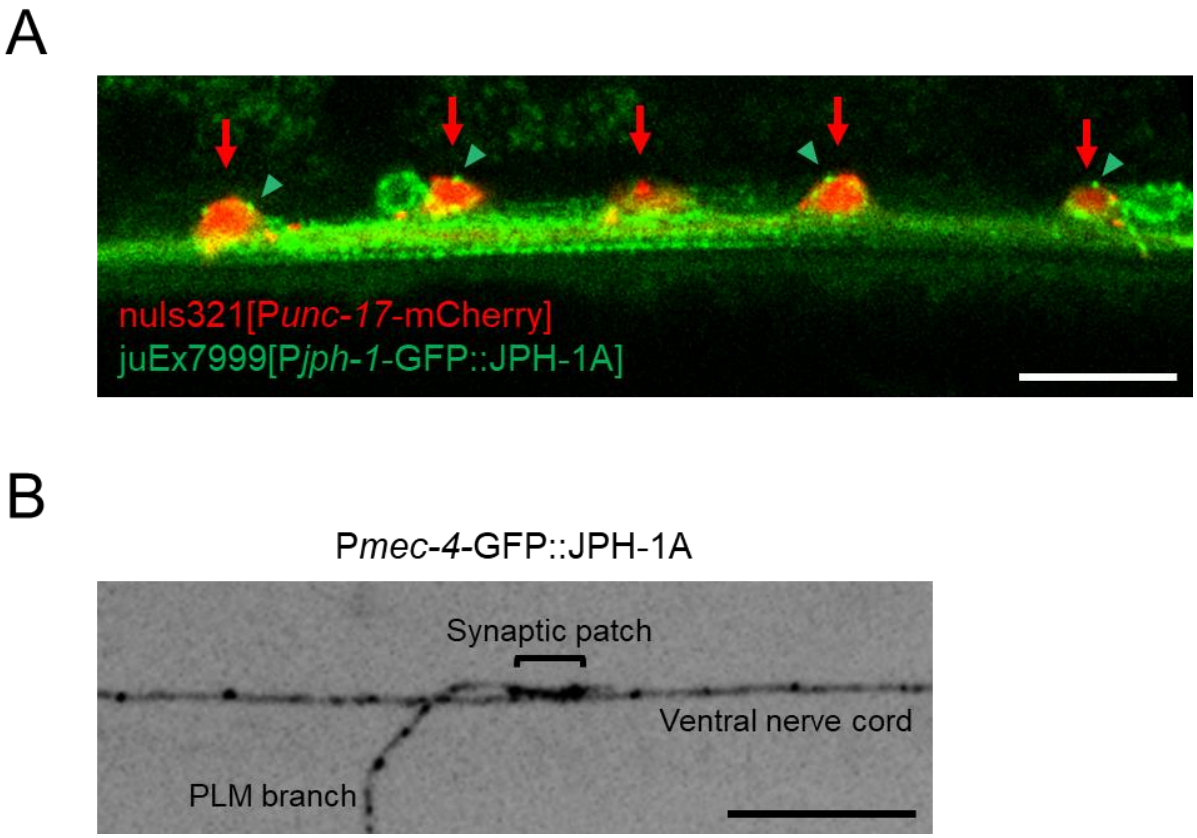

Figure 13. *jph-1* is expressed in cholinergic motor neurons and touch receptor neurons.
A) *jph-1* is expressed in cholinergic neurons. Single plane confocal image of ventral nerve cord of L4 animal expressing mCherry in cholinergic neurons [P*unc-17*-mCherry(*nuIs321*)] and JPH-1A under the *jph-1* promoter [P*jph-1*-GFP::JPH-1A(*juEx7999*)]. Red arrows indicate cholinergic neuron cell bodies. Green arrowheads indicate JPH-1A puncta in cholinergic neurons. Scale bar, 10 µm.
B) JPH-1A is present where the PLM touch receptor neuron synapses onto the ventral nerve cord. Confocal projection of JPH-1A expressed in touch neurons [P*mec-4*-GFP::JPH-1A(*juSi388*)]. Scale bar, 10 µm.

Figure 14. Additional data on pharmacological responses of *jph-1(0)* and *jph-1(0); esyt-2(0)*
A) *jph-1* null mutants *ju1683* and *ju1684* have the same response to levamisole as wild type animals.
B)*jph-1* null mutants *ju1683* and *ju1684* are both aldicarb resistant. Statistical significance shown between *jph1-(ju1684)* and wild type.
C) *jph-1(ju1684);esyt-2(ju1408)* double mutants exhibit a wild-type response to aldicarb. Statistical significance shown between *jph-1(ju1684)* and *jph-1;esyt-2*.
D) *esyt-2(ju1409)* animals are levamisole resistant compared to wild-type animals. Statistical significance shown between *esyt-2(ju1409)* and wild type.
13-15 animals tested per genotype per trial, n=3 trials. Data are shown as individual data points and mean±SEM. Statistics: One-way ANOVA with Tukey's post-test. ns not significant, *$p<0.05$, **$p<0.01$, ***$p<0.001$.

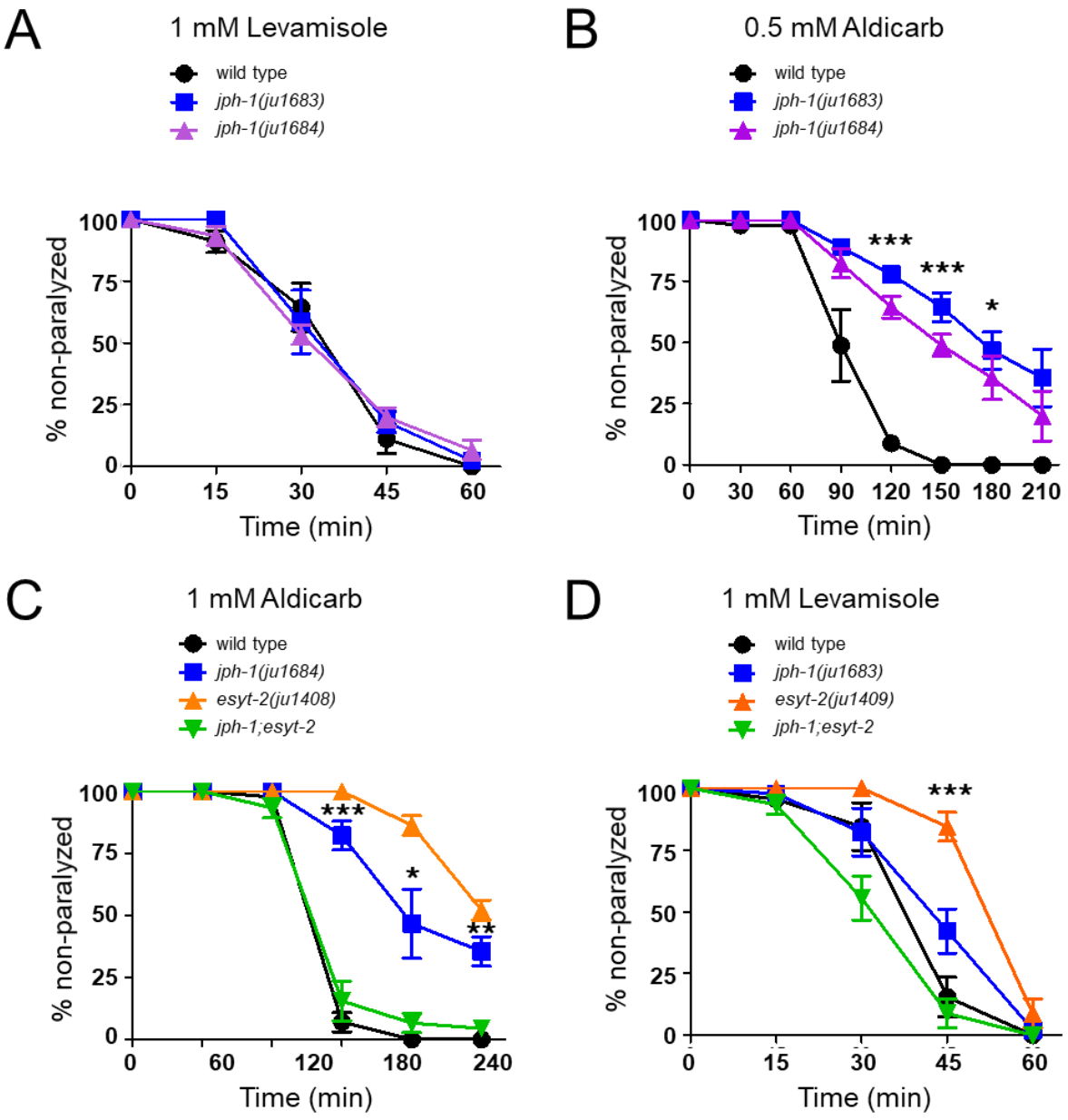
A
1 mM Levamisole
wild type
jph-1(ju1683)
jph-1(ju1684)
% non-paralyzed
Time (min)
B
0.5 mM Aldicarb
wild type
jph-1(ju1683)
jph-1(ju1684)
% non-paralyzed
Time (min)
***
***
*
C
1 mM Aldicarb
wild type
jph-1(ju1684)
esyt-2(ju1408)
jph-1;esyt-2
% non-paralyzed
Time (min)
***
*
**
D
1 mM Levamisole
wild type
jph-1(ju1683)
esyt-2(ju1409)
jph-1;esyt-2
% non-paralyzed
Time (min)
***

Figure 15. *jph-1* and *esyt-2* null mutants are aldicarb resistant and exhibit mutual suppression.

A) *jph-1(ju1683)* animals are resistant to aldicarb compared to wild-type animals. Aldicarb resistance was rescued by expression of a fosmid containing *jph-1* genomic DNA (*juEx3390*). Statistical significance shown between *jph-1(ju1683)* and *jph-1*;*Ex[jph-1(+) fosmid]*.

B) *esyt-2(ju1409)* animals are resistant to aldicarb compared to wild-type animals. Aldicarb resistance was rescued by expression of *esyt-2* genomic DNA (*juEx7581*). Statistical significance shown between *esyt-2(ju1409)* and *esyt-2*;*Ex[esyt-2 gDNA]*.

C) *jph-1(ju1683);esyt-2(ju1409)* double mutants exhibit a wild-type response to aldicarb. Statistical significance shown between *jph-1(ju1683)* and *jph-1;esyt-2*.

D) Expression of *esyt-2* genomic DNA (*juEx7581*) restores aldicarb resistance to *jph-1(ju1683); esyt-2(ju1409)* double mutants. Statistical significance shown between *jph-1*;*esyt-2* and *jph-1;esyt-2*;*Ex[esyt-2 gDNA]*.

13-15 animals tested per genotype per trial, n=3 trials. Data are shown as individual data points and mean±SEM. Statistics: One-way ANOVA with Tukey's post-test. ns not significant, *$p<0.05$, **$p<0.01$, ***$p<0.001$.

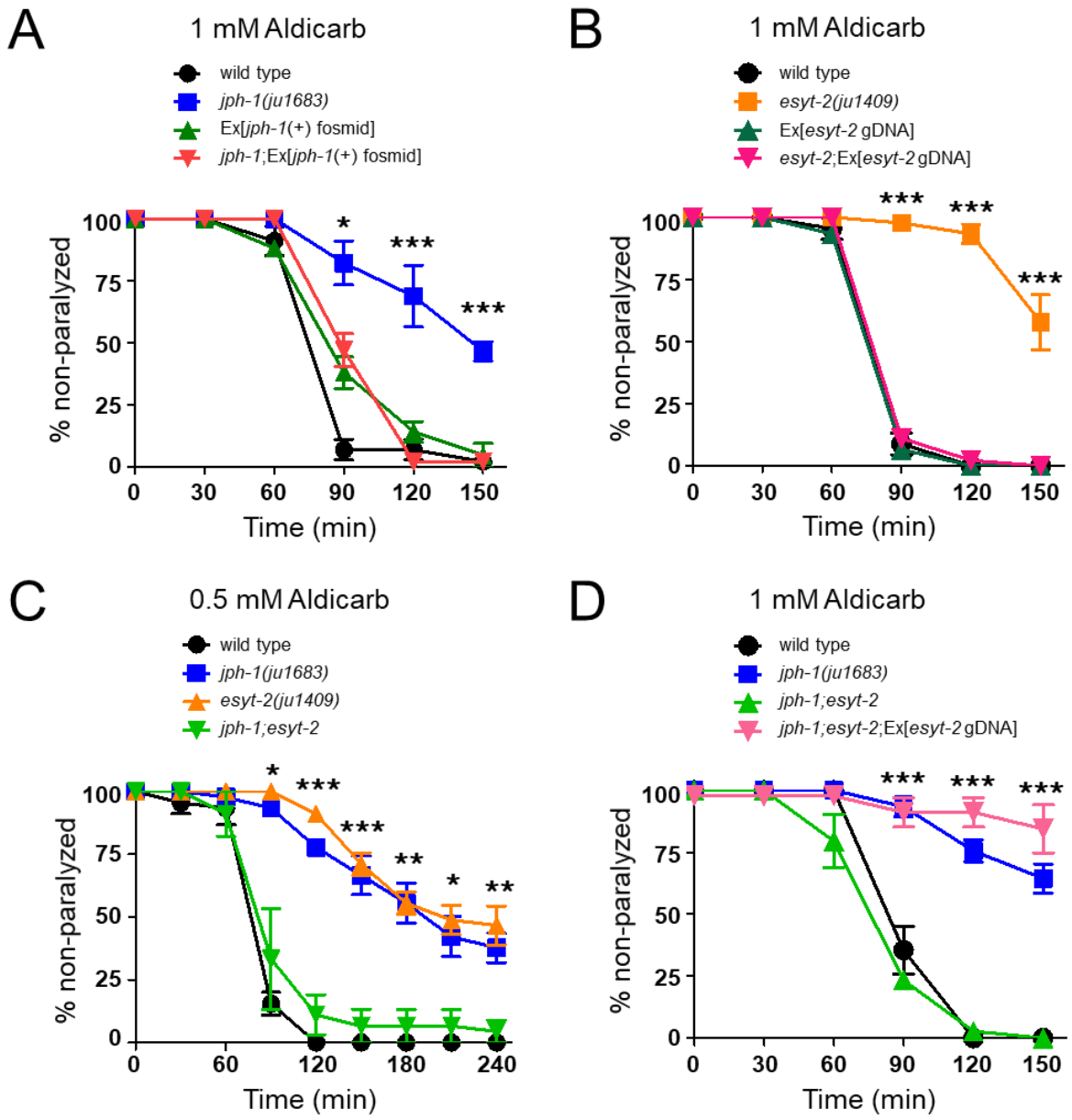
A
1 mM Aldicarb
wild type
jph-1(ju1683)
Ex[jph-1(+) fosmid]
jph-1;Ex[jph-1(+) fosmid]
% non-paralyzed
Time (min)
B
1 mM Aldicarb
wild type
esyt-2(ju1409)
Ex[esyt-2 gDNA]
esyt-2;Ex[esyt-2 gDNA]
C
0.5 mM Aldicarb
wild type
jph-1(ju1683)
esyt-2(ju1409)
jph-1;esyt-2
D
1 mM Aldicarb
wild type
jph-1(ju1683)
jph-1;esyt-2
jph-1;esyt-2;Ex[esyt-2 gDNA]

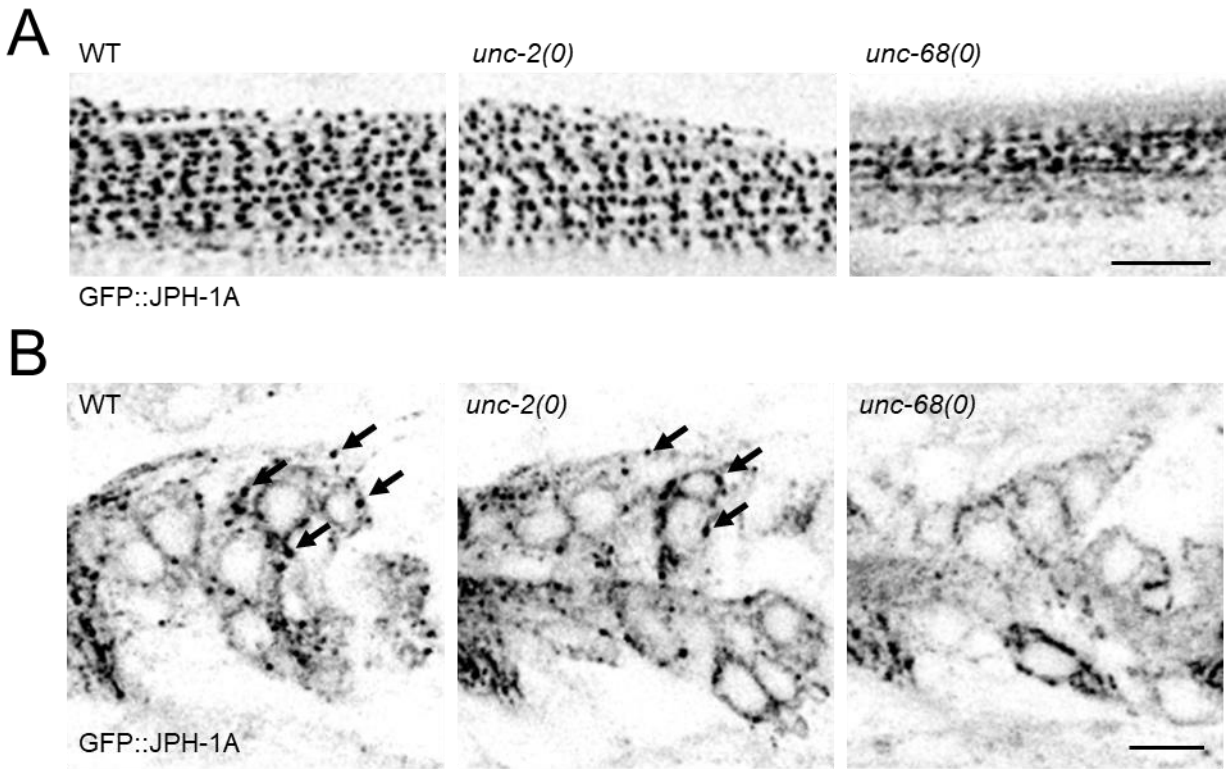

Figure 16. *unc-68* is required for JPH-1A localization.
Shown are single-plane confocal images of GFP::JPH-1A expressed under the *jph-1* promoter [P*jph-1*-GFP::JPH-1A(*juEx7999*)] in wild-type (WT), *unc-2(e55)*, and *unc-68(e540)* backgrounds. **A**) In the body wall muscle, JPH-1A localizes to row of puncta in WT and *unc-2(e55)* animals, while in *unc-68(e540)* animals JPH-1A puncta are less distinct.
B) In neurons of the head ganglia, JPH-1A localizes to reticulate structures surrounding the nucleus and forms puncta in the cell periphery of WT and *unc-2(e55)* animals, but not *unc-68(e540)* mutants. Arrows mark some of the GFP::JPH-1A puncta.
WT and *unc-2(e55)* images were taken at 2% laser power and *unc-68(e55)* was taken at 4.5% laser power to compensate for the slight variation in expression level. Scale bar, 5 µm.

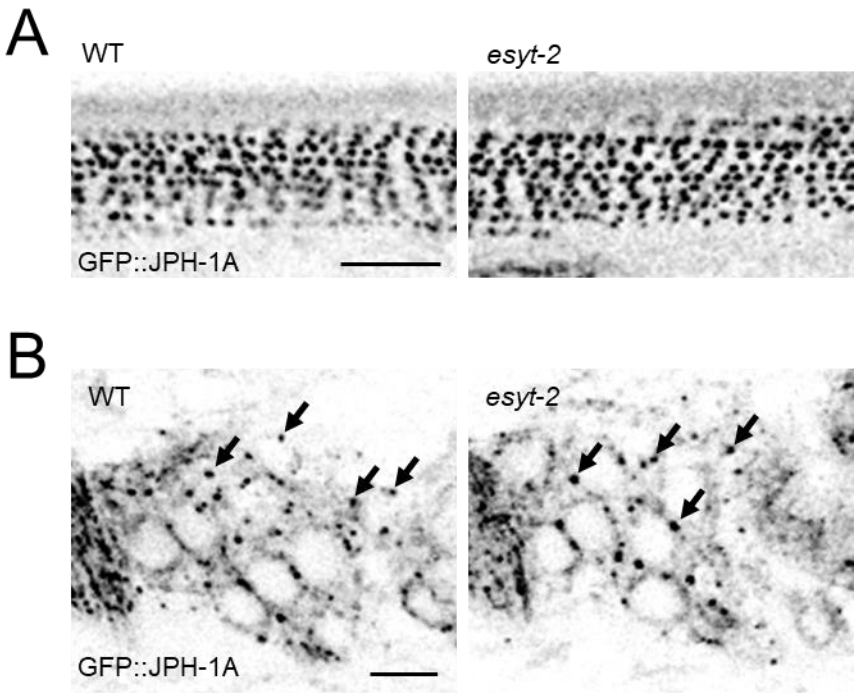

Figure 17. JPH-1A localization is unaltered in *esyt-2(0)*
Shown are single-plane confocal images of GFP::JPH-1A expressed under the *jph-1* promoter [P*jph-1*-GFP::JPH-1A(*juSi387*)] in wild-type and *esyt-2(ju1409)* backgrounds.
A) In the body wall muscle, JPH-1A localizes to rows of puncta in wild type and *esyt-2(ju1409)* animals.
B) In neurons of the head ganglia, JPH-1A localizes to reticulate structures surrounding the nucleus and forms puncta in the cell periphery of wild type and *esyt-2(ju1409)* animals. Arrows mark some of the GFP::JPH-1A puncta.
Scale bar, 5 μm.

Tables

Table 1. Strains and genotypes

Strain	Genotype
N2	wild type
CZ27358	*jph-1(ju1683) I*
CZ27360	*jph-1(ju1684) I*
CZ28073	*jph-1(ju1683) I; juEx3390[jph-1 fosmid WRM0622aB02]*
CZ28260	*jph-1(ju1683) I; juEx3392[jph-1 fosmid WRM0623aF07]*
CZ27162	*juEx8014[Pjph-1-GFP]*
CZ27161	*juEx8013[Pjph-1-GFP]*
CZ28024	*jph-1(ju1683) I; juEx7999[Pjph-1-GFP::JPH-1A]*
CZ27777	*jph-1(ju1683) I; juSi387[Pjph-1-GFP::JPH-1A] IV*
CZ27603	*jph-1(ju1683) I; juEx8037[Pjph-1-GFP::JPH-1B]*
CZ27606	*jph-1(ju1683) I; juEx8038[Pjph-1-GFP::JPH-1B]*
CZ27364	*juSi387[Pjph-1-GFP::JPH-1A] IV*
CZ28264	*nuTi144 [Pmyo-3 GFP 1-10 G418] I; unc-68(nu664) V; juEx8103[Pjph-1-mKate2::JPH-1A]*
CZ28263	*nuTi144 [Pmyo-3 GFP 1-10 G418] I; egl-19(nu674) IV; juEx8103[Pjph-1-mKate2::JPH-1A]*
CZ27404	*juSi387[Pjph-1-GFP::JPH-1A] IV; juIs540[Pmec-4-mKate2::ESYT-2] X*
CZ27569	*juEx8038[Pjph-1-GFP::JPH-1B]*
CZ24806	*eat-4(ky5)*
CZ27782	*jph-1(ju1683) I; juEx8041[Pmyo-2-GFP::JPH-1A]*
CZ28120	*jph-1(ju1683) I; juEx8022[Pmyo-3-GFP::JPH-1A]*
CZ28121	*jph-1(ju1683) I; juEx8023[Pmyo-3-GFP::JPH-1A]*
CZ28051	*jph-1(ju1683) I; juSi389(Prab-3-GFP::JPH-1A] IV*
CZ13170	*jph-1(ok2823) I*
CZ13990	*jph-1(ok2823) I; juEx3390[jph-1 fosmid WRM0622aB02]*
CZ27483	*jph-1(ok2823) I; juEx3392[jph-1 fosmid WRM0623aF07]*
CZ10969	*muIs32(Pmec-7-GFP) II*
CZ26391	*jph-1(ok2823) I; muIs32[Pmec-7-GFP] II*
CZ27359	*jph-1(ju1683) I; muIs32[Pmec-7-GFP] II*
CZ27778	*jph-1(ju1683) I; muIs32[Pmec-7-GFP] II; juSi387[Pjph-1-GFP::JPH-1A]IV*
CZ27783	*jph-1(ju1683) I; muIs32[Pmec-7-GFP] II; juEx8041[Pmyo-2-GFP::JPH-1A]*
CZ27910	*jph-1(ju1683) I; muIs32[Pmec-7-GFP] II; juSi388[Pmec-4-GFP::JPH-1A]IV*
OD2984	*ltSi953[Pmec-18-Degron-SL2-mKate2; cb-unc-119(+)]II; unc-119(ed3)III*
CZ27842	*jph-1(ju1683) I; ltSi953[Pmec-18-Degron-SL2-mKate2; cb-unc-119(+)] II; juSi387[Pjph-1-GFP::JPH-1A] IV; unc-119(ed3)?III*
CZ27361	*jph-1(ju1684) I; muIs32[Pmec-7-GFP] II*
CZ27536	*juEx8035[Pjph-1-GFP::JPH-1(ok2823)]*

Table 1. Strains and genotypes, Continued

Strain	Genotype
CZ28262	*nuIs321[Punc-17-mCherry]; juEx7999[Pjph-1-GFP::JPH-1A]*
CZ27875	*juSi388[Pmec-4-GFP::JPH-1A] IV*
CZ26322	*esyt-2(ju1409) III*
CZ28238	*esyt-2(ju1409) III;juEx7581 [esyt-2 gDNA]*
CZ28070	*jph-1(ju1683) I; esyt-2(ju1409) III*
CZ26389	*esyt-2(ju1408) III*
CZ28241	*jph-1(ju1684) I; esyt-2(ju1408) III*
CZ28282	*jph-1(ju1683) I; esyt-2(ju1409) III; juEx7581 [esyt-2 gDNA]*
CB540	*unc-68(e540) V*
CZ28026	*jph-1(ju1683) I; unc-68(e540)V; juEx7999[Pjph-1-GFP::JPH-1A]*
CZ26691	*egl-19(ad1006lf) IV*
DA695	*egl-19(ad695gf) IV*
CZ27905	*jph-1(ju1683) I; egl-19(ad695gf) IV*
CB55	*unc-2(e55) X*
CZ28054	*jph-1(ju1683) I; unc-2(e55) X; juEx7999[Pjph-1-GFP::JPH-1A]*
QW47	*unc-2(zf35gf) X*
CZ27903	*jph-1(ju1683) I; unc-2(zf35gf) X*
CZ28025	*unc-68(e540) V; juEx7999[Pjph-1-GFP::JPH-1A]*
CZ28053	*unc-2(e55) X; juEx7999[Pjph-1-GFP::JPH-1A]*
CZ28055	*esyt-2(ju1409) III; juSi387[Pjph-1-GFP::JPH-1A] IV*

Table 2. Plasmids

Plasmid name	Description
pCZGY3516	P*jph-1*-GFP::JPH-1A
pCZGY3519	P*jph-1*-GFP::JPH-1A with homology arms for CRISPR/Cas9 knock-in
pCZGY3525	P*jph-1*-GFP::JPH-1B
pCZGY3344	P*mec-4*-mKate2::ESYT-2
pCZGY3518	P*jph-1*-GFP
pCZGY3523	P*myo-2*-GFP::JPH-1A
pCZGY3522	P*rab-3*-GFP::JPH-1A with homology arms for CRISPR/Cas9 knock-in
pCZGY3535	P*myo-3*-GFP::JPH-1A
pCZGY3520	P*mec-4*-GFP::JPH-1A with homology arms for CRISPR/Cas9 knock-in
pCZGY2750	P*eft-3*:Cas9 + cxTi10882 sgRNA
pCFJ90	P*myo-2*-mCherry
pCFJ104	P*myo-3*-mCherry
pCZGY3529	P*jph-1*-GFP::JPH-1(*ok2823*)
WRM0622aB02	Fosmid containing jph-1
WRM0623aF07	Fosmid containing jph-1
pKP3315	P*myo-3* split GFP 1-10 miniMOS G418
pKP3318	*egl-19* exon 1 gRNA 5'-TTACCTGACATGATGGACAC-3'
pKP3319	*egl-19* exon 1 x7 GFP FP11 with with homology arms for CRISPR/Cas9 knock-in
pKP3320	*unc-68A* exon 31 gRNA 5'-GATGCTGCAGCCACGGGCGG-3'
pKP3321	*unc-68A* exon 31 x7 GFP FP11 with 1kb with homology arms for CRISPR/Cas9 knock-in
pGW28	*unc-58* gRNA co-CRISPR 5'-ATCCACGCACATGGTCACTA-3'
pDD162	P*eft-3*-CAS9 (Goldstein Lab)

Table 3. Transgenes

Transgene name	**Injected DNA**	**Injected conc.** (ng/µL)	**Coinjection marker and conc.**	**Source**
juEx3390[jph-1 fosmid WRM0622aB02]	fosmid WRM0622aB02	10	P*ttx-3*-RFP (30 ng/µL)	This manuscript
juEx3392[jph-1 fosmid WRM0623aF07]	fosmid WRM0623aF07	10	P*ttx-3*-RFP (30 ng/µL)	This manuscript
juEx8014[Pjph-1-GFP]	pCZGY3518	2.5	P*unc-122*-RFP (50 ng/µL)	This manuscript
juEx8013[Pjph-1-GFP]	pCZGY3518	2.5	P*unc-122*-RFP (50 ng/µL)	This manuscript
juEx7999[Pjph-1-GFP::JPH-1A]	pCZGY3516	2.5	P*unc-122*-RFP (50 ng/µL)	This manuscript
juSi387[Pjph-1-GFP::JPH-1A]	pCZGY3519	2.5		This manuscript
juEx8037[Pjph-1-GFP::JPH-1B]	pCZGY3525	2.5	P*unc-122*-RFP (50 ng/µL)	This manuscript
juEx8038[Pjph-1-GFP::JPH-1B]	pCZGY3525	2.5	P*unc-122*-RFP (50 ng/µL)	This manuscript
juIs540[Pmec-4-mKate2::ESYT-2]				Kim *et al.*, 2018
juEx8041[Pmyo-2-GFP::JPH-1A]	pCZGY3523	0.125	P*unc-122*-RFP (50 ng/µL)	This manuscript
juEx8022[Pmyo-3-GFP::JPH-1A]	pCZGY3535	2.5	P*unc-122*-RFP (50 ng/µL)	This manuscript
juEx8023[Pmyo-3-GFP::JPH-1A]	pCZGY3535	2.5	P*unc-122*-RFP (50 ng/µL)	This manuscript
juSi389(Prab-3-GFP::JPH-1A]	pCZGY3522	10		This manuscript
juSi388[Pmec-4-GFP::JPH-1A]	pCZGY3520	2.5		This manuscript
ltSi953[pOD2087/pSW408]				Wang *et al.*, 2017
juEx8035[Pjph-1-GFP::JPH-1(ok2823)]	pCZGY3529	2.5	P*unc-122*-RFP (50 ng/µL)	This manuscript
nuTi144	pKP3315	10		This manuscript

Table 4. Cloning primers

Cloning primers		
Name	**Sequence**	**Purpose**
YJ12558	gacgtaggtgtgtcagcag	5' flanking primer to amplify *jph-1* cDNA
YJ12559	cctgaggagaagtgtgtctg	3' flanking primer to amplify *jph-1* cDNA
YJ12560	atgaatggaggcagatttgac	Forward primer to amplify *jph-1* from start codon
YJ12561	ctacgaagaagacttcttcttcttc	Reverse primer to amplify *jph-1* isoform A to stop codon
YJ12562	ctaatatgtgagggtgtgtaccg	Reverse primer to amplify *jph-1* isoform B to stop codon
YJ12563	tgttctgccattaccagcccg	Forward primer to amplify 4.5 kb *jph-1* promoter
YJ12564	ttcccatttgccgtactgctg	Reverse primer to amplify 4.5 kb *jph-1* promoter
AF-JA-76	attttgtggtataaaatagccgagttaggaaacaaattt ttctttcaggtttctcagtagtgaccatgtgcgtggatc ttgcgtccacacatctcaaggcgtactt	*unc-58(gf)* coCRISPR repair oligo

Table 5. Genotyping primers

Genotyping primer sets			
Name	**Sequence**	**Purpose**	**Product size**
YJ12565 YJ12566 YJ12567	gacgacggcggaacctatg tcaggtacgttctagtcggt gtcttgctggtcaacgtcgt	Genotype *jph-1(ju1683)* and *jph-1(ju1684)*	WT 154 bp, *ju1683* 250 bp, *ju1683* 294 bp, cDNA no product
YJ10503 YJ10504 YJ10686	ggaacaaaggagttcagatcctgtg ggaagacccttagttccaaacaagtg tttttcagaaatatatgccgaggatgttc	Genotype all single copy insertion (*juSi*) lines	WT 562 bp, *juSi* 744 bp
YJ12568 YJ12569 YJ12570	gtctacgatcaagtggttca gaacaatagacaccgatgga atcaacctggcacgataatt	Genotype *jph-1(ok2823)*	WT 273 bp, *ok2823* 390 bp, cDNA 870 bp
YJ12571 YJ12572	ggattccacgaactgttgatg cttttcagcagcattcacc	Amplify area flanking *unc-68(e540)* for sequencing	453 bp
YJ12573 YJ12574	gtacttcgaactgatgcaatgtc gtgaaatcatcgcatctccg	Amplify area flanking *egl-19(ad695gf)* for sequencing	370 bp
YJ12575 YJ12576	gaatgatccaccacgggttg catcagaatgagcgtgttgcag	Amplify area flanking *unc-2(zf35gf)* for sequencing	478 bp
YJ12052 YJ12577 YJ12578	taaagtaacagccgcgccaa aatatgtgctagcaagtattttga ctttgccactgtgtccattg	Genotype *esyt-2(ju1408)* and *esyt-2(ju1409)*	WT 324 bp, *ju1408* 733 bp, *ju1409* 733 bp
YJ12582 YJ12583	cgcggccccagtcgccacatggtgtgacg gggtacggtattgcgaaagctggc	Genotype *nuTi144*	WT 612 bp, *nuSi144* no product
YJ12582 YJ12584	cgcggccccagtcgccacatggtgtgacg agctagcgacggcaaatact	Genotype *nuTi144*	WT no product, *nuSi144* 500bp
YJ12585 YJ12586	gatctactgtctttgtgctaaagctgtctgg ccaaagtaaaggacctaacccgtcaaaatatcc	Genotype *egl-19(nu674)*	WT 2297 bp, nu674 2723 bp
YJ12585 YJ12587	gatctactgtctttgtgctaaagctgtctgg cgtactcgtgaagaaccatgtgatcacg	Genotype *egl-19(nu674)*	WT no product, *nu674* 1185 bp
YJ12588 YJ12589	cgtgaagagctgaactatgtg cccaactggtagtaatctcttc	Genotype *unc-68(nu664)*	WT 549 bp, *nu664* 975 bp

Table 6. CRISPR crRNA sequences

crRNAs		
Name	**Sequence**	**Purpose**
YJ12590	5'-rCrCrGrUrCrCrGrGrUrArArCrArCrCrUrArUrCrA-3'	Target *jph-1* exon 1
YJ12591	5’-rArCrGrArCrGrUrUrGrArCrCrArGrCrArArGrArC-3’	Target *jph-1* exon 9

Table 7. Summary of growth phenotypes of *jph-1* mutants and relevant transgenic animals.
[1] a fosmid containing the entire genomic locus of *jph-1* [WRM0622aB02(*juEx3390*) or WRM0623aF07(*juEx3392*)]
[2] transgenic expression of JPH-1A under its own promoter [P*jph-1*-GFP::JPH-1A(*juSi387* or *juEx7999*)], in pharyngeal muscle [P*myo-2*-GFP::JPH-1A(*juEx8041*)], in body wall muscle [P*myo-3*-GFP::JPH-1A(*juEx8022* or *juEx8023*)], in neurons [P*rab-3*-GFP::JPH-1A(*juSi389*)]
[3]JPH-1B [P*jph-1*-GFP::JPH-1B(*juEx8037* or *juEx8038*)].

Genotype	**Transgene**	**Days to L4 (20°C)**	**Body size at L4**
wild type	none	2	Normal
jph-1(ju1683)	none	3 to 4	Small
jph-1(ju1683)	Fosmid with genomic *jph-1*[1]	2	Normal
jph-1(ju1683)	JPH-1A[2]	2	Normal
jph-1(ju1683)	JPH-1B[3]	3 to 5	Small
eat-4(ky5)	None	2	Normal
jph-1(ju1683)	JPH-1A in pharyngeal muscle[2]	2	Normal
jph-1(ju1683)	JPH-1A in body wall muscle[2]	3 to 4	Small
jph-1(ju1683)	JPH-1A in neurons[2]	3 to 4	Small
jph-1(ok2823)	None	3 to 4	Small
jph-1(ok2823)	Fosmid with genomic *jph-1*[1]	2	Normal

Table 8. Summary of growth rates and movement of double mutants of *jph-1(0)* with calcium channels and *esyt-2* mutants.
All alleles are null unless otherwise annotated as gain-of-function (gf) or partial loss-of-function (lf).

Genotype	Days to L4 (20°C)	Movement
jph-1(ju1683)	3 to 4	Partial flaccid paralysis
unc-68(e540)	2 to 3	Partial flaccid paralysis
egl-19(ad1006lf)	2	Partial flaccid paralysis
egl-19(ad695gf)	2	Normal
unc-2(e55)	2	Paralyzed
unc-2(zf35gf)	2	Hyperactive
esyt-2(ju1409)	2	Normal
jph-1(ju1683); unc-68(e540)	4 to 6	Severe flaccid paralysis
jph-1(ju1683); unc-68(e540); juEx7999 [P*jph-1*-GFP::JPH-1A]	3 to 4	Partial flaccid paralysis
jph-1(ju1683); egl-19(ad1006lf)	Lethal	
jph-1(ju1683); egl-19(ad695gf)	4 to 5	Partial flaccid paralysis
jph-1(ju1683); unc-2(e55)	4 to 7	Paralyzed
jph-1(ju1683); unc-2(zf35gf)	5 to 7	Partial flaccid paralysis
jph-1(ju1683); esyt-2(ju1409)	3 to 5	Partial flaccid paralysis

References

Andrusiak MG, Sharifnia P, Lyu X, Wang Z, Dickey AM, Wu Z, Chisholm AD, Jin Y. 2019. Inhibition of Axon Regeneration by Liquid-like TIAR-2 Granules. *Neuron* **104**:290-304.e8. doi:10.1016/j.neuron.2019.07.004

Avery L. 1993. The genetics of feeding in *Caenorhabditis elegans*. *Genetics* **133**:897–917.

Avery L, Horvitz HR. 1989. Pharyngeal pumping continues after laser killing of the pharyngeal nervous system of *C. elegans. Neuron* **3**:473–485. doi:10.1016/0896-6273(89)90206-7

Avery L, You Y-J. 2012. *C. elegans* feeding. *WormBook* 1–23. doi:10.1895/wormbook.1.150.1

Beavers DL, Wang W, Ather S, Voigt N, Garbino A, Dixit SS, Landstrom AP, Li N, Wang Q, Olivotto I, Dobrev D, Ackerman MJ, Wehrens XHT. 2013. Mutation E169K in junctophilin-2 causes atrial fibrillation due to impaired RyR2 stabilization. *J Am Coll Cardiol* **62**:2010–2019. doi:10.1016/j.jacc.2013.06.052

Brenner S. 1974. The genetics of *Caenorhabditis elegans. Genetics* **77**:71–94.

Calpena E, Del Amo VL, Chakraborty M, Llamusi B, Artero R, Espinós C, Galindo MI. 2018. The *Drosophila* junctophilin gene is functionally equivalent to its four mammalian counterparts and is a modifier of a Huntingtin poly-Q expansion and the Notch pathway. *DMM Dis Model Mech* **11**. doi:10.1242/dmm.029082

Chen B, Guo A, Zhang C, Chen R, Zhu Y, Hong J, Kutschke W, Zimmerman K, Weiss RM, Zingman L, Anderson ME, Wehrens XHT, Song LS. 2013. Critical roles of junctophilin-2 in T-tubule and excitation-contraction coupling maturation during postnatal development. *Cardiovasc Res* **100**:54–62. doi:10.1093/cvr/cvt180

El-Gebali S, Mistry J, Bateman A, Eddy SR, Luciani A, Potter SC, Qureshi M, Richardson LJ, Salazar GA, Smart A, Sonnhammer ELL, Hirsh L, Paladin L, Piovesan D, Tosatto SCE, Finn RD. 2019. The Pfam protein families database in 2019. *Nucleic Acids Res* **47**:D427–D432. doi:10.1093/nar/gky995

El Mouridi S, Lecroisey C, Tardy P, Mercier M, Leclercq-Blondel A, Zariohi N, Boulin T. 2017. Reliable CRISPR/Cas9 genome engineering in *Caenorhabditis elegans* using a single efficient sgRNA and an easily recognizable phenotype. *G3 Genes, Genomes, Genet* **7**:1429–1437. doi:10.1534/g3.117.040824

Frøkjær-Jensen C, Davis MW, Sarov M, Taylor J, Flibotte S, LaBella M, Pozniakovsky A, Moerman DG, Jorgensen EM. 2014. Random and targeted transgene insertion in *Caenorhabditis elegans* using a modified Mos1 transposon. *Nat Methods* **11**:529–534. doi:10.1038/nmeth.2889

Frøkjær-Jensen C, Wayne Davis M, Hopkins CE, Newman BJ, Thummel JM, Olesen SP, Grunnet M, Jorgensen EM. 2008. Single-copy insertion of transgenes in *Caenorhabditis elegans*. *Nat Genet* **40**:1375–1383. doi:10.1038/ng.248

Garbino A, Van Oort RJ, Dixit SS, Landstrom AP, Ackerman MJ, Wehrens XHT. 2009. Molecular evolution of the junctophilin gene family. *Physiol Genomics* **37**:175–186. doi:10.1152/physiolgenomics.00017.2009

Ghosh-Roy A, Wu Z, Goncharov A, Jin Y, Chisholm AD. 2010. Calcium and cyclic AMP promote axonal regeneration in *Caenorhabditis elegans* and require DLK-1 kinase. *J Neurosci* **30**:3175–3183. doi:10.1523/JNEUROSCI.5464-09.2010

Giordano F, Saheki Y, Idevall-Hagren O, Colombo SF, Pirruccello M, Milosevic I, Gracheva EO, Bagriantsev SN, Borgese N, De Camilli P. 2013. PI(4,5)P2-Dependent and Ca2+-Regulated ER-PM interactions mediated by the extended synaptotagmins. *Cell* **153**:1494–1509. doi:10.1016/j.cell.2013.05.026

Gjorgjieva J, Biron D, Haspel G. 2014. Neurobiology of *Caenorhabditis elegans* locomotion: Where do we stand? *Bioscience* **64**:476–486. doi:10.1093/biosci/biu058

Golini L, Chouabe C, Berthier C, Cusimano V, Fornaro M, Bonvallet R, Formoso L, Giacomello E, Jacquemond V, Sorrentino V. 2011. Junctophilin 1 and 2 proteins interact with the L-type Ca 2+ channel dihydropyridine receptors (DHPRs) in skeletal muscle. *J Biol Chem* **286**:43717–43725. doi:10.1074/jbc.M111.292755

Goodman MB, Hall DH, Avery L, Lockery SR. 1998. Active currents regulate sensitivity and dynamic range in *C. elegans* neurons. *Neuron* **20**:763–772. doi:10.1016/S0896-6273(00)81014-4

Guo A, Wang Yihui, Chen B, Wang Yunhao, Yuan J, Zhang L, Hall D, Wu J, Shi Y, Zhu Q, Chen C, Thiel WH, Zhan X, Weiss RM, Zhan F, Musselman CA, Pufall M, Zhu W, Au KF, Hong J, Anderson ME, Grueter CE, Song LS. 2018. E-C coupling structural protein junctophilin-2 encodes a stress-adaptive transcription regulator. *Science (80-)* **362**:1–14. doi:10.1126/science.aan3303

Hirata Y, Brotto M, Weisleder N, Chu Y, Lin P, Zhao X, Thornton A, Komazaki S, Takeshima H, Ma J, Pan Z. 2006. Uncoupling store-operated Ca2+ entry and altered Ca2+ release from sarcoplasmic reticulum through silencing of junctophilin genes. *Biophys J* **90**:4418–4427. doi:10.1529/biophysj.105.076570

Hirve N, Rajanikanth V, Hogan PG, Gudlur A. 2018. Coiled-Coil Formation Conveys a STIM1 Signal from ER Lumen to Cytoplasm. *Cell Rep* **22**:72–83. doi:10.1016/j.celrep.2017.12.030

Huang YC, Pirri JK, Rayes D, Gao S, Mulcahy B, Grant J, Saheki Y, Francis MM, Zhen M, Alkema MJ. 2019. Gain-of-function mutations in the UNC-2/CaV2α channel lead to excitation-dominant synaptic transmission in *C. elegans*. *Elife* **8**:1–28. doi:10.7554/eLife.45905

Ito K, Komazaki S, Sasamoto K, Yoshida M, Nishi M, Kitamura K, Takeshima H. 2001. Deficiency of triad junction and contraction in mutant skeletal muscle lacking junctophilin type 1. *J Cell Biol* **154**:1059–1067. doi:10.1083/jcb.200105040

Kakizawa S, Kishimoto Y, Hashimoto K, Miyazaki T, Furutani K, Shimizu H, Fukaya M, Nishi M, Sakagami H, Ikeda A, Kondo H, Kano M, Watanabe M, Iino M, Takeshima H. 2007. Junctophilin-mediated channel crosstalk essential for cerebellar synaptic plasticity. *EMBO J* **26**:1924–1933. doi:10.1038/sj.emboj.7601639

Kigerl KA, Zane K, Adam K, Sullivan MB, Popovich PG. 2020. The spinal cord-gut-immune axis as a master regulator of health and neurological function after spinal cord injury. *Exp Neurol* **323**.

Kikuma K, Li X, Kim D, Sutter D, Dickman DK. 2017. Extended synaptotagmin localizes to presynaptic ER and promotes neurotransmission and synaptic growth in *Drosophila*. *Genetics* **207**:993–1006. doi:10.1534/genetics.117.300261

Kim KW, Tang NH, Piggott CA, Andrusiak MG, Park S, Zhu M, Kurup N, Cherra SJ, Wu Z, Chisholm AD, Jin Y. 2018. Expanded genetic screening in caenorhabditis elegans identifies new regulators and an inhibitory role for NAD $^{+}$ in axon regeneration. *Elife* **7**. doi:10.7554/eLife.39756

Kobuna H, Inoue T, Shibata M, Gengyo-Ando K, Yamamoto A, Mitani S, Arai H. 2010. Multivesicular body formation requires OSBP-related proteins and cholesterol. *PLoS Genet* **6**. doi:10.1371/journal.pgen.1001055

Lainé V, Ségor JR, Zhan H, Bessereau JL, Jospin M. 2014. Hyperactivation of L-type voltage-gated Ca2+ channels in *Caenorhabditis elegans* striated muscle can result from point mutations in the IS6 or the IIIS4 segment of the α1 subunit. *J Exp Biol* **217**:3805–3814. doi:10.1242/jeb.106732

Landstrom AP, Beavers DL, Wehrens XHT. 2014. The junctophilin family of proteins: From bench to bedside. *Trends Mol Med* **20**:353–362. doi:10.1016/j.molmed.2014.02.004

Landstrom AP, Kellen CA, Dixit SS, Van Oort RJ, Garbino A, Weisleder N, Ma J, Wehrens XHT, Ackerman MJ. 2011. Junctophilin-2 expression silencing causes cardiocyte hypertrophy and abnormal intracellular calcium-handling. *Circ Hear Fail* **4**:214–223. doi:10.1161/CIRCHEARTFAILURE.110.958694

Lang AB, John Peter ATAT, Walter P, Kornmann B. 2015. ER-mitochondrial junctions can be bypassed by dominant mutations in the endosomal protein Vps13. *J Cell Biol* **210**:883–890. doi:10.1083/jcb.201502105

Lee RYN, Lobel L, Hengartner M, Horvitz HR, Avery L. 1997. Mutations in the α1 subunit of an L-type voltage-activated Ca2+ channel cause myotonia in *Caenorhabditis elegans*. *EMBO J* **16**:6066–6076. doi:10.1093/emboj/16.20.6066

Lee RYN, Sawin ER, Chalfie M, Horvitz HR, Avery L. 1999. EAT-4, a Homolog of a Mammalian Sodium-Dependent Inorganic Phosphate Cotransporter, Is Necessary for Glutamatergic Neurotransmission in *Caenorhabditis elegans*. *J Neurosci* **19**:159–167.

Letunic I, Bork P. 2018. 20 years of the SMART protein domain annotation resource. *Nucleic Acids Res* **46**:D493–D496. doi:10.1093/nar/gkx922

Lewis JA, Wu CH, Berg H, Levine JH. 1980. The genetics of levamisole resistance in the nematode *Caenorhabditis elegans*. *Genetics* **95**:905–928.

Li H, Ding X, Lopez JR, Takeshima H, Ma J, Allen PD, Eltit JM. 2010. Impaired Orai1-mediated resting Ca2+ entry reduces the cytosolic [Ca2+] and sarcoplasmic reticulum Ca2+ loading in quiescent junctophilin 1 knock-out myotubes. *J Biol Chem* **285**:39171–39179. doi:10.1074/jbc.M110.149690

Liu Q, Chen B, Yankova M, Morest DK, Maryon E, Hand AR, Nonet ML, Wang ZW. 2005. Presynaptic ryanodine receptors are required for normal quantal size at the *Caenorhabditis elegans* neuromuscular junction. *J Neurosci* **25**:6745–6754. doi:10.1523/JNEUROSCI.1730-05.2005

Madeira F, Park YM, Lee J, Buso N, Gur T, Madhusoodanan N, Basutkar P, Tivey ARN, Potter SC, Finn RD, Lopez R. 2019. The EMBL-EBI search and sequence analysis tools APIs in 2019. *Nucleic Acids Res* **47**:W636–W641. doi:10.1093/nar/gkz268

Manford AG, Stefan CJ, Yuan HL, MacGurn JA, Emr SD. 2012. ER-to-Plasma Membrane Tethering Proteins Regulate Cell Signaling and ER Morphology. *Dev Cell* **23**:1129–1140. doi:10.1016/j.devcel.2012.11.004

Maryon EB, Coronado R, Anderson P. 1996. unc-68 encodes a ryanodine receptor involved in regulating *C. elegans* body-wall muscle contraction. *J Cell Biol* **134**:885–893. doi:10.1083/jcb.134.4.885

Maryon EB, Saari B, Anderson P. 1998. Muscle-specific functions of ryanodine receptor channels in *Caenorhabditis elegans*. *J Cell Sci* **111**:2885–2895.

Mathews EA, García E, Santi CM, Mullen GP, Thacker C, Moerman DG, Snutch TP. 2003. Critical residues of the *Caenorhabditis elegans* unc-2 voltage-gated calcium channel that affect behavioral and physiological properties. *J Neurosci* **23**:6537–6545. doi:10.1523/JNEUROSCI.23-16-06537.2003

Mello CC, Kramer JM, Stinchcomb D, Ambros V. 1991. Efficient gene transfer in *C.elegans*: Extrachromosomal maintenance and integration of transforming sequences. *EMBO J* **10**:3959–3970. doi:10.1002/j.1460-2075.1991.tb04966.x

Mesmin B, Bigay J, Moser Von Filseck J, Lacas-Gervais S, Drin G, Antonny B. 2013. XA four-step cycle driven by PI(4)P hydrolysis directs sterol/PI(4)P exchange by the ER-Golgi Tether OSBP. *Cell* **155**:830. doi:10.1016/j.cell.2013.09.056

Miller KG, Alfonso A, Nguyen M, Crowell JA, Johnson CD, Rand JB. 1996. A genetic selection for *Caenorhabditis elegans* synaptic transmission mutants. *Proc Natl Acad Sci U S A* **93**:12593–12598. doi:10.1073/pnas.93.22.12593

Moriguchi S, Nishi M, Komazaki S, Sakagami H, Miyazaki T, Masumiya H, Saito SY, Watanabe M, Kondo H, Yawo H, Fukunaga K, Takeshima H. 2006. Functional uncoupling between Ca2+ release and afterhyperpolarization in mutant hippocampal neurons lacking junctophilins. *Proc Natl Acad Sci U S A* **103**:10811–10816. doi:10.1073/pnas.0509863103

Nakada T, Kashihara T, Komatsu M, Kojima K, Takeshita T, Yamada M. 2018. Physical interaction of junctophilin and the CaV1.1 C terminus is crucial for skeletal muscle contraction. *Proc Natl Acad Sci U S A* **115**:4507–4512. doi:10.1073/pnas.1716649115

Nishi M, Mizushima A, Nakagawara K ichi, Takeshima H. 2000. Characterization of human junctophilin subtype genes. *Biochem Biophys Res Commun* **273**:920–927. doi:10.1006/bbrc.2000.3011

Nishi M, Sakagami H, Komazaki S, Kondo H, Takeshima H. 2003. Coexpression of junctophilin type 3 and type 4 in brain. *Mol Brain Res* **118**:102–110. doi:10.1016/S0169-328X(03)00341-3

Paix A, Folkmann A, Rasoloson D, Seydoux G. 2015. High efficiency, homology-directed genome editing in *Caenorhabditis elegans* using CRISPR-Cas9ribonucleoprotein complexes. *Genetics* **201**:47–54. doi:10.1534/genetics.115.179382

Phillips MJ, Voeltz GK. 2016. Structure and function of ER membrane contact sites with other organelles. *Nat Rev Mol Cell Biol* **17**:69–82. doi:10.1038/nrm.2015.8

Phimister AJ, Lango J, Eun HL, Ernst-Russell MA, Takeshima H, Jianjie M, Allen PD, Pessah IN. 2007. Conformation-dependent stability of junctophilin 1 (JP1) and Ryanodine Receptor Type 1 (RyR1) channel complex is mediated by their hyper-reactive thiols. *J Biol Chem* **282**:8667–8677. doi:10.1074/jbc.M609936200

Porter KR, Palade GE. 1957. STUDIES ON THE ENDOPLASMIC RETICULUM III. Its Form and Distribution in Striated Muscle Cells. *J Biophys Biochem Cytol* **3**:269–300.

Pritchard HAT, Griffin CS, Yamasaki E, Thakore P, Lane C, Greenstein AS, Earley S. 2019. Nanoscale coupling of junctophilin-2 and ryanodine receptors regulates vascular smooth muscle cell contractility. *Proc Natl Acad Sci U S A* **116**:21874–21881. doi:10.1073/pnas.1911304116

Reynolds JO, Chiang DY, Wang W, Beavers DL, Dixit SS, Skapura DG, Landstrom AP, Song LS, Ackerman MJ, Wehrens XHT. 2013. Junctophilin-2 is necessary for T-tubule maturation during mouse heart development. *Cardiovasc Res* **100**:44–53. doi:10.1093/cvr/cvt133

Saeki T, Suzuki Y, Yamamura H, Takeshima H, Imaizumi Y. 2019. A junctophilin-caveolin interaction enables efficient coupling between ryanodine receptors and BKCa channels in the Ca2+ microdomain of vascular smooth muscle. *J Biol Chem* **294**:13093–13105. doi:10.1074/jbc.RA119.008342

Saheki Y, Bargmann CI. 2009. Presynaptic CaV2 calcium channel traffic requires CALF-1 and the α 2 subunit UNC-36. *Nat Neurosci* **12**:1257–1265. doi:10.1038/nn.2383

Saheki Y, De Camilli P. 2017. The Extended-Synaptotagmins. *Biochim Biophys Acta - Mol Cell Res* **1864**:1490–1493. doi:10.1016/j.bbamcr.2017.03.013

Sahu G, Wazen RM, Colarusso P, Chen SRW, Zamponi GW, Turner RW. 2019. Junctophilin Proteins Tether a Cav1-RyR2-KCa3.1 Tripartite Complex to Regulate Neuronal Excitability. *Cell Rep* **28**:2427-2442.e6. doi:10.1016/j.celrep.2019.07.075

Schafer WR, Sanchez BM, Kenyon CJ. 1996. Genes affecting sensitivity to serotonin in *Caenorhabditis elegans*. *Genetics* **143**:1219–1230.

Sun L, Shay J, McLoed M, Roodhouse K, Chung SH, Clark CM, Pirri JK, Alkema MJ, Gabel C V. 2014. Neuronal regeneration in *C. elegans* requires subcellular calcium release by ryanodine receptor channels and can be enhanced by optogenetic stimulation. *J Neurosci* **34**:15947–15956. doi:10.1523/JNEUROSCI.4238-13.2014

Takeshima H, Komazaki S, Nishi M, Iino M, Kangawa K. 2000. Junctophilins: A novel family of junctional membrane complex proteins. *Mol Cell* **6**:11–22. doi:10.1016/s1097-2765(00)00003-4

Trojanowski NF, Fang-Yen C. 2015. Simultaneous Optogenetic Stimulation of Individual Pharyngeal Neurons and Monitoring of Feeding Behavior in Intact *C. elegans* In: Biron D, Haspel G, editors. *C. elegans*: Methods and Applications. Totowa, NJ: Humana Press. pp. 105–119. doi:10.1007/978-1-4939-2842-2_9

Valm AM, Cohen S, Legant WR, Melunis J, Hershberg U, Wait E, Cohen AR, Davidson MW, Betzig E, Lippincott-Schwartz J. 2017. Applying systems-level spectral imaging and analysis to reveal the organelle interactome. *Nature* **546**:162–167. doi:10.1038/nature22369

Van Oort RJ, Garbino A, Wang W, Dixit SS, Landstrom AP, Gaur N, De Almeida AC, Skapura DG, Rudy Y, Burns AR, Ackerman MJ, Wehrens XHT. 2011. Disrupted junctional membrane complexes and hyperactive ryanodine receptors after acute junctophilin knockdown in mice. *Circulation* **123**:979–988. doi:10.1161/CIRCULATIONAHA.110.006437

Von Stetina SE, Treinin M, Miller DM. 2006. The Motor Circuit. *Int Rev Neurobiol* **69**:125–167. doi:10.1016/S0074-7742(05)69005-8

Wang S, Tang NH, Lara-Gonzalez P, Zhao Z, Cheerambathur DK, Prevo B, Chisholm AD, Desai A, Oegema K. 2017. A toolkit for GFP-mediated tissue-specific protein degradation in *C. elegans*. *Dev* **144**:2694–2701. doi:10.1242/dev.150094

Woo JS, Kim DH, Allen PD, Lee EH. 2008. TRPC3-interacting triadic proteins in skeletal muscle. *Biochem J* **411**:399–405. doi:10.1042/BJ20071504

Wu Z, Ghosh-Roy A, Yanik MF, Zhang JZ, Jin Y, Chisholm AD. 2007. *Caenorhabditis elegans* neuronal regeneration is influenced by life stage, ephrin signaling, and synaptic branching. *Proc Natl Acad Sci U S A* **104**:15132–15137. doi:10.1073/pnas.0707001104

Yoshida M, Sugimoto A, Ohshima Y, Takeshima H. 2001. Important role of junctophilin in nematode motor function. *Biochem Biophys Res Commun* **289**:234–239. doi:10.1006/bbrc.2001.5951

Ziman AP, Gómez-Viquez NL, Bloch RJ, Lederer WJ. 2010. Excitation-contraction coupling changes during postnatal cardiac development. *J Mol Cell Cardiol* **48**:379–386. doi:10.1016/j.yjmcc.2009.09.016

Chapter 4:

Discussion and Future Directions

As the catalogue of membrane contact sites (MCSs) grows and MCSs have been identified for all membrane-bound organelles, the field has begun to shift from identifying MCSs to determining their functions (Prinz et al., 2020). The work presented in this dissertation delves into the function of endoplasmic reticulum (ER) – plasma membrane (PM) contact sites issue by examining *Caenorhabditis elegans* mutants affecting conserved ER-PM contact site components. I show that individually, most ER-PM components are dispensable for axon regeneration after injury, suggesting redundancy among MCS proteins. I find that the *C. elegans* junctophilin *jph-1* functions in muscles and neurons and is required for a variety of roles, including feeding, locomotion, axon regeneration, and neurotransmission. In this chapter, I discuss my results and identify future directions that can expand on the data shown in this dissertation and build our understanding of the functions of ER-PM contact sites.

Roles of ER-PM contact sites in axon regeneration

Following the identification of ER-PM contacts in muscles by electron microscopy (Porter and Palade, 1957), neurons were the second tissue in which MCSs were identified (Rosenbluth, 1962). In this study, electron microscopy revealed ER-PM contact sites in both peripheral and central nervous system neurons and near synapses. In recent years, it has been shown that neuron depolarization causes a reversible decrease in ER-PM contact area (Tao-Cheng, 2018). The voltage-gated potassium channel Kv2.1, which also acts as an ER-PM tether, couples PM-localized voltage-gated calcium channels and ER-localized ryanodine receptor (RyR) calcium channels in neurons (Vierra et al., 2019). Other ER-PM contact site proteins have been identified, including extended-synaptotagmins, which control lipid homeostasis by clearing diacylglycerol from the PM (Saheki et al., 2016). However, much of the research of ER-PM contact sites has been

performed in cultured cell lines, and while many ER-PM contact site proteins are neuronally expressed, their functions have not been validated in neurons (Fowler et al., 2019).

To address the functions of ER-PM contact sites in neurons, I examined neurons under the stress condition of axon injury. MCS proteins often act redundantly, and phenotypes are frequently not visible unless the cell or organism is subjected to stress (Manford et al., 2012). I performed axon injury experiments on *C. elegans* mutants of conserved ER-PM contact site components. This comprised of the *C. elegans* homologs of the ER-PM tethers extended-synaptotagmin, junctophilin, and anoctamin, and the lipid transfer protein family oxysterol binding protein (OSBP) – related proteins (ORPs) which localize to ER-PM contact sites. In addition to single mutants, I tested *anoh-1;anoh-2* double mutants and *obr-1;obr-2;obr-3;obr-4* quadruple mutants to mutate the entire anoctamin and ORP protein families in *C. elegans*.

Apart from the ORP quadruple mutant and the junctophilin *jph-1* mutant, I did not observe significant changes to axon regeneration. This suggests that ER-PM contact site proteins act redundantly, such that individual mutations are insufficient to cause observable changes in axon regeneration. Consistent with this, knocking out all three E-Syts in mice showed no observable changes to animal health or brain morphology (Sclip et al., 2016; Tremblay and Moss, 2016). An alternative explanation is that most ER-PM contact site proteins are not required for axon regeneration. In Chapter 3, I show that *jph-1* is required in the pharyngeal muscle, but not neurons, for axon regeneration. This may be due to *jph-1*'s role in feeding, which could provide necessary nutrients for axon injury repair and regrowth. The inability of neuronal expression of *jph-1* to rescue axon regeneration suggests that neuronal ER-PM contacts may not play an important role in axon regeneration. Answering this question will require the construction of additional

compound mutants to delete multiple ER-PM contact site proteins simultaneously and eliminate the possibility of compensation by redundant proteins.

Tissue-specific roles of ER-PM contact site proteins junctophilin and extended-synaptotagmin

In Chapter 3, I address the tissue-specific roles of the *C. elegans* junctophilin *jph-1*. I generated *jph-1(0)* mutants, which are small, slow-growing, and uncoordinated. Using a transcriptional reporter, I show that *jph-1* is expressed in neurons and muscles. I demonstrate that the small and slow-growing phenotypes are due to the absence of *jph-1* from the pharyngeal muscle, where it is required for the muscle contraction that drives feeding. Reduced nutrient intake is likely the cause of the delayed development of *jph-1(0)* mutants, as similar effects are seen in starved animals (Avery, 1993; Avery and Horvitz, 1989).

I show that the slow and uncoordinated locomotion phenotype is due to the absence of *jph-1* from the body wall muscle. In the body wall muscle, JPH-1 co-localizes with RyR/UNC-68 and the voltage-gated calcium channel Cav1/EGL-19. Animals with mutations in *unc-68* or *egl-19* show partial flaccid paralysis, similar to *jph-1(0)* mutants (Lee et al., 1997; Maryon et al., 1996). JPH-1 is likely required to couple the entry of calcium through the PM-localized EGL-19 to the opening of the ER-localized UNC-68. However, it is not clear if JPH-1 is required for the generation of ER-PM contacts, the localization of EGL-19 and UNC-68 to ER-PM contacts, or both. The latter can be addressed by examining the localization of EGL-19 and UNC-68 reporters in *jph-1(0)* mutants. JPH-1 localization in *unc-68(0)* mutants is more diffuse, suggesting that these proteins may be required for each others' localization. Addressing if JPH-1 generates ER-PM contacts in the body wall muscle will require the examination of ER-PM contacts in *jph-1(0)*

mutants. Electron microscopy is the gold standard for studying ER-PM contacts. However, methods to examine ER-PM contacts using fluorescence microscopy, which have recently been developed, may offer a more tractable alternative (Scorrano et al., 2019).

Expression in pharyngeal and body wall muscles is sufficient to rescue the overt phenotypes of *jph-1(0)* mutants. However, *jph-1* is also expressed in many neurons. To address the role of ER-PM contacts in neurons, I examined both *jph-1* and the neuronally expressed ER-PM contact protein extended-synaptotagmin, which is encoded by *esyt-2*. In Chapter 2, I show that *esyt-2* is expressed in *C. elegans* neurons and localizes to ER-PM contact sites. In Chapter 3, I assess neurotransmission at the neuromuscular junction in *jph-1* and *esyt-2* mutants using pharmacological assays. Both *jph-1(0)* and *esyt-2(0)* are resistant to the drug aldicarb, suggesting that they have defects in neurotransmission. Unexpectedly, *jph-1(0);esyt-2(0)* double mutants have a wild-type response to aldicarb, suggesting that *jph-1* and *esyt-2* have antagonistic roles in neurotransmission. Dissecting this interaction will require determining whether *jph-1* and *esyt-2* act pre- or post-synaptically in neurotransmission. *jph-1(0)* display a wild-type response to the drug levamisole, suggesting that they do not function downstream of the levamisole-sensitive acetylcholine receptors in the muscle. However, neuronal expression of *jph-1* does not rescue aldicarb resistance in *jph-1(0)* mutants. A P*esyt-2*-GFP transcriptional reporter is expressed exclusively in neurons, but *esyt-2(0)* mutants show slight levamisole resistance, which is an indicator of post-synaptic activity. Future experiments using tissue-specific *jph-1* knockouts and tissue-specific *esyt-2* rescue transgenes may show where *jph-1* and *esyt-2* act, starting the process of unravelling how these genes regulate neurotransmission.

The work I present in my dissertation demonstrates that ER-PM contact site proteins play critical roles in diverse tissue types and support tissue-specific functions. In addition, I thoroughly

characterize the genes *jph-1* and *esyt-2* in *C. elegans*, laying the groundwork for their future study. Next steps include expanding on the mechanistic details about how ER-PM contact site proteins perform their tissue-specific functions. *C. elegans* is an excellent model to continue studying ER-PM contact site proteins. By taking advantage of the ability to perform live-imaging in intact animals and the availability of genetic tools, *C. elegans* will likely play an important role in dissecting the functions of ER-PM contact site proteins.

References

Avery L. 1993. The genetics of feeding in Caenorhabditis elegans. *Genetics* **133**:897–917.

Avery L, Horvitz HR. 1989. Pharyngeal pumping continues after laser killing of the pharyngeal nervous system of C. elegans. *Neuron* **3**:473–485. doi:10.1016/0896-6273(89)90206-7

Fowler PC, Garcia-Pardo ME, Simpson JC, O'Sullivan NC. 2019. NeurodegenERation: The Central Role for ER Contacts in Neuronal Function and Axonopathy, Lessons From Hereditary Spastic Paraplegias and Related Diseases. *Front Neurosci* **13**:1–20. doi:10.3389/fnins.2019.01051

Lee RYN, Lobel L, Hengartner M, Horvitz HR, Avery L. 1997. Mutations in the α1 subunit of an L-type voltage-activated Ca2+ channel cause myotonia in Caenorhabditis elegans. *EMBO J* **16**:6066–6076. doi:10.1093/emboj/16.20.6066

Manford AG, Stefan CJ, Yuan HL, MacGurn JA, Emr SD. 2012. ER-to-Plasma Membrane Tethering Proteins Regulate Cell Signaling and ER Morphology. *Dev Cell* **23**:1129–1140. doi:10.1016/j.devcel.2012.11.004

Maryon EB, Coronado R, Anderson P. 1996. unc-68 encodes a ryanodine receptor involved in regulating C. elegans body-wall muscle contraction. *J Cell Biol* **134**:885–893. doi:10.1083/jcb.134.4.885

Porter KR, Palade GE. 1957. STUDIES ON THE ENDOPLASMIC RETICULUM III. Its Form and Distribution in Striated Muscle Cells. *J Biophys Biochem Cytol* **3**:269–300.

Prinz WA, Toulmay A, Balla T. 2020. The functional universe of membrane contact sites. *Nat Rev Mol Cell Biol* **21**:7–24. doi:10.1038/s41580-019-0180-9

Rosenbluth J. 1962. Subsurface cisterns and their relationship to the neuronal plasma membrane. *J Cell Biol* **13**:405–421. doi:10.1083/jcb.13.3.405

Saheki Y, Bian X, Schauder CM, Sawaki Y, Surma MA, Klose C, Pincet F, Reinisch KM, De Camilli P. 2016. Control of plasma membrane lipid homeostasis by the extended synaptotagmins. *Nat Cell Biol* **18**:504–515. doi:10.1038/ncb3339

Sclip A, Bacaj T, Giam LR, Südhof TC. 2016. Extended Synaptotagmin (ESyt) triple knock-out mice are viable and fertile without obvious endoplasmic reticulum dysfunction. *PLoS One* **11**:1–17. doi:10.1371/journal.pone.0158295

Scorrano L, De Matteis MA, Emr S, Giordano F, Hajnóczky G, Kornmann B, Lackner LL, Levine TP, Pellegrini L, Reinisch K, Rizzuto R, Simmen T, Stenmark H, Ungermann C, Schuldiner M. 2019. Coming together to define membrane contact sites. *Nat Commun* **10**:1–11. doi:10.1038/s41467-019-09253-3

Tao-Cheng JH. 2018. Activity-dependent decrease in contact areas between subsurface cisterns and plasma membrane of hippocampal neurons. *Mol Brain* **11**:1–8. doi:10.1186/s13041-018-0366-7

Tremblay MG, Moss T. 2016. Loss of all 3 Extended Synaptotagmins does not affect normal mouse development, viability or fertility. *Cell Cycle* **15**:2360–2366. doi:10.1080/15384101.2016.1203494

Vierra NC, Kirmiz M, van der List D, Santana LF, Trimmer JS. 2019. Kv2.1 mediates spatial and functional coupling of L-type calcium channels and ryanodine receptors in neurons. *bioRxiv* 1–42. doi:10.1101/702514